DYRK1A in cancer: good or evil?

Defining properties of DYRK1A kinase as a novel tumor driver

Jacopo Boni

TESI DOCTORAL UPF / 2019

THESIS SUPERVISOR

Dra. Susana de la Luna

Gene Regulation, Stem Cells and Cancer Programme

Centre for Genomic Regulation

DEPARTMENT OF EXPERIMENTAL AND HEALTH SCIENCES

Universitat Pompeu Fabra Barcelona

Centre for Genomic Regulation

Ai miei pensieri,

A come ero ieri,

E anche per me.

(Ivano Fossati - Dedicato)

There's no dark side of the moon really. As a matter of fact, it's all dyrk.

(Pink Floyd – Eclipse)

Table of contents

Materials and Methods

Results

Abstract

Genes encoding for protein kinases are the most frequently mutated genes in cancer, as kinases play pivotal roles in the regulation of cellular pathways that are crucial for malignant transformation. DYRK (dual-specificity tyrosine-regulated kinases) are an evolutionary conserved family of protein kinases, which participate in the regulation of critical cellular processes important for tumor development. In this Thesis work, the putative role of the DYRK family members as drivers in cancer has been explored through an extensive analysis of The Cancer Genome Atlas-TCGA data. The expression of DYRK genes was found altered in tumor samples, and the member DYRK1A emerged as the most promising candidate to act as a tumor driver. The impact of DYRK1A cancer-associated somatic mutations has been evaluated through specific functional screens, which showed that most of the mutations analyzed lead to loss of activity and/or protein stability. By using a CRIPSR/Cas9-based approach, *DYRK1Awt/wt* genotype has been restored in HEC59, a heterozygous *DYRK1A*-mutated endometrial carcinoma cell line. Reversion to the wt genotype reduced cell survival and strongly impaired HEC59 clonogenic capacity, while complete *DYRK1A* loss led to opposite phenotypes. Mouse xenograft experiments showed reduced tumor volume and delayed growth of the modified cells compared to parental HEC59, indicating that variations in *DYRK1A* dosage negatively affect tumor growth *in vivo*. Finally, an integrated analysis of transcriptome-proteome-phosphoproteome profiles in DYRK1A-edited clones provided hints on molecular mechanisms dependent on DYRK1A dosage in endometrial cancer such as activation of the interferon-STAT1 pathway in reverted DYRK1A-WT cells. Other possible mechanisms for DYRK1A-mediated tumor suppressive function are also discussed. All together, the results provide evidence that DYRK1A is a novel tumor driver.

Resumen

Los genes que codifican para proteína quinasas son los genes más frecuentemente mutados en cáncer, ya que las quinasas juegan un papel fundamental en la regulación de procesos cruciales para la transformación tumoral. Las quinasas DYRK (dual-specificity tyrosine-regulated kinases) son una familia de proteína quinasas evolutivamente conservadas, que participan en la regulación de procesos celulares como proliferación, diferenciación y supervivencia. En esta Tesis se ha estudiado el potencial de los miembros de la familia DYRK de actuar como *drivers* en cáncer. Mediante un extenso análisis de datos de *The Cancer Genome Atlas*-TCGA, se ha encontrado que los genes DYRK están alterados en tumores, y el miembro DYRK1A resultó ser el candidato más prometedor. El impacto de mutaciones somáticas en *DYRK1A* se ha evaluado mediante ensayos funcionales, y se ha demostrado que la mayoría de las mutaciones analizadas causan pérdida de actividad y/o estabilidad. Utilizando la técnica CRIPSR/Cas9 de edición genética, se ha restaurado el genotipo *DYRK1Awt/wt* en células HEC59, una línea celular tumoral de cáncer de endometrio haploinsuficiente para DYRK1A. La reversión al genotipo *wt/wt* afecta el potencial clonogénico de estas células, muy probablemente debido a una reducción en supervivencia, mientras que la pérdida total de *DYRK1A* conlleva la aparición de fenotipos opuestos. Los tumores generados por inyección en ratones de células HEC59 con distintas dosis de *DYRK1A* manifiestan retraso en su desarrollo y un volumen tumoral reducido, en comparación con los tumores derivados de la línea parental haploinsuficiente, lo que indica que tanto la ganancia de DYRK1A como su pérdida afectan negativamente al crecimiento tumoral *in vivo*. Finalmente, se ha llevado a cabo un análisis de los perfiles de transcriptoma-proteoma-fosfoproteoma de HEC59 y los clones derivados, para identificar mecanismos moleculares dependientes de la dosis de DYRK1A en cáncer de endometrio. El

análisis ha revelado la activación en la ruta del interferon/STAT1 en células DYRK1A-WT revertidas; se discuten además otros posibles mecanismos responsables de la función supresora de tumores mediada por DYRK1A. En conjunto, los resultados descritos sugieren que DYRK1A es un nuevo driver tumoral.

Introduction

1. Dual-specificity tyrosine-regulated kinases (DYRKs)

1.1. The DYRK subfamily of kinases

Protein kinases represent one of the largest and most widely studied superfamiy of proteins, and comprises over 500 members in humans (Manning et al., 2002) (Figure I.1A). Dual-specificity tyrosine-regulated kinases (DYRKs) belong to the CMGC group of kinases, which also includes Cyclin-dependent kinases (CDKs), Mitogen-activated protein kinases (MAPKs), CDK-like kinases (CDKLs), Serine-arginine-rich protein kinases (SRPKs), Cdc2-like kinases (CLKs) and RCK family (Figure I.1B). In turn, DYRK family is formed by 3 subfamilies: the DYRK subfamily, Homodomain-interacting kinases (HIPKs) and pre-messenger RNA processing protein 4 kinases (PRP4Ks) (Aranda et al., 2011). From now on, DYRK will refer to the DYRK subfamily. In humans, there are 5 DYRK members, divided phylogenetically in two classes: class I DYRKs are DYRK1A and DYRK1B, whereas class II DYRKs include DYRK2, DYRK3 and DYRK4 (Figure I.1B).

Even though all DYRK members share a highly conserved catalytic domain and a DYRK-specific motif, the DYRK homology (DH)-box, class I and class II DYRKs present class-specific domains (Figure I.2). In particular, class II DYRKs are characterized by the N-terminal autophosphorylation accessory region (NAPA), which is essential for catalytic activation (Kinstrie et al., 2010).

1.2. DYRK genes expression

DYRK1A was the first member of the family to be identified, by infering its sequence homology with the *mnb* gene in *D. melanogaster* (Guimera et al., 1996). Mammalian DYRK genes were then identified and characterized by amplifying and cloning DYRK1A-homologous sequences using total cDNA from 3T3-L1 cells (Becker et al., 1998). DYRKs expression is controlled by alternative promoters generating transcripts with distinct 5'-untranslated regions (UTR); moreover, alternative splicing events generate multiple protein isoforms (Aranda, et al., 2011; Guimera et al., 1999; Papadopoulos et al., 2011).

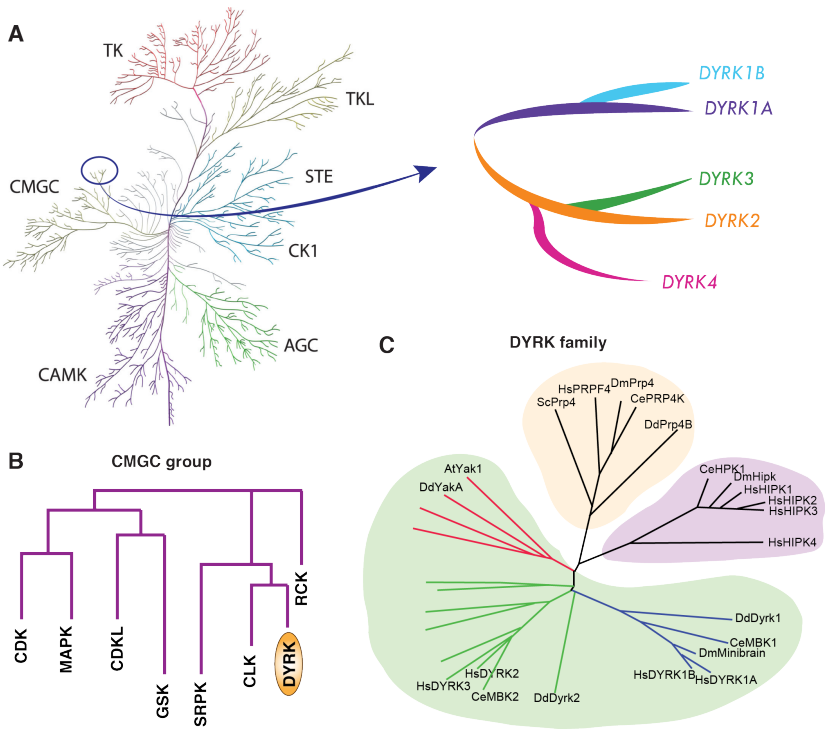

Figure I.1 Phylogenetic organization of the DYRK family of kinases. **A)** The DYRK subfamily of kinases in the human kinome tree. AGC (containing protein kinases A, G and C); CAMK (calcium/calmodulin-dependent protein kinase); CK1 (casein kinase 1); CMGC (containing cyclin-dependent kinase, MAPK, glycogen synthase kinase 3 and CDC2-like); STE (homologues of yeast sterile 7, sterile 11 and sterile 20); TK (tyrosine kinase); TKL (tyrosine kinase-like). Adapted from (Manning et al., 2002). **B)** Evolutionary relationship among the different subfamilies of the CMGC group of protein kinases (see text for the complete name of the subfamilies). **C)** Evolutionary tree of DYRK family of kinases: PRP4K (in orange), HIPK (in violet) and DYRK (in green). At: *Arabidopsis thaliana*; Ce: *Caenorhabditis elegans*; Dd: *Dictyostelium discoideum*; Dm: *Drosophila melanogaster*; Hs: *Homo sapiens*; Sc: *Saccharomyces cerevisiae*; Sp: *Schizosaccharomyces pombe*. Adapted from (Aranda et al., 2011).

Among the DYRK family members, class I *DYRKs* appear to be ubiquitously expressed in all human tissues, with *DYRK1A* levels homogeneously represented and *DYRK1B* most highly expressed in testis and skeletal muscle (Leder et al., 1999)(Figure I.3), whereas the expression of class II members follows a tissue-restricted profile (Becker, et al., 1998)(Figure I.3). *DYRK2* expression is low in most human tissues, except for the intestinal tract (Figure I.3). Murine *Dyrk3* was initially found expressed in testis and in the erythroid lineage

(Zhang et al., 2005), whereas in humans, expression appears restricted almost exclusively to the testis (Figure I.3). Finally, DYRK4 was also found highly expressed in testis in mouse (Sacher et al., 2007) (Figure I.3), with differentially regulated splicing variants (Papadopoulos, et al., 2011).

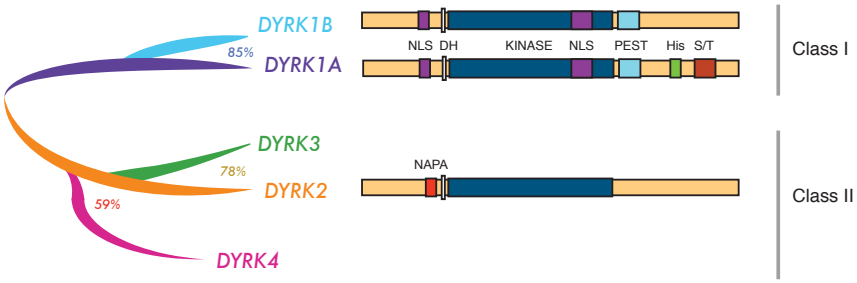

Figure I.2 Classification and protein structure of human DYRK subfamily members. Schematic representation of mammalian DYRK family of kinases indicating phylogeny, grade of homology and protein domains. Shared domains among all members are the catalytic domain (KINASE) domain and the DYRK-homology box (DH). Class I DYRKs present two nuclear localization signals (NLS1 and NLS2) and a PEST motif. DYRK1A includes also a tract of 13 consecutive histidine residues (His) and a region enriched in serine/threonine residues at the C-terminus. Class II DYRKs show a common structure with the characteristic NAPA domain at the N-terminus.

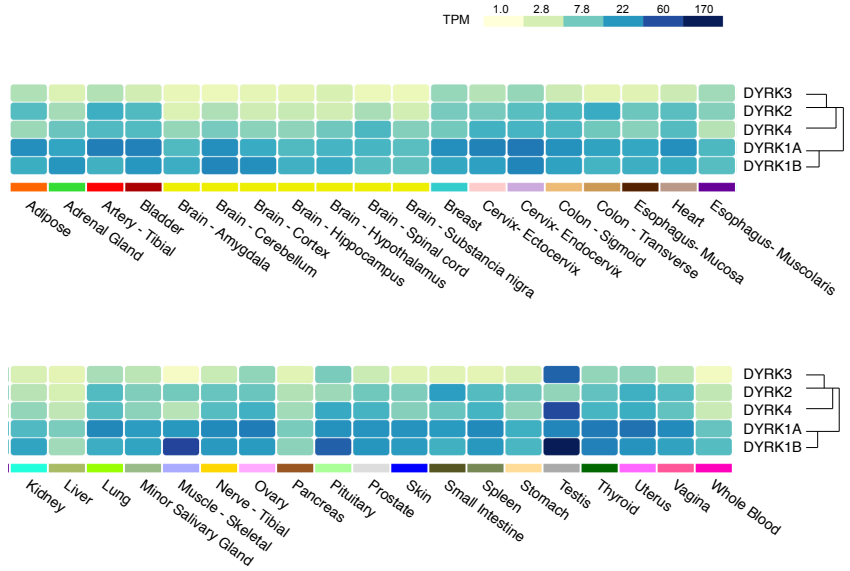

Figure I.3 DYRKs gene expression. Heatmap showing RNA expression levels in TPM (transcript per million) of DYRK family genes across human tissues. Data obtained and figure adapted from the Genotype-tissue expression (GTEx) portal.

1.3. The protein kinase DYRK1A

Human *DYRK1A* gene is located in the chromosome 21 (HSA21), mapping in the Down syndrome (DS) critical region (DSCR), and certainly represents the most extensively studied member of the family. The particular interest on this kinase is mainly due to its importance in tissue development and in DS etiology (Arbones et al., 2019). For the purpose of this thesis work, which considers the whole family of DYRK kinases but focuses especially on the member DYRK1A, a more detailed description of what is currently known about this kinase, including activation, mechanisms of regulation and its implication in human disease, is provided in this section.

1.3.1. Mechanism of activation

The definition “dual-specificity” is due to the ability of DYRK kinases to phosphorylate both tyrosine (Y) and serine/threonine (S/T) residues, even though Y-phosphorylation is restricted to the autophosphorylation activity. As most of protein kinases, full activation of DYRK kinases depends on the phosphorylation of a Y-residue within the activation loop, which leads to a crucial conformational switch from an inactive to an active state (Himpel et al., 2001; Kentrup et al., 1996; Nolen et al., 2004). For DYRK kinases, this key event results from an autocatalytic reaction, which occurs during protein synthesis (in the case of DYRK1A in Y321), generating a constitutively active kinase (Lochhead et al., 2005). In addition, Lochhead and colleagues provided experimental evidence that DYRK1A nascent kinase forms a folding intermediate, which has Y-specificity and is able to catalyze autophosphorylation during protein maturation. Thus, once mature, the Y321-phosphorylated kinase is folded, and its residue-specificity shifts to S/T (Lochhead, et al., 2005). Nevertheless, this model has been questioned by other studies. In particular, it has been shown that Y321 dephosphorylation does not trigger a complete loss of activity *in vitro* (Adayev et al., 2007; Becker and Sippl, 2011), and other investigators even claimed that mature DYRK1A retains Y-phosphorylation activity (Walte et al., 2013).

DYRK1A has been proposed to be a proline-directed kinase, with a RPX(S/T)P consensus sequence (Himpel et al., 2000); however, this specificity does not seem to be so stringent, with other residues (S, A and V) allowed in the P+1 position (Soundararajan et al., 2013).

The regulation of protein kinases is crucial for the normal cell function. As the other members of the family, DYRK1A is constitutively active, thus requiring other mechanisms for regulation; these may include modulation of DYRK1A enzymatic activity by allosteric mechanisms and interaction with regulatory proteins and intracellular protein levels. In turn, the protein accumulation levels depend on the interplay between different molecular mechanisms, which concurrently participate to rule protein turnover. Finally, a third layer of regulation is defined by the distribution of the kinase in distinct cellular compartments, which determines differential substrate accessibility. All these aspects are discussed in the next sections.

1.3.2. Protein expression

Protein amounts directly depend on gene expression levels and post-transcriptional regulatory events. As previously mentioned, *DYRK1A* is expressed through distinct transcripts, due to alternative promoters (Figure I.4A), with different activity and regulation (Maenz et al., 2008). Alternative splicing events give rise to two distinct protein isoforms, different in 9 aa at the non-catalytic N-terminus (Guimera, et al., 1999), and with no reported differences in terms of expression levels and function (Figure I.4B). A 29 aa-shorter isoform might be produced as a result of pB promoter usage and exon 2 skipping (Figure I.4A) (Maenz, et al., 2008). Several transcription factors have been shown to modulate *DYRK1A* expression, including E2F1 (Maenz, et al., 2008), RE1 silencing transcription factor (REST) (Lu et al., 2011), Nuclear factor of activated T-cells (NFAT) (Lee et al., 2009), and T-box transcription factor 5 (TBX5), the latter during miR-10b-induced, invasive breast tumorigenesis (Kim et al., 2016). Post-transcriptional regulation is mediated by specific microRNAs (miRNAs): miR-199b and

miR-1246 (da Costa Martins et al., 2010; Zhang et al., 2011). Finally, results from our group demonstrated that DYRK1A transcript and protein levels seem to be cell cycle-dependent, increasing during cell cycle progression and reaching the maximum during the G2/M phase (Di Vona and de la Luna, unpublished results).

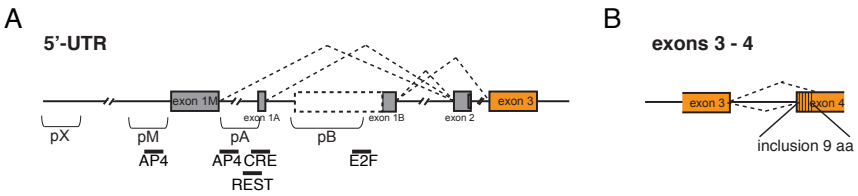

Figure I.4 Promoter usage and alternative splicing events in DYRK1A. A) Distinct promoters control *DYRK1A* expression (see text for more information on promoters pA, pB and pM). The existence of an upstream promoter (pX) is inferred from the presence of active-transcription-chromatin marks based on ENCODE data. **B**) The use of an alternative splicing acceptor site in exon 4 regulates the inclusion/exclusion of a segment of 27 nucleotides, and thereby of a 9 amino acid region. Adapted from (Aranda et al., 2011).

1.3.3. Protein stability

DYRK1A is targeted to proteasome degradation, as it has been proven to be sensitive to proteasome inhibitors (Alvarez, 2004). However, a clear regulatory mechanism for DYRK1A degradation has not been elucidated yet. By looking at the protein domains, the presence of a PEST motif suggests that DYRK1A protein may have a short half-life, since this type of sequence has been generally associated to fast degradation (Rogers et al., 1986). Few cellular factors have been shown to be regulators of DYRK1A turnover; among these, the chaperone Heat shock protein 90 (HSP90) and the co-chaperone Cell division cycle 37 (CDC37) interact with DYRK1A during its maturation process (Sonamoto et al., 2015). The scaffold protein DDB1 and CUL4 associated factor 7 (DCAF7; also named WDR68 or HAN11) forms a complex with DYRK1A (Glenewinkel et al., 2016; Skurat and Dietrich, 2004). This interaction is also conserved in evolution and it has been confirmed in zebrafish and in *D. melanogaster* (Nissen et al., 2006; Yang et al., 2016), suggesting a role for this complex to modulate

DYRK1A activity during development and cell differentiation. Recently, Yousefelahiyeh and colleagues showed that DYRK1A protein levels are reduced in DCAF7-knock-out cells and that such decrease does not depend on proteasome activity (Yousefelahiyeh et al., 2018).

Interestingly, DYRK1A stability and catalytic activity could be functionally linked, since an inactive form by mutation in the ATP binding site, K188R, has a shorter half-life compared with the WT protein (Alvarez, 2004). This could represent a cellular mechanism to promote degradation of non-functional kinases. Supporting this model, intramolecular autophosphorylation on S97 by a folding intermediate seems to play a central role in preventing protein degradation (Kii et al., 2016). In this context, results from our lab also demonstrated that Nemo-like kinase phosphorylates DYRK1A in several residues and proposed that these events mediate its degradation via proteasome, suggesting that other kinases could be involved in the regulation of DYRK1A stability (Arató, 2010).

1.3.4. Subcellular localization

DYRK1A localizes in different cellular compartments, depending on the cell type, adding another layer of complexity in DYRK1A regulation. Despite of a prevalent cytosolic enrichment observed in different cell lines (Di Vona et al., 2015) (and unpublished results from our group), and in central nervous system (CNS) tissues (Hammerle et al., 2003; Wegiel et al., 2004), endogenous DYRK1A localization in cell nuclei of primary cerebellar cells and C2C12 myoblasts has been shown (Fernandez-Martinez et al., 2009; Marti et al., 2003). Moreover, DYRK1A accumulation in cell nuclei following ectopic expression has been observed in other cell types of the CNS (Sitz et al., 2004; Yabut et al., 2010), and in several human cell lines (Alvarez et al., 2003; Rozen et al., 2018). Besides, DYRK1A associates to specific cellular structures, both in the cytoplasm and in the nucleus, including synaptic membranes, vesicles and cytoskeletal fractions (Aranda et al., 2008; Kaczmarski et al., 2014; Murakami et al., 2009; Wegiel, et al., 2004). In

the nucleus, DYRK1A is found in high molecular weight complexes and it is recruited to chromatin at proximal promoters where it regulates gene expression (Di Vona, et al., 2015). In addition, different DYRK1A phosphorylated forms show distinct cellular distribution (Kaczmarski, et al., 2014; Kida et al., 2011), indicating that DYRK1A post-translational modifications are also implicated in this type of regulation.

When ectopically expressed, DYRK1A mostly accumulates in the nucleus thanks to two nuclear localization signals (NLS) (Figure I.2), both necessary for full DYRK1A nuclear translocation (Alvarez et al., 2007). The kinase shuttles between the nucleus and the cytosol through a dedicated nuclear export signal (de la Luna's lab, unpublished results). It is therefore possible that the different subcellular localization between the endogenous DYRK1A and the overexpressed one could be due to alterations in the equilibrium between the export and import mechanisms. Within the nucleus, DYRK1A is found concentrated to nuclear speckles (Alvarez, et al., 2007). The His-repeat at the non-catalytic C-terminus (Figure I.2) has been proved to be responsible for the accumulation in nuclear speckles, suggesting possible interactions with other factors involved in RNA metabolism, gene expression and splicing regulation (Galganski et al., 2017; Salichs et al., 2009).

1.3.5. Modulation of kinase activity

As for other CMGC group kinases, dephosphorylation of the activation loop-tyrosine might represent a mechanism for DYRK1A inactivation in cells. Nevertheless, no phosphatases targeting DYRK1A have been identified so far.

DYRK1A-interacting proteins have been shown to modulate DYRK1A activity. Results from our group indicate that binding of the regulatory factor 14-3-3β, which is mediated by an autophosphorylation event on the S520 residue (S529 in the longest isoform) enhances DYRK1A enzymatic activity (Alvarez, et al., 2007). DYRK1A interacts with

another member of the same family of proteins, 14-3-3ε, which also resulted in increased DYRK1A activity (Kim et al., 2004). The scaffold protein DCAF7 has been also shown to modulate DYRK1A activity, by helping in substrate recruitment (Glenewinkel, et al., 2016). Other DYRK1A activity-modulating factors are Sprouty-related protein with an EVH1 domain 1/2 (SPRED1/2) proteins, which have been found to compete for substrate binding, thereby inhibiting its kinase activity (Li et al., 2010). Finally, the Large tumor suppressor kinase 2 (LATS2) was found to phosphorylate DYRK1A and increase its ability to phosphorylate Lin52, a member of the DREAM (dimerization partner/DP retinoblastoma-like, E2F and MuvB) complex (Tschop et al., 2011).

1.3.6. DYRK1A in disease

DYRK1A is a dosage sensitive gene, meaning that little variations in protein amounts give rise to severe phenotypes; both germline gene extra-dosage as well as haploinsufficiency are associated to developmental defects and human pathologies (Arbones, et al., 2019). As mentioned in previous sections, DYRK1A is located in the DSCR and it is found 1.5-fold overexpressed in DS individuals (Dowjat et al., 2007; Guimera, et al., 1996). Several DYRK1A-overexpressing mouse models have been shown to reproduce morphological and cognitive defects associated to DS: altered special learning, impaired motor abilities (Altafaj et al., 2001), memory defects (Ahn et al., 2006), abnormal retinal size and function (Laguna et al., 2008), skeletal alterations (Blazek et al., 2015), and higher risk to develop childhood leukemia (Malinge et al., 2012). Interestingly, several works have shown that genetic or pharmacological normalization of DYRK1A levels in mice models with partial trisomy rescued some of the abnormal traits associated with DS, including impaired learning skills, cognitive deficits, hippocampal development-associated memory defects, abnormal skeletal and retina phenotypes (Blazek, et al., 2015; De la Torre et al., 2014; Garcia-Cerro et al., 2014; Laguna et al., 2013).

Human population genomic studies include *DYRK1A* among the intolerant to loss-of-function (LoF) genes, highlighting *DYRK1A* as a highly essential gene (Lek et al., 2016). It is not surprising then, that *Dyrk1a*$^{-/-}$ mice are embryonic lethal (death at E10.5-E13.5) (Fotaki et al., 2002) and that *DYRK1A* haploinsufficiency is associated to a specific human disease. In diploid organisms, functional loss of one allele can cause haploinsufficiency when the reduced amount of the gene product is not able to preserve normal function, therefore giving rise to specific phenotypes. The first indications that loss of one copy of *DYRK1A* caused developmental defects and could be linked to pathological traits came from studies on *mnb* haploinsufficient flies (Tejedor et al., 1995) and *Dyrk1a*$^{+/-}$ mice (Fotaki, et al., 2002). In addition to a smaller brain and body size, *Dyrk1a* heterozygous mice showed seizures, cognitive deficits, autistic-like behaviors (Arranz et al., 2019; Raveau et al., 2018), which are common to those showed by individuals with *DYRK1A* haploinsufficiency. After the identification of *DYRK1A* truncations and *de novo* missense mutations in clinical cases of intellectual disability (ID) and autism spectrum disorder (ASD) patients with specific pathological traits (Courcet et al., 2012; Moller et al., 2008; van Bon et al., 2011), in 2016 *van Bon et al*. stated that DYRK1A haploinsufficiency was, in fact, a novel syndrome (DHS) causing a specific clinical phenotype, characterized by ID, ASD, microcephaly, intrauterine growth retardation, seizures and a specific facial gestalt (van Bon et al., 2016). During the last years many more cases of *DYRK1A de novo* disrupting mutations have been identified and DHS is currently considered a rare developmental syndrome within ASD, included in the Online Mendelian Inheritance in Man database as mental retardation autosomal dominant 7 (MRD7; OMIM:614104), and in the Orphanet (ORPHA:464306)(Bronicki et al., 2015; Earl et al., 2017; Ji et al., 2015; Luco et al., 2016). Moreover, our group recently published an extensive biochemical characterization of all *DYRK1A* missense mutations reported so far, which shows that most of these

variants cause total impairment of DYRK1A kinase activity (Arranz, et al., 2019).

One of the most frequently studied DYRK1A substrates is *Tau* (Woods et al., 2001), an important microtubule associated protein (MAP) in neurons. Hyperphosphorylated forms of Tau have been extensively associated to Alzheimer's disease (AD) onset (Harrison and Owen, 2016). Moreover, DYRK1A also phosphorylates Amyloid precursor protein (Ryoo et al., 2008), suggesting that DYRK1A might influence the formation of Aβ peptides. High mRNA levels of DYRK1A were found in the hippocampus of AD patients (Kimura et al., 2007) and DYRK1A inhibition improved pathological phenotypes in mice models of AD (Branca et al., 2017), providing additional evidence for a possible role of DYRK1A dysregulation in AD. Furthermore, alterations in DYRK1A expression levels have been also associated to Parkinson's disease (Barallobre et al., 2014; Cen et al., 2016).

Altered DYRK1A levels have been also linked to heart defects (Hille et al., 2016; Kuhn et al., 2009; Raaf et al., 2010) and bone homeostasis (Lee, et al., 2009). Finally, several reports suggest that targeting DYRK1A leads to an increase in pancreatic β-cells proliferation, thus making DYRK1A inhibition through chemical compounds a potential therapeutic solution for treating diabetes (Belgardt and Lammert, 2016; Kumar et al., 2018; Wang et al., 2019).

Experimental evidence achieved during last years also suggest that DYRK1A, as well as others members of the family, might participate in tumor formation and DYRKs' expression levels have been found altered in certain cancer types. These findings will be discussed more exhaustively in the next chapter.

2. DYRK kinases in cancer

2.1. The cancer genomics revolution

Cancer is one of the leading causes of death worldwide. In 2018, 18 million new cases were diagnosed and it is predicted that this number will rise to 24 million new cases in 2040 (International Agency of Research on Cancer, GLOBOCAN 2018) (Ferlay et al., 2019). Cancer encompasses a set of diseases that arise as a consequence of uncontrolled proliferation and spreading of transformed malignant cells. In the late 70s, researchers discovered the first cancer-causing genes, demonstrating what had been speculated for decades: cancer is provoked by alterations of the DNA genomic sequence (Stehelin et al., 1976; Tabin et al., 1982). As a consequence of the new availability of human genetic information, cancer genomics emerged as a new field and involved research efforts to collect sequencing data from cancer samples, aimed to identify recurrent genomic alterations in cancer cells. The first on-line Catalogue of Somatic Mutations in Cancer (COSMIC), a curated collection of mutations in cancer samples available for research community, was created in 2004 (Bamford et al., 2004). In this line, in 2006 National Center Institute (NCI) launched a pilot project named The Cancer Genome Atlas (TCGA), and a full project in 2009; in parallel, an international research unit launched the International Cancer Genome Consortium (ICGC) (International Cancer Genome et al., 2010). In an outstanding article published in Nature Reviews in 2009, Michael Stratton, Peter Campbell and Andrew Futreal stated “we look forward to the explosion of information about cancer genomes that is imminent and the insights into the process of oncogenesis that this promises to generate” (Stratton et al., 2009). Indeed, thanks to further advances in sequencing technologies, which have considerably improved their sensitivity and resolution capacity, the field has exploded in the last decade. Many independent large-scale studies aimed to sequence and analyze hundreds to thousands of tumor samples, covering different tumor types, were conceived (Meyerson et al., 2010;

Vogelstein et al., 2013; Zhang et al., 2018). Other platforms of cancer data annotation and visualization, such as cBio Cancer Genomics Portal (cBioPortal) (Cerami et al., 2012) and IntOGen (Gonzalez-Perez et al., 2013) appeared. The last event in this story is the publication of the Pan-Cancer Atlas by the TCGA consortium: an extended comprehensive analysis of more than 11,000 tumor samples spanning 33 tumor types, based on multiple genome-wide platforms (Hoadley et al., 2018).

2.2. Discovery of new cancer driver genes

One of the main goal of cancer genomics is to identify new cancer-related genes and to understand how they participate to tumor initiation and progression. As previously mentioned, cancer is a disease of the genome. Neoplastic transformation of a normal cell into a cancer cell and the following steps of tumor progression are driven by accumulation of genetic alterations that confer selective growth and survival advantages (Figure I.5). These mutations are called “driver” mutations, and they must be distinguished from the vast majority of mutations (“passengers”) present in tumor genomes that do not contribute to the malignant phenotype of the cell. Indeed, driver mutations are estimated to represent only the 1-2.5% of the total number of mutations in cancer samples (Vogelstein, et al., 2013). Such mutations occur in genes responsible for the oncogenic properties of cancer cells, which are therefore defined as *cancer driver genes*.

As suggested by Vogelstein and colleagues, it is likely that all major cancer driver genes, the ones that are recurrently found mutated in tumor cells, have already been identified (Vogelstein, et al., 2013). However, there is a broad land of low frequency-mutated genes that contribute to the oncogenic phenotype, which are harder to identify. These low-penetrance genes, which were defined as the “hills” of the cancer landscape to distinguish them from the high frequency-mutated genes (“mountains”) (Wood et al., 2007), are the ones that determine intratumor and intertumor heterogeneity (Garraway and Lander, 2013).

Driver genes that are mutated less frequently in tumors represent a potential source of tumor-specific targets to be exploited for personalized therapies. Thus, one major challenge of cancer genomic research has been to develop efficient computational tools to analyze cancer mutation patterns that could disclose new driver genes and pathways. Several methods have been described so far (Dimitrakopoulos and Beerenwinkel, 2017; Tokheim et al., 2016), each method considering different parameters to define the likelihood of a gene to be a tumor driver and thus generating lists of potential driver genes. For instance, Tumor Suppressor and Oncogene (TUSON) explorer was developed to predict the potential of a given gene to function as tumor suppressor or oncogene, computing profiles of somatic mutations and copy number alterations (Davoli et al., 2013). Other approaches, such as HotNet2 (Leiserson et al., 2015), consider alterations in whole pathways and gene networks, rather than single-gene lesions. The previously mentioned IntOGen platform includes complementary algorithms to identify driver genes by detecting different types of biases (Gonzalez-Perez, et al., 2013), such as the accumulation of high-impact mutations (OncodriveFM, (Gonzalez-Perez and Lopez-Bigas, 2012)) or the clustering in particular regions of the protein sequence (OncodriveCLUST, (Tamborero et al., 2013)). These last methods are considered in this Thesis work and a more accurate description is found in the Materials and Methods section. Following the release of the Pan-Cancer Atlas, a collaborative effort by several cancer computational groups resulted in the most extensive exploration of cancer data to identify driver genes to date (Bailey et al., 2018). The study was carried out integrating 26 different tools and generated a list of 299 putative driver genes (Bailey, et al., 2018).

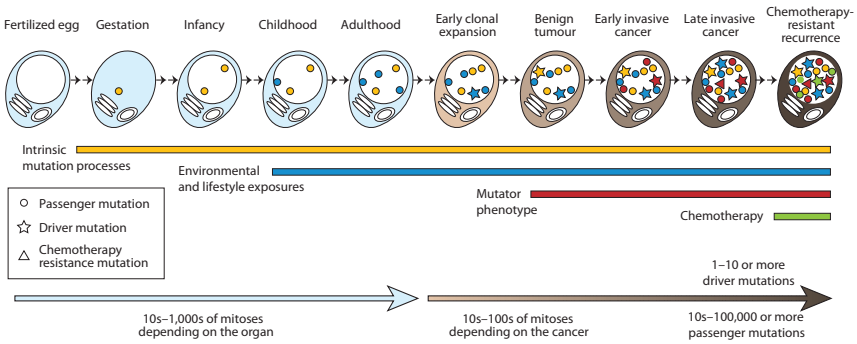

Figure I.5 Accumulation of mutations during development and cancer formation-progression. Representation of passenger and driver mutation events occurring since the very first mitotic cell divisions in embryogenesis until tumor formation and progression in the adult organism, encompassing organism life periods and cancer stages. Intrinsic mutation processes and environmental effects are the leading causes of accumulation of mutations; dysregulation of the DNA damage machinery components can lead to a mutator phenotype characterized by an accelerated mutational process and eventual chemotherapy can also enhance the mutation burden. Adapted from (Stratton, et al., 2009).

2.3. Protein kinases are tumor drivers

Protein kinases catalyze reaction by which the gamma phosphate of an ATP molecule is transferred to the hydroxyl group of a substrate. This simple chemical event represents the most common post-translational modification in living systems and dramatically affects the function of the substrate, thus playing a central role in the modulation of most cellular processes. Notably, mutations in kinase genes are associated to many types of human disorders, including cancer (Lahiry et al., 2010).

The protein product of the first discovered oncogene, the cellular homologous of the *v-Src* gene of the Rous Sarcoma virus, was found to have kinase activity (Collett and Erikson, 1978; Stehelin, et al., 1976). Forty years later, many other oncogenes and tumor suppressor genes are known to encode for protein kinases, and dysregulation of signaling pathways caused by mutated protein kinases is extensively associated to tumor initiation and progression (Fleuren et al., 2016; Gross et al., 2015).

In 2004, the first census of genes mutated and casually implicated in cancer, the Cancer Gene Census, was published (Futreal et al., 2004), and it revealed that the most common domain encoded by cancer genes is the kinase domain (Futreal, et al., 2004). Thus, following cancer genomic studies uncovered driver mutations in larger groups of protein kinases (Greenman et al., 2007; Kan et al., 2010). More recently, lists of cancer driver genes provided by the analysis and interpretation of cancer genomic data generated in large-scale studies confirmed a strong enrichment for protein kinases (Fleuren, et al., 2016) (Figure I.6). Interestingly, DYRK1A appears as a tumor driver kinase in the lists provided by Fleuren and colleagues (Figure I.6), since it was included among the potential tumor drivers from the analysis with the previously mentioned TUSON method (Davoli, et al., 2013).

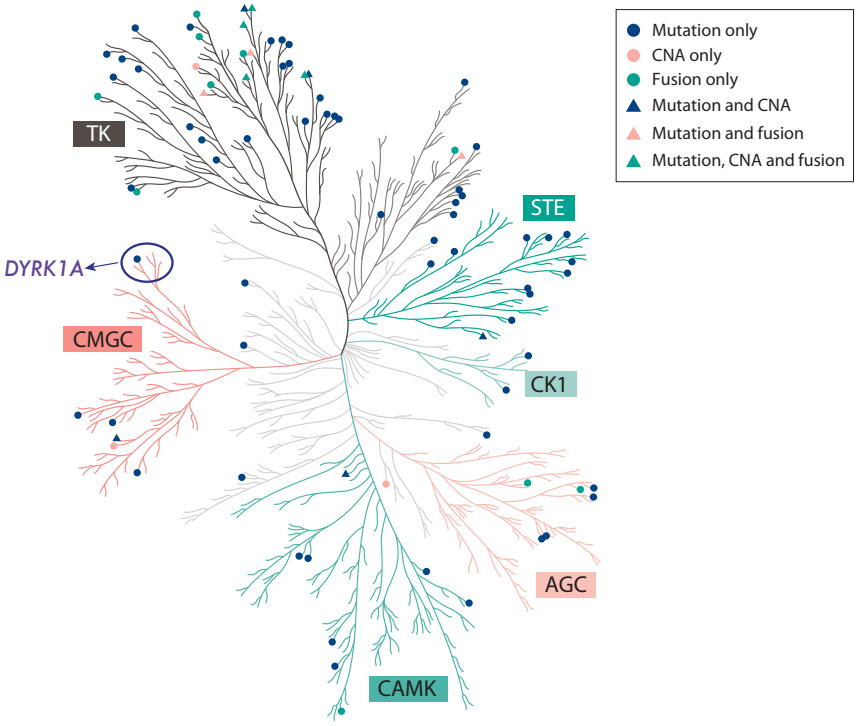

Figure I.6 Driver kinases and their cancer-associated alterations. Human kinome phylogenetic tree showing 89 driver kinases extracted from cancer genomic studies and the type of genetic alterations found in tumor samples. The DYRK family is highlighted with a purple circle. DYRK1A is the only member of the family included in the list and it is marked with a blue point (mutation only). Adapted from (Fleuren et al., 2016).

While cancer genomic studies were collecting new data on cancer somatic mutations occurring on kinase genes, high-throughput RNAi screens started to provide exciting new insight on kinase-dependency by tumor cells (Baldwin et al., 2008; Baldwin et al., 2010; Bommi-Reddy et al., 2008; Grueneberg et al., 2008; Grueneberg et al., 2008). All these pieces of information contributed to identify novel tumor-specific driver kinases that represent potential targets for new therapeutic interventions. Indeed, kinases are easily targeted with small molecules. Considering the link between altered protein kinase activity and onset of human pathologies, it is not surprising that many kinase inhibitors have already been identified and approved for therapies. In 1995, the first kinase inhibitor (Fasudil, targeting ROCK kinase) was approved for treatment of cerebral vasospasm (Shibuya et al., 1992). Studies aimed at targeting the *BCR-ABL* fusion gene, which causes the expression of constitutively active ABL kinase (Koretzky, 2007), led to the discovery of a phenyl-amino-pyrimidine ABL inhibitor later called Imatinib by Novartis (Buchdunger et al., 2001; Druker et al., 1996). Imatinib was approved by the Federal Drug Administration (FDA) for the treatment of chronic myeloid leukemia in 2001 and represents the first kinase inhibitor approved by the FDA for cancer therapy. In the following years, other inhibitors targeting well known cancer kinases like Erlotinib (targeting Epidermal growth factor receptor [EGFR]) and Sofarenib (targeting Raf, Vascular endothelial growth factor receptor [VEGFR] and Platelet-derived growth factor receptor [PDGFR]β) were approved for non-small-cell lung cancer and renal cell carcinoma, respectively (Bonomi, 2003; Escudier et al., 2007). Identification of novel kinases contributing to tumor initiation/progression prompted academic and pharmaceutical researchers to put major efforts in drug discovery. To date, there are 41 kinase inhibitors, targeting single or multiple tumor driver kinases, approved by FDA for cancer treatment, with hundreds of additional compounds currently under clinical trials (Bhullar et al., 2018).

However, specificity of kinase inhibitors is a noteworthy issue. Most of the compounds currently used in research and clinics target the ATP-binding pocket, which is conserved throughout the kinome and thus compromised specificity. Independent studies have examined the specificity of widely used kinase inhibitors demonstrating that most of them have low specificity (Bain et al., 2007; Fabian et al., 2005; Fedorov et al., 2007; Karaman et al., 2008).

Although many novel kinases potentially involved in cancer development have been identified in genomic studies and functional screens, there is a strong need for further cellular and molecular studies to better elucidate how they participate in oncogenic processes. Academic and pharmaceutical research remains largely biased towards kinases that are most extensively described so far (Fedorov et al., 2010), while efforts to understand cellular mechanisms regulated by novel putative driver kinases should be improved.

2.4. DYRK1A in cancer

DYRK1A kinase is a pleiotropic factor that phosphorylates a broad group of substrates involved in many different cellular processes. As remarked by Vogelstein et al., the pathways that are responsible for selective growth advantage in cancer cells are limited and can be organized in three core cellular processes: cell fate, cell survival and genome maintenance (Vogelstein, et al., 2013). Strikingly, DYRK1A phosphorylates and modulates the activity of several cellular factors regulating cellular processes that are included in the three categories (Figure I.7).

In the past decade, a number of research works have ascribed to DYRK1A opposite functions in cancer, drawing a complex scenario. In fact, DYRK1A is suggested to act both as a tumor suppressor and as a tumor promoter, in different biological contexts (Figure I.8). The pieces of research regarding potential functions of DYRK1A in mediating tumor initiation/progression are summarized in the next sections.

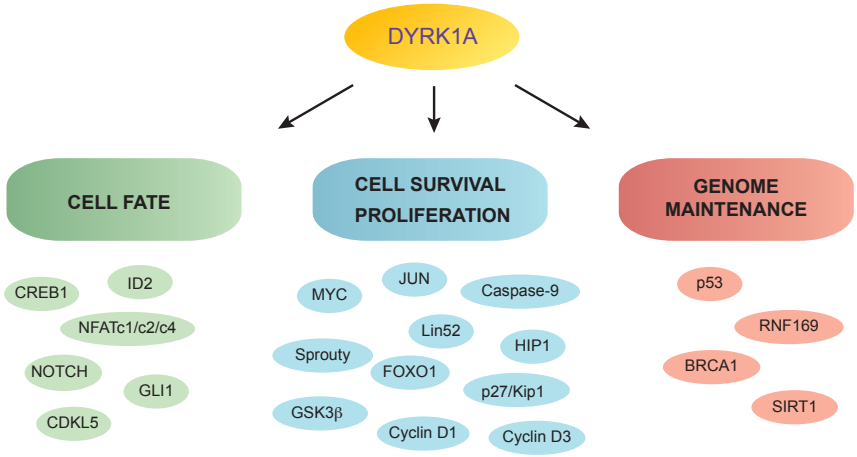

Figure I.7 DYRK1A substrates involved in cancer-related cellular processes. Substrates of DYRK1A that are described to participate in cell fate decisions (green), cell survival regulation and/or proliferation (light blue) or genomic stability maintenance (red) pathways. Many of these proteins are ascribed to more than one cancer-related core process (see the text for more details). BRCA1 (Barba, 2017), Caspase-9 (Laguna, et al., 2008), CDK5L (Oi et al., 2017), CREB1 (Yang et al., 2001), Cyclin D1 (Chen et al., 2013), Cyclin D3 (Thompson et al., 2015), FOXO1 (Woods et al., 2001), GLI1 (Mao et al., 2002), GSK3β (Song et al., 2015), HIP1 (Kang et al., 2005), ID2 (Lee et al., 2016), JUN (Morton et al., 2003), Lin52 (Litovchick et al., 2011), MYC (Liu et al., 2014), NFATc1/c2/c4 (Arron et al., 2006), NOTCH (Fernandez-Martinez, et al., 2009), p27/KIP (Soppa et al., 2014), p53 (Park et al., 2010), RNF169 (Roewenstrunk, 2016), SIRT1 (Guo et al., 2010), Sprouty (Aranda, et al., 2008).

2.4.1. The interaction of DYRK1A with viral oncoproteins

The first evidence of a role of DYRK1A in cell immortalization derives from studies on oncogenic viruses, which suggested a role for DYRK1A in cell transformation in oncovirus-associated cancer models. As the *S. cerevisiae* DYRK Yak1p, both DYRK1A and DYRK1B bind to the adenovirus oncoprotein E1A (Komorek et al., 2010; Zhang et al., 2001) (Figure I.8), which is responsible for adenovirus-induced oncogenic transformation (Frisch and Mymryk, 2002). This interaction is dependent on the scaffold protein DCAF7, which serves as an adaptor for DYRK1A-E1A binding, which in turn might promote the phosphorylation of E1A at S89 (Glenewinkel, et al., 2016). This interaction appears to contribute to the adenovirus ability to regulate the Interferon (IFN) response (Zemke and Berk, 2017). Another important

viral oncoprotein regulated by DYRK1A is the human papilloma virus (HPV) E7 protein (Figure I.8). By using primary mouse keratinocytes, Chang and colleagues showed that *Dyrk1a* mRNA levels were increased when cells were immortalized by infection with the high risk HPV strain 16 (HPV16) and that *Dyrk1a* expression levels correlated with those of the virus regulatory protein E7 (Chang et al., 2007). Analysis of cervical lesions from HPV-derived patient samples showed that DYRK1A protein levels were increased, compared with the respective normal tissue (Chang, et al., 2007). A molecular mechanism by which DYRK1A interacts and phosphorylates the HPV16 E7, thus increasing its stability, has been proposed (Liang et al., 2008).

2.4.2. DYRK1A is engaged in cell cycle regulation

Cell cycle entry/arrest is based on the activation of key regulators in response to external stimuli, which leads to changes in gene expression. Uncontrolled proliferation of cancer cells is often a consequence of disruption of cell cycle checkpoints; indeed, cellular factors involved in the fine-tuned regulation of cell cycle are often found altered in cancer (Kastan and Bartek, 2004). DYRK kinases have been described as cell cycle kinases (Becker, 2012) and DYRK1A phosphorylates key cell cycle modulators like Cyclin D1 and $p27^{Kip1}$, thus promoting cell cycle exit (Chen, et al., 2013; Soppa, et al., 2014) (Figure I.8). Indeed, the activity of DYRK1A on Cyclin D1 and D3 is linked to differentiation decisions in cells from different origin as neurons and lymphocytes (Najas et al., 2015; Thompson, et al., 2015).

Several groups have reported interactomes of DYRK1A based on proteomic approaches. The cell cycle regulators retinoblastoma protein (pRB) or pRB-like proteins-like p107 and p130 are detected as DYRK1A interacting proteins (Varjosalo et al., 2013), although no functional roles for these interactions have been defined.

The dimerization partner (DP), RB-like, E2F and multi-vulval class B (MuvB) complex (DREAM complex) is a highly conserved, master

mediator of cell cycle arrest in G0 (quiescence) and a repressor of cell cycle progression-gene expression (Sadasivam and DeCaprio, 2013). DYRK1A was shown to be a DREAM complex kinase, since it phosphorylates the DREAM key component Lin52. Phosphorylation of Lin52 on S28 promotes DREAM complex assembly and thereby triggers cell cycle exit (Litovchick, et al., 2011) (Figure I.8). Moreover, the DYRK1A/DREAM complex appears to be required for cell entry in oncogene-induced senescence (Litovchick, et al., 2011). The activation of the DREAM complex by DYRK1A was suggested to be the mechanism responsible for ovarian cancer cell dormancy (MacDonald et al., 2017), a particular quiescent state in which ovarian cells form spheroids, escape chemotherapy-induced apoptosis and migrate from the primary tumor site (Shield et al., 2009). Moreover, DYRK1A has been shown to mediate a similar mechanism in gastroinstestinal stromal tumor (GIST) cells quiescence induced by treatment with imatinib (Boichuk et al., 2013).

2.4.3. DYRK1A modulates Receptor tyrosine kinases (RTKs)-dependent signaling

A very important family of kinases involved in cancer-pathways is the receptor tyrosine kinases (RTK) one. By coupling growth factor ligand-binding and signaling cascade activation, RTKs represent key regulators of many cellular processes, such as cell proliferation and survival, which are crucial for development and organogenesis (Lemmon and Schlessinger, 2010); RTKs dysregulation is associated to cancer onset and metastasis (Du and Lovly, 2018). They are found altered at high frequencies in tumors, either by activating mutations or overexpression, which lead to the hyperactivity of the downstream signaling (Du and Lovly, 2018). Strikingly, 28 RTKs out of 58 known ones are found in the list of tumor driver kinases provided by Fleuren and colleagues (Fleuren, et al., 2016). Moreover, most of the kinase inhibitors and monoclonal antibodies approved for cancer therapy target RTK proteins (Bhullar, et al., 2018).

EGFR is one of the most extensively characterized RTKs (Lemmon et al., 2014). *EGFR* amplification and/or gain-of-function mutations are found in many cancer types such as lung cancer (Sharma et al., 2007) and glioblastoma (Eskilsson et al., 2018). Our lab and collaborators showed that DYRK1A prevents EGFR endocytosis-mediated degradation by phosphorylating the RTK-negative regulator Sprouty2 in neural stem cells (Ferron et al., 2010) (Figure I.8). Following this observation, Pozo and colleagues showed that DYRK1A depletion reduced EGFR levels in glioblastoma cell lines and proposed that EGFR degradation was prevented by DYRK1A also in brain tumors. Notably, they also showed that DYRK1A levels are upregulated in glioma patient samples and correlate with EGFR levels (Pozo et al., 2013).

Last year, our group and collaborators published a study in which we proposed a similar correlation between the RTK c-MET, the receptor of hepatocyte growth factor (HGF), and DYRK1A protein expression levels in pancreatic ductal adenocarcinoma (PDAC) tumor samples (Luna et al., 2018) (Figure I.8). *MET* is another well-established oncogene found altered in many types of cancer, and the HGF-MET axis is often associated with activation of migration and invasion pathways in cancer cells (Birchmeier et al., 2003; Spina et al., 2015). Our data shows that DYRK1A promotes tumor progression through the stabilization of c-MET (Luna, et al., 2018). As results included in this article have been part of my research work during this PhD project, it is included as Annex I.

Another RTK regulated by DYRK1A is VEGFR2, which acts as a major regulator of the biogenesis and sprouting of blood vessels (angiogenesis), by inducing proliferation, migration and invasion of endothelial cells (Herbert and Stainier, 2011) (Figure I.8). Results from our group in primary endothelial cells support a pro-angiogenic role for DYRK1A, since DYRK1A depletion caused defects in VEGFR2-dependent signaling and reduction of the angiogenic transcriptional

response. Mechanistically, these effects appear to be the result of reduced VEGFR2 accumulation (Rozen, et al., 2018).

Altogether, these works provide evidence of a general role for DYRK1A in positively regulating the stability of RTK receptors in different physiological contexts.

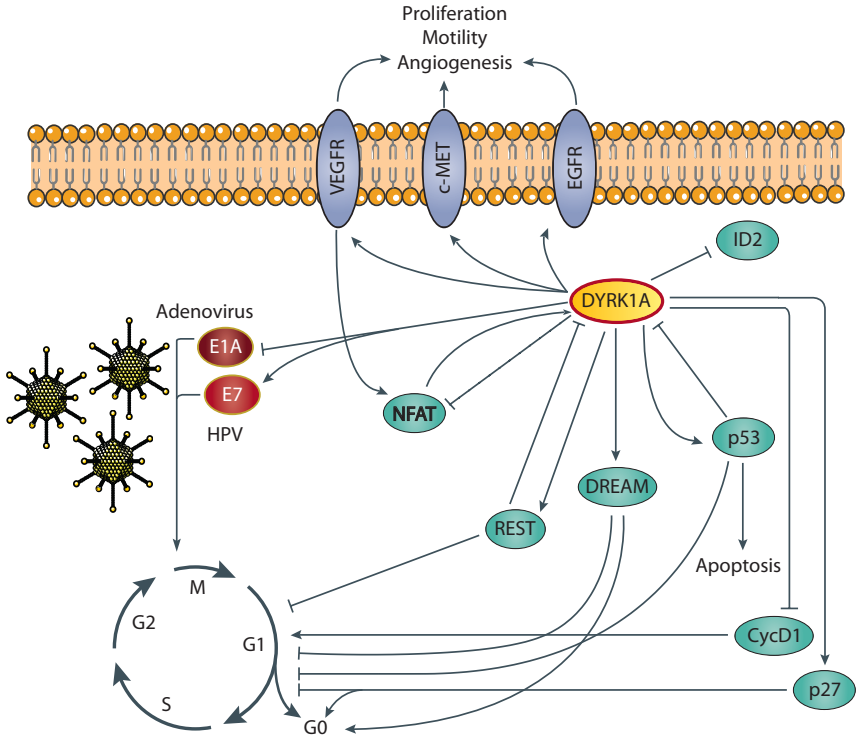

Figure I.8 DYRK1A modulates cellular factors involved in tumorigenesis. Overview of DYRK1A and its interaction with cellular factors involved neoplastic transformation and cancer-related pathways. Pro-tumorigenic and tumor-suppressive functions have been proposed by independent research works and they are summarized in this scheme (see text). Viral oncoproteins are indicated with red ovals, RTK with purple ovals and intracellular factors and complexes with green ovals. Adapted from (Nizetic and Groet, 2012).

2.4.4. Regulation of NFAT proteins by DYRK1A

NFAT proteins represent a conserved family of transcription factors involved in vertebrate development and immune system function, which are activated in response to increased Ca^{++} intracellular levels in response to the activation of many different signaling pathways including RTKs (Macian, 2005). As regulators of cellular processes

including cell growth, survival and angiogenesis, dysregulation of NFAT proteins is linked to tumor progression (Mancini and Toker, 2009). DYRK1A was found to be a regulator of NFAT signaling pathway in a RNAi screen in *Drosophila* (Gwack et al., 2006); since NFAT activation and translocation to the nucleus is prevented by hyperphosphorylation, DYRK1A was proposed to act as a negative regulator of NFAT proteins, and overexpression of DYRK1A in DS models was suggested to impair normal NFAT function (Arron, et al., 2006) (Figure I.8). The effect of DYRK1A overexpression in negatively regulating NFAT activation has been shown in several pathological scenarios such as the promotion of megakaryoblastic leukemia (Malinge, et al., 2012), bone homeostasis (Lee, et al., 2009), or cardiomyocyte hypertrophy (Kuhn, et al., 2009). Nevertheless, our group proposed an opposite role for DYRK1A in regulating NFAT signaling in endothelial cells. Indeed, DYRK1A was shown to promote VEGF-dependent NFAT activation, since loss of DYRK1A activity, either through knockdown or inhibition, had a dramatic negative impact on VEGF/Ca^{++}/NFAT signaling, with severe consequences on physiological angiogenis (Rozen, et al., 2018). Together, these findings indicate that changes in DYRK1A dosage might have different outcomes on NFAT signaling, depending on the cellular context. A potential negative feedback loop regulatory mechanism between NFATc1 and DYRK1A has also been proposed, adding further complexity to this crucial molecular partnership (Lee, et al., 2009) (Figure I.8).

2.4.5. DYRK1A in cancer: some extra clues

Besides the targets described in the previous sections, DYRK1A regulates cellular factors that are extensively described to participate in malignant transformation processes, as it is the case of the tumor suppressor p53. *TP53* represents the most frequently mutated gene in cancer, with variants that promote tumor initiation either by suppressing p53 expression/activity or through gain of function (Martincorena and Campbell, 2015; Sabapathy and Lane, 2018). It encodes for the tumor-

suppressor protein p53, whose function has been extensively studied both in physiological and pathological conditions. Transcriptional regulation, DNA damage repair, induction of apoptosis and cell cycle restrain are among the complex network of p53 cellular functions (Kastenhuber and Lowe, 2017). DYRK1A phosphorylates p53 on S15, enhancing its activity and thus promoting cell cycle arrest in neuronal embryonic cells (Park, et al., 2010) (Figure I.8). Moreover, p53 negatively regulates DYRK1A by inducing the expression of the microRNA miR-1246, which in turns suppresses DYRK1A expression (Zhang, et al., 2011), suggesting a negative feedback regulatory mechanism (Figure I.8).

Inhibitor of DNA binding 2 (ID2) is a transcriptional inhibitor, which has been found to enhance cancer cells stemness and invasive capacity (Lasorella et al., 2014). Despite the tumor-promoting role supported in glioblastoma (Pozo, et al., 2013), both class I kinases DYRK1A and DYRK1B phosphorylate ID2 on T27, preventing its binding to von-Hippel Lindau and thus hampering its oncogenic function in glioblastoma models (Lee, et al., 2016) (Figure I.8). Moreover, low levels of DYRK1A/DYRK1B were associated to poor clinical outcome in glioma patients.

Dosage imbalance of DYRK1A was found to alter the cellular levels of REST transcription factor (Canzonetta et al., 2008; Lepagnol-Bestel et al., 2009), a key regulator of neuronal development, which has been found to exert a potent tumor suppressive role and prevent epithelial cell transformation (Westbrook et al., 2005). As well as for p53, a negative feedback loop governing the DYRK1A-REST interplay has been suggested (Lu, et al., 2011) (Figure I.8).

Additional critical pathways modulated by DYRK1A are the Hedgehog (HH) and Notch signaling pathways. They play major roles in vertebrate development and dysregulation of these pathways promote tumor formation and progression (Aster et al., 2017; Gupta et al., 2010).

DYRK1A interacts and phosphorylates the intracellular domain of Notch and thus weakens its function in neural cells both in cell culture and *in vivo* (Fernandez-Martinez, et al., 2009). On the other hand, DYRK1A phosphorylates and thus promotes nuclear translocation and transcriptional activity of Glioma-associated oncogene homologous 1 (GLI1), a major downstream effector of HH signaling (Ehe et al., 2017; Mao, et al., 2002; Schneider et al., 2015).

Finally, a direct role for DYRK1A in promoting tumor progression has been suggested by additional research efforts. Increased DYRK1A protein levels were observed in tissue microarrys of head and neck squamous cell carcinoma (HNSCC) samples, and DYRK1A knockdown or chemical inactivation in HNSCC cell lines led to impaired proliferation and invasion (Radhakrishnan et al., 2016). By analyzing RNA-seq TCGA data, Kim and colleagues found *DYRK1A* downregulation in breast cancer samples; DYRK1A was proposed to act as a tumor suppressor in mice models of breast carcinoma and that its expression was dependent on the transcription factor TBX5, which is in turn suppressed by the oncogenic microRNA miR-10b (Kim, et al., 2016).

2.4.6. Down syndrome and cancer

Thanks to the increase of life expectancy of DS individuals in the last decades (Zhu et al., 2013), epidemiologic studies aimed at defining the incidence of common human pathologies and comparing with normal population have become more and more accurate. These studies have demonstrated that people with DS have a marked lower incidence of most solid tumors (Boker et al., 2001; Hasle et al., 2000; Hasle, 2001; Patja et al., 2006) and reduced cancer-associated mortality (Hill et al., 2003; Yang et al., 2002), compared with age-adjusted non-DS population. The only exceptions are germ cell tumors, in particular testicular germ cell tumors (Hasle, 2001; Hill, et al., 2003), and childhood leukemia (Lee et al., 2016). Indeed, DS children have 10 to 50-fold increased risk of developing acute lymphoblastic leukemia and acute myeloid leukemia (AML) (Hasle, 2001). Moreover, acute

megakaryoblastic leukemia (AMKL), which is preceded by transient myeloproliferative disorder, a particular malignancy characterized by megakaryoblast clonal expansion, has a 500-fold increased incidence in DS children (Al-Kasim et al., 2002). Overexpression of RUNX1, a tumor suppressor gene located in HSA21, was proposed as the main factor responsible for the perturbation of early hematopoietic differentiation (De Vita et al., 2010), while mutations in *GATA1* are detected in nearly all AMKL affected DS infants (Wechsler et al., 2002). Additionally, Malinge and colleagues suggested DYRK1A as a potent, megakaryoblastic oncogene (Malinge, et al., 2012); their model relies on the negative regulation of NFAT proteins by DYRK1A, as NFAT factors were previously indicated as regulators of myeloid differentiation (Kiani et al., 2007). In line with this model, both Regulator of calcineurin 1 (RCAN1/DSCR1) and DYRK1A-dependent negative regulation of NFAT proteins was proposed as potential cause of the lower solid tumors incidence in DS (Baek et al., 2009).

However, and in conflict with this model, DYRK1A expression levels were found reduced in AML patient samples and moreover, overexpression of DYRK1A led to impaired AML cell proliferation by inducing cell cycle arrest (Liu, et al., 2014). Much more research would be required to better delineate the role of the overexpression of DYRK1A in protecting trisomic tissues from cancer appearance and progression.

2.4.7. DYRK1A inhibitors and their impact in cancer

Given the functional impact of DYRK1A overexpression in DS, intense efforts have been dedicated to identify specific inhibitors with potential use as therapeutic tools (Jarhad et al., 2018). However, as many kinase inhibitors, none of the DYRK1A inhibitors described to date are strictly specific for DYRK1A, which limits data interpretation and highlights the need of novel, highly-specific inhibitors for research and clinical trials. A small summary on those most widely used follows.

The natural ATP-competitor that has been most largely used as DYRK1A inhibitor is the β–carboline alkaloid harmine (Bain, et al., 2007; Gockler et al., 2009). Given the good results in attenuating DYRK1A overexpression effects in mouse models (Laguna, et al., 2008), harmine was suggested as a promising compound for clinical trials of DS therapy or other DYRK1A-associated pathologies (Wang et al., 2015): however, its capability to inhibit also monoamine oxidase enzymes (Kim et al., 1997) complicates its application in clinics. Notably, harmine has cytotoxic effects in different cancer cell lines (Cao et al., 2011; Ishida et al., 1999; Luna, et al., 2018; Pozo, et al., 2013; Radhakrishnan, et al., 2016; Uhl et al., 2018; Zhang et al., 2016) and synergistic effects with anti-tumor drugs (Atteya et al., 2017; Boichuk, et al., 2013; MacDonald, et al., 2017); moreover, harmine treatment in glioma and pancreatic ductal carcinoma xenografts inhibits tumor growth (Luna, et al., 2018; Pozo, et al., 2013).

Another natural compound that has DYRK1A inhibitory capacity and rescues DYRK1A overexpression-associated phenotypes is the polyphenol derivative of the green tea leaves epigallocatechin gallate (EGCG) (De la Torre, et al., 2014; Guedj et al., 2009; McElyea et al., 2016). EGCG is currently under clinical trial for treatment of DS individuals (de la Torre et al., 2016). The anti-cancer properties of green tea and its derivatives, including EGCG, have been proved in many studies with animal models thanks to their potential targeting of many different intracellular pathways (Yang et al., 2009).

Other DYRK1A inhibitors with reported anti-tumor effects are roscovitine and its derivatives, which are currently in clinical trials (Demange et al., 2013). However, these compounds show higher specificity for members of the CDK family, which might explain their anti-proliferative properties. A Casein kinase 2 inhibitor, CX-4945 (Silmitasertib), with pro-apoptotic and anti-angiogenic effects (Siddiqui-Jain et al., 2010) and currently tested in clinical trials for multiple myeloma and cholangiocarcinoma, has been recently reported to act as

a potent inhibitor of DYRK1A and to restore neurological defects in *minibrain*-overexpressing *Drosophila* models (Kim et al., 2016).

Lately, promising results have been achieved with two derivatives of benzothiazole, called INDY and FINDY, which attenuate malformations caused by DYRK1A high dosage *in Xenopus laevis* (Kii, et al., 2016; Ogawa et al., 2010). Of note, INDY shows similar properties as harmine in compromising ovarian cancer spheroids viability (MacDonald, et al., 2017).

2.5. Other DYRKs in cancer

Other members of the DYRK family of kinases have been associated to cancer-related cellular processes and found altered in tumors. In particular, many indications of this link have been collected for human class I DYRK1B and class II DYRK2, which are described in the next sections.

2.5.1. DYRK1B in cancer

Evidence that the DYRK1A closest paralogue, DYRK1B - also named *minibrain*-related kinase (Mirk) - plays a role in promoting tumor progression in specific biological contexts has been provided during the last years. A string of research contributions proposed a pro-tumorigenic role for DYRK1B in different tumor types, supported by increased DYRK1B protein levels in tumor samples, which include liposarcoma (Chen et al., 2018), rhabdomyosarcoma (Mercer et al., 2006), osteosarcoma (Yang et al., 2010), lung (Gao et al., 2009), breast (Chen et al., 2017), ovarian (Friedman, 2013; Gao et al., 2012) and pancreatic cancer (Deng et al., 2006; Deng and Friedman, 2014). The chromosomal region containing *DYRK1B* (19q13.2) has been found amplified in ovarian cancer samples and cell lines (Hu et al., 2011; Thompson et al., 1996), as well as in PDAC samples (Kuuselo et al., 2007; Luna, et al., 2018). Supporting a functional role for DYRK1B amplification and overexpression PDAC, treatment of PANC1-derived xenografts with a DYRK1B inhibitor reduced tumor growth (Deng and

Friedman, 2014). In agreement with these findings, we showed that DYRK1B knockdown impaired PANC-1 cells proliferation, migration and invasion (Luna, et al., 2018)(Annex I).

DYRK1B phosphorylates many DYRK1A substrates, including cell cycle regulators such as Cyclin D1, $p27^{Kip1}$ and Lin52 (Deng et al., 2004; Litovchick, et al., 2011; Zou et al., 2004). Therefore, DYRK1B overexpression has been suggested to promote the maintenance of a reversible quiescent state in cancer cells, while DYRK1B knockdown has been linked to cell cycle entry, increased DNA damage, enhanced apoptosis and increased sensitivity to reactive oxygen species and chemotherapeutic drugs (Deng et al., 2009; Ewton et al., 2011; Hu and Friedman, 2010; Hu, et al., 2011; Hu et al., 2013; Jin et al., 2009).

2.5.2. DYRK2 in cancer

DYRK2 represents the class II DYRK member with more research contributions, mostly related to its ability to modulate tumor progression. The first evidence derives from genomic analysis and differential gene expression studies, which underscored DYRK2 overexpresssion as associated to its genomic locus amplification in esophageal and lung adenocarcinomas (Miller et al., 2003), GIST tumors (Koon et al., 2004), gastric adenocarcinoma (Gorringe et al., 2005), liposarcomas (Italiano et al., 2008) and gliomas (Maher et al., 2006; Shen et al., 2017).

DYRK2 phosphorylates and modulates key factors involved in cell cycle arrest/progression (Becker, 2012; Nihira and Yoshida, 2015). Thus, DYRK2 phosphorylates and, thereby enhances, the degradation rate of the pro-proliferative transcription factors c-Jun and c-Myc (Taira et al., 2012). Moreover, DYRK2 was found downregulated in different tumor types and its expression inversely correlated with c-Jun/c-Myc expression and with aggressiveness of breast tumors (Taira, et al., 2012).

Epithelial-to-mesenchymal transition (EMT) is a cellular transformation process that plays a role in embryonic development and is implicated in

cancer progression to invasive stages (Brabletz et al., 2018). DYRK2 phosphorylates and primes for ubiquitination-mediated degradation Snail (Mimoto et al., 2013), a transcriptional repressor that promotes EMT (de Herreros et al., 2010), providing additional evidence that DYRK2 prevents the activation of aggressive phenotypes in breast cancer cells. In clear contrast with this model, Guo and colleagues proposed a pro-oncogenic function for DYRK2 in breast cancer, as it was shown to promote breast cancer cell proliferation and tumor growth in xenograft models through direct phosphorylation of the 26S proteasome (Guo et al., 2016); in addition, high levels of DYRK2 correlated with poor prognosis in breast cancer patients (Guo, et al., 2016). The publication did not discussed any on the conflicting results with previous reports. Recently, the natural drug curcumin was found to act as a potent inhibitor of DYRK2, to impair cell proliferation and invasion and to induce apoptosis in myeloma and breast cancer cell lines (Banerjee et al., 2018).

DYRK2 has been also described as a regulator of other cancer-related processes, such as DNA-damage response and apoptosis. In particular, DYRK2 phosphorylates p53 and positively regulate p53-mediated apoptosis in response to DNA damage (Taira et al., 2007). This mechanism is dependent on the kinase ATM, which phosphorylates DYRK2, allowing DYRK2 escaping from MDM2-mediated degradation in the cell nuclei (Taira et al., 2010). Whether this process has an impact on the role of DYRK2 on cancer progression was not further explored.

Objectives

Although substantial improvements have been achieved in research and clinical practice, cancer still represents a severe threat to human health. Thanks to recent advances in sequencing technologies and computational tools, many new tumor driver genes have been identified. Protein kinases, which orchestrate a complex network of signaling pathways and thus regulate cellular processes responsible for the maintenance of tissue homeostasis, are found dysregulated at high frequencies in cancer cells. Indeed, the kinase domain represents the most frequently mutated domain in cancer. DYRK protein kinases participate in the regulation of cell fate and cell survival and have been found altered in tumor samples, but little is known about their role in cancer. Thus, the aims of this Thesis work are:

i. to interrogate cancer genomics and transcriptomics data to generate a comprehensive description of the profile of alterations of DYRK genes in tumor samples and to determine their potential role as tumor drivers.

Once the member/s of the family that most likely may function as tumor driver/s were identified:

ii. to characterize the impact of cancer-associated mutations on the function of the kinase.
iii. to further investigate how they contribute to tumor initiation and tumor progression, through specific cellular and *in vivo* models.

Materials and Methods

1. Plasmids

The plasmids listed in this section were purchased from companies, provided from other research groups, or generated during the thesis work by cloning or mutagenesis, as indicated. The identity of the cloned sequences was checked by DNA sequencing.

1.1. Backbone vectors

- pcDNA-3: mammalian expression vector (Invitrogen).
- pEFGP-C1: mammalian expression vector to express green fluorescent protein (GFP) under the control of a cytomegalovirus (CMV) promoter (Clonetech).

1.2. Mammalian expression vectors for tagged proteins

- pHA-DYRK1A plasmids: expression vectors encoding human DYRK1A (754 aa isoform; Acc. No. NM_130436) with an N-terminal influenza hemagglutinin (HA) tag (Alvarez et al., 2003).
- All the DYRK1A variants listed below were generated by site-directed mutagenesis, using specific 5'-end phosphorylated primers (Table MM.1) and pHA-DYRK1A as template.

Table MM.1 Primers used for mutagenesis with the mutated codon highlighted in bold.

DYRK1A variant*	Mutagenesis primer	Description
Y147H	5'-GATGATGATAACTATGAT**CAT**A-TTGTAAAAAACGGAG-3'	Variant found in cancer databases.
R158C	5'-CGGAGAAAAGTGGATGGAT**TGT**T-ACGAAATTGACTCCTTG-3'	Variant found in cancer databases.
R158H	5'-CGGAGAAAAGTGGATGGATCATT-ACGAAATTGACTCCTTG-3'	Variant found in cancer databases.
E160K	5'-GAAAAGTGGATGGATCGTTAC-**AAA**ATTGACTCCTTGATAGGC-3'	Variant found in cancer databases.
K188N	5'-GCAAGAATGGGTTGCCATT**AAT**A-TAATAAAGAACAAGAAGGC-3'	Variant found in cancer databases.
K188R**	5'-GCAAGAATGGGTTGCCATT**AGA**A-TAATAAAGAACAAGAAGGC-3'	Catalytic inactive variant, used as negative control in functional assays (Alvarez et al., 2003).

K188T	5'-GCAAGAATGGGTTGCCATT**ACA**A-TAATAAAGAACAAGAAGGC-3'	Variant found in cancer databases.
L207V	5'AGATAGAAGTGCGACTT**GTT**G-AGCTCATGAACAAACATGAC-3'	Variant found in cancer databases.
D247H	5'-ATTGGTGTTTCTCAGCAA**GTG**A-TAGAGGTTGTAGGACAGC-3'	Variant found in cancer databases.
D247N	5'-ATTGGTGTTTCTCAGCAA**GTT**A-TAGAGGTTGTAGGACAGC-3'	Variant found in cancer databases.
L261R	5'-TTGCGCAAACTTTCGTGT**TCG**G-TTCAAAGAGACCCCTCG-3'	Variant found in cancer databases.
A277V	5'-CACTGCACTGCTTTTCCTT**GTG**-ACTCCAGAACTTAGTATCA-3'	Variant found in cancer databases.
I283V	5'-TTTTAGATCACAGTGAAT**GAC**A-CTAAGTTCTGGAGTCGCAAG-3'	Variant found in cancer databases.
C286Y	GAACTTAGTATCATTCAC**TAT**G-ATCTAAAACCTGAAAATATC-3'	Variant found in cancer databases.
R300H	5'-CAACTATCTTGATTGCACT**GTG**T-TTGGGGTTACAAAGAAGG-3'	Variant found in cancer databases.
R300P	5'-CAACTATCTTGATTGCACT**GGG**T-TTGGGGTTACAAAGAAGG-3'	Variant found in cancer databases.
S311F	5'-GATAGTTGACTTTGGCAGT**TTT**T-GTCAGTTGGGGCAGAGG-3'	Variant found in cancer databases.
S311P	5'-GATAGTTGACTTTGGCAGT**CCT**T-GTCAGTTGGGGCAGAGG-3'	Variant found in cancer databases.
S311Y	5'-GATAGTTGACTTTGGCAGT**TAT**T-GTCAGTTGGGGCAGAGG-3'	Variant found in cancer databases.
Q313L	5'-GACTTTGGCAGTTCTTGT**CTG**-TTGGGGCAGAGGGTAAG-3'	Variant found in cancer databases.
Y321C	5'-GGGGCAGAGGATATACCAG-**TGT**ATTCAGAGTCGCTTTTATCG-3'	Variant found in cancer databases.
R328L	5'-TATTCAGAGTCGCTTTTAT**CTG**T-CTCCAGAGGTGCTACTGGG-3'	Variant found in cancer databases.
R328Q	5'-TATTCAGAGTCGCTTTTAT**CAG**T-CTCCAGAGGTGCTACTGGG-3'	Variant found in cancer databases.
S346F	5'-CCTTGCCATTGATATGTGG**TTC**C-TCGGGTGTATTTTGGTTG-3'	Variant found in cancer databases.
G348W	5'-ATTGATATGTGGTCCCTC**TGG**T-GTATTTTGGTTGAAATGC-3'	Variant found in cancer databases.

R438H	5'-GGAGGACCTGGTGGGCGA**CAT**G-CTGGGGAGTCAGGTCATACG-3'	Variant found in cancer databases.
R467Q	5'-TGATTATGACCCCAAAACT**CAA**A-TTCAACCTTATTATGC-3'	Variant found in cancer databases.
R559C	5' AGACACACAGTCCCCAGG**TGT**G-TCAGCAATTTCCTGCTCCTC 3'	Variant found in cancer databases.

*, aa numbers refer to the longest isoform of DYRK1A (763 aa; Acc. No. NM_1396.4), to maintain the numbering of cancer databases.
**, the DYRK1A-K188R variant is indicated in this thesis manuscript as KD (kinase dead).

1.3 Plasmids for the production of lentiviral particles.

- pCMV-VSV-G: lentiviral packaging vector expressing the vesicular stomatitis virus G envelope protein; obtained from Addgene (plasmid #8454, (Stewart et al., 2003)).
- pCMV-dR8.91: second generation packaging plasmid encoding for the human immunodeficiency 1 virus *gag*, *pol* and *rev* genes (Zufferey et al., 1997); kindly provided by D. Trono (Laboratory of Virology and Genetics, Ëcole Polytechnique Fédérale de Lausanne, Switzerland).
- pWPXL: lentiviral transfer vector, encoding GFP protein under the control of Elongation factor 1-alpha (EF-1α) promoter; obtained from Addgene (plasmid #12257).
- pWPI: bicistronic lentiviral transfer vector, encoding the GFP protein under the control of EF-1α promoter and an internal ribosomal entry site (IRES), to allow independent translation; obtained from Addgene (plasmid #12254).
- pLv-DYRK1A-GFP: lentiviral transfer vector encoding for human DYRK1A (754 aa isoform) fused to GFP (Di Vona et al., 2015).
- pLv-DYRK1A-IRES-GFP: lentiviral transfer vector encoding for DYRK1A (754 aa isoform; Acc. No. NM_130436) and IRES-GFP (Rozen et al., 2018).

1.4. Plasmids for genome editing

- PX458: multicistronic expression vector encoding for *Streptococcus pyogenes* Cas9 and GFP, separated by a 2A

peptide, under the control of CMV promoter; obtained from Addgene (plasmid #48138; (Ran et al., 2013)).

- The following plasmids were generated by cloning single guide RNA (sgRNA) sequences (Table MM.2) in the PX458 vector, under the control of the U6 promoter at the Protein Technologies Facility (CRG).

Table MM.2 Plasmids for genome editing of the endometrial cancer cell lines.

Vector name	sgRNA sequence
pEN-sgRNA60	5'-GCCCTCTGCCCCAACTGACA-3'
pEN-sgRNA61	5'-GTTTGGCAGTCCTTGTCAGT-3'
pEN-sgRNA63	5'-GTGGCAGTCCTTGTCAGTTG-3'
pHEC-sgRNA76	5'-GCGCTTTTATCAGTCTCCAG-3'
pHEC-sgRNA86	5'-GGCATTCCCAGTAGCACCTC-3'

2. Techniques for DNA manipulation

2.1. Purification of plasmids

Plasmid DNA was extracted from bacterial cultures using the QIAGEN Plasmid Mini or Maxi Kit (Qiagen), depending on the volume of the culture (3 ml for Mini, 200 ml for Maxi), following the manufacturer's instructions.

2.2. DNA sequencing

Plasmids were sequenced using the Sanger sequencing method with 100-300 ng DNA, 3.2 pmol primers, and the Big Dye Terminator v3.1 Ready Reaction Cycle Sequencing Kit (Applied Biosystems), at the Genomic Sequencing Service (UPF-PRBB, Barcelona). The Polymerase Chain Reaction (PCR) conditions are in Table MM.3.

Table MM.3 PCR conditions for the sequencing reaction.

	T	time
Denaturation	95ºC	3 min
39 cycles	95ºC	10 s
	55ºC	30 s
	60ºC	1 min

2.3. Analysis of genomic DNA

Genomic DNA (gDNA) was extracted from HEC59 and EN cell lines and the clones generated during CRISPR (clustered regularly interspaced short palindromic repeats)-mediated genome editing, for genotyping. Cells were lysed in gDNA lysis buffer (25 mM NaOH, 0.2 mM ethylendiamine tetracetic acid [EDTA]) and incubated for 30 min at 98ºC. Neutralization buffer (40 nM Tris-HCl pH 8.0) was added and samples were centrifuged at 4,000x*g* for 10 min at room temperature. The DNA-containing supernatant was isolated and DNA was quantified with NanoDrop.

The detection of the genomic fragment for genotyping was performed by PCR with 0.5-1 µg gDNA,10 pmol primers, and a PCR Master Mix 2x reagent (Promega) PCR conditions are in Table MM.4.

Table MM.4 PCR conditions.

	T	time
Denaturation	95ºC	60 s
40 cycles	95ºC	30 s
	57-60ºC	30 s
	72ºC	45 s
Elongation	72ºC	5 min

The PCR products were separated by electrophoresis in a 1% agarose gel to confirm the expected size. The identity of the PCR product was further confirmed by digestion with restriction enzymes and DNA sequencing. In this case, the DNA was purified using the QIAGEN PCR product purification kit (Qiagen).

The *DYRK1A* genotype was determined by either Sanger sequencing of the PCR product as described above (template DNA amount reduced to 10-20 ng) or by digestion with restriction enzymes.

All restriction enzymes were purchased from New England BioLabs and the digestion reaction was performed by incubating 50-100 ng of PCR DNA with 1-5 units of enzyme for 1 h at the conditions indicated by the provider.

2.4. Site-directed mutagenesis

Point mutations were introduced in plasmids using the QuickChange® Site-directed Mutagenesis Kit (Stratagene), following the manufacturer's instructions. The 5'-end phosphorylated primers (Table MM.1) were purchased from Fisher Scientific. Mutations were confirmed by DNA sequencing.

3. Cell culture and *in vivo* models

3.1. Cell lines

The following human cell lines have been used in this work:

- HEK-293T: epithelial cell line derived from human embryonic kidney transformed with the large T antigen of SV40 virus.
- HeLa: epithelial cell line derived from human cervical adenocarcinoma.
- HEC59: epithelial cell line derived from human endometrial endometrioid carcinoma.
- EN: epithelial cell line derived from human endometrial endometrioid carcinoma.

HEK-293T and HeLa cells were obtained from the American Type Culture Collection (www.atcc.org). HEC59 cells were purchased from the Japanese Collection of Research Biorecourses (JCRB) Cell Bank (cellbank.nibiohn.go.jp/english). The EN cell line was obtained from the Leibniz-Institut DSMZ-German Collection of Microorganisms and Cell

Cultures (www.dsmz.de). HEK-293T and HeLa cells were grown in Dulbecco's Modified Eagle's Medium (DMEM, GIBCO, Thermo Fisher Scientific) supplemented with 10% (v/v) fetal bovine serum (FBS; GIBCO, Thermo Fisher Scientific) and antibiotics (100 U/ml penicillin and 100 U/ml streptomycin, Invitrogen) at 37°C and in a 5% CO_2 atmosphere. HEC59 and EN cells were grown in the same conditions, except for the FBS concentration that was increased to 20%.

3.2. Cell transfection

For the DYRK1A enzymatic activity screen, HEK-293T were transfected in 100-mm plates with 7.5 or 15 µg DNA depending on the production/stability levels of the protein variant, using the calcium phosphate method (Graham and van der Eb, 1973). For the DYRK1A stability screen, HEK-293T cells were transfected in MW6 plates with 3.3 µg DNA per well (3.0 µg pHA-DYRK1A plasmid and 0.3 µg pEGFP). The DNA-calcium phosphate precipitate was removed after 16-20 h by washing the cells with phosphate-buffered saline (PBS) and adding fresh medium. Cells were processed 48 h post-transfection, according to the purpose of the experiment.

For genome editing, HEC59 and EN were transfected in MW6 plates with 2.5 µg of plasmid plus 4.0 µg of single-stranded donor oligonucleotide (ssODN) using Lipofectamine® 3000 transfection kit (Thermo Fisher Scientific), following the manufacturer's instructions. Cells were washed after 16-20 h post-transfection with PBS and fresh medium was added. Cells were processed 48 h post-transfection for cell sorting.

3.3 Production of lentiviral particles

To generate lentiviral particles stocks, HEK-293T cells were seeded at a density of $2.5x10^6$ in 100-mm plates and transfected with 3.4 µg of pCMV-VSV-G envelope plasmid, 6.3 µg of pCMV-dR8.91 packaging construct and 9.8 µg of the specific transfer plasmid using the calcium phosphate precipitation method. Fresh DMEM medium was added 24 h

post-transfection, and the lentivirus containing supernatant was harvested at 48 h and 72 h post-transfection. The lentivirus-containing supernatant was centrifuged at 1,000x*g* for 10 min at 4°C and filtered through 0.45 µm filters (Millipore). Viral particles were concentrated by centrifuging the media at 20,000 rpm for 2 h at 4°C using a SW32Ti rotor in a Beckman Coulter centrifuge, and the pellet was resuspended in PBS and stored at -80°C.

3.4. Cell transduction with lentiviral particles

Cells were trypsinized and resuspended in growth medium containing 5 µg/ml of hexadimethrine bromide (Polybrene, Sigma). The concentrated virus was added to cells in suspension at variable concentrations depending on the viral titers obtained. The cells were washed with PBS 24 h post-infection and fresh medium was added. Finally, the cells were processed 72h post-infection, according to the purpose of the experiment.

3.5. Generation of CRISPR-Cas9-edited clones

EN and HEC59 cells transfected with specific sgRNA-Cas9 vector and ssODN were trypsinized and centrifuged at 300x*g* for 5 min. Cell pellets were resuspended in growth medium supplemented with 5 µg/ml of 4',6-diamino-2-phenylindole (DAPI; Roche). GFP+ cells were selected by fluorescence-activated cell sorting (FACS), using the FACSAria SORP or the Influx cell sorters (Becton Dickinson), at the CRG/UPF Flow Cytometry Core Facility. The sorted cells were seeded in MW96 plates, previously filled with conditioned medium, at 1 cell/well density. Dead cells, identified as DAPI+, were excluded. The cells were grown for 2-3 weeks until the wells were fully confluent. Colonies were then split 1:2 in two wells, one for genotyping and the other for maintenance.

The conditioned medium was prepared by collecting media from 2-3 days-growing EN and HEC59 cells. Media were centrifuged at 1,000x*g* for 10 min and filtered using 0.45 µM filters, to remove cells, cell debris and possible contaminants.

3.6. Colony formation assays

The ability of HEC59 and EN cell lines to divide and form colonies was determined by clonogenic assays. Cells were seeded at low density (1.0 - 2.5x10^3 cells/well, depending on the cell line) in MW6 plates, in triplicate. Cells were grown for 3-4 weeks until colonies were visible. Colonies were stained with methylene blue (Sigma; 0.2% [w/v] methylene blue in 50% [v/v] methanol) for 10 min and washed with H_2O. The number of colonies was determined using the image software Fiji (Schindelin et al., 2012).

3.7. Cell growth assays

To assess HEC59 and EN cell proliferation rate, cells were seeded in MW6 plates at 2.0x10^5 cells/well density, in triplicate. Cells were counted each day during 5 days, using an automatic cell counter (Countess, Invitrogen). Growth curves were generated by normalizing all counts to the values obtained the first day.

3.8. FACS analysis of cell cycle parameters

EN and HEC59 cells at 50-70% confluency (0.5 - 1x10^6) were trypsinized and washed in PBS by centrifugation at 300x*g* for 5 min at room temperature. Cell pellets were fixed by adding dropwise 500 µl of cold 70% (v/v) ethanol while vortexing and stored at -20ºC. Samples were processed after, at least, 24 h: cells were centrifuged and washed with PBS to remove residual ethanol, and DNA staining performed by resuspending the pellet in 400-800 µl of DAPI solution (5 µg/ml DAPI in PBS). Cells were analyzed with a LSR-II flow cytometer (Becton Dickinson) using the FACSDiva Software v6.1.2 (Becton Dickinson). The cell cycle profile was determined with the program ModFit v3.2 (Verity Software).

To determine the population of dead cells in the HEC59-derived clones, the same protocol was applied, but the growth media were also harvested to also include floating dead cells.

3.9. Mouse xenografts

The HEC59 parental cell line and the CRISPR-derived clones were used for xenografts experiments in mice. $2x10^6$ cells were inoculated subcutaneously into the flanks of athymic nude-*Foxn1*^{nu} mice (Envigo) in collaboration with Giulia Raimondi (Cristina Fillat's group, Institut d'Investigacions Biomèdiques Pi i Sunyer, Barcelona). Tumors were measured every 3-4 days and tumor volume was determined using the formula: volume= $\pi/6 \times$ length $\times$ width^2. Relative tumor growth was calculated normalizing every measure with the first value recorded. Statistical analysis was applied to end-point data. Mice were sacrificed at 35 days after cell inoculation, and tumors were removed. Each tumor was cut in half and either fixed with 4% paraformaldehyde and embedded in paraffin or quickly frozen in liquid nitrogen for further analysis.

4. Techniques for protein analysis

4.1. Preparation of cell lysates

Total cell lysates were obtained by resuspending the cells in SDS buffer (25 mM Tris-Cl pH 7.5, 1% [w/v] sodium dodecil sulfate [SDS], 1 mM EDTA, 10 mM sodium pyrophosphate [Na-PPi], 20 mM β-glycerolphosphate) and boiling at 98ºC for 20 min.

Soluble extracts were prepared by resuspending the cells in HEPES lysis buffer (50 mM 4-[2-hydroxyethyl]-1-piperazineethanesulfonic acid [HEPES] pH 7.4, 150 mM NaCl, 2 mM EDTA, 1% [v/v] Nonidet P-40 [NP-40] [Sigma]), supplemented with a protease inhibitor cocktail (complete Mini; Roche Diagnostic) and phosphatase inhibitors (2 mM sodium orthovanadate, 30 mM Na-PPi, and 25 mM NaF). Cell lysates were incubated at 4ºC for 30 min and centrifuged at maximum speed for 30 min at 4ºC, to separate insoluble cellular components.

Protein quantification was done with the BCA Protein Assay Kit (Pierce - Thermo Scientific), following manufacturer's instructions.

4.2. Western Blot (WB) assay

Protein extracts were denatured by adding 6x loading buffer (350 mM Tris-HCl pH 6.8, 30% [v/v] glycerol, 10% SDS, 600 mM dithiothreitol [DTT], 0.012% [w/v] bromophenol blue) and incubation at 98ºC for 10 min. Proteins were resolved by SDS-polyacrylamide gel electrophoresis (SDS-PAGE), using different acrylamide percentage gels (depending on the molecular weight of the proteins to detect) at 130 V in 1x running buffer (25 mM Tris-base, 200 mM glycine, 0.1% SDS). Proteins were transferred onto Hybond-ECL nitrocellulose membranes (Amersham Biosciences) at 400 mA for 1 h at 4ºC in 1x transfer buffer (25 mM Tris-HCl pH 8.3, 200 mM glycine, 20% [v/v] methanol). Protein trapping on nitrocellulose membranes was confirmed by Ponceau (Sigma) staining.

Membranes were then blocked with 10% (w/v) non-fat milk (Cell Signaling Technologies) diluted in TBS-T (10 mM Tris-HCl pH 7.5, 100 mM NaCl, 0.1% [v/v] Tween-20 [Sigma]) for 1 h at room temperature and incubated with the primary antibody (Table MM.5), diluted in 5% (w/v) non-fat milk, overnight at 4ºC. Membranes were then washed 3 times with TBS-T (10 min each at room temperature), and incubated with horseradish peroxidase (HRP)-conjugated secondary antibodies (Table MM.6), diluted in 5% (w/v) non-fat milk, for 1 h at room temperature. After three TBS-T washes, membranes were incubated with ECL Western Lightning® Plus ECL (Perkin Elmer) and exposed in a LAS-3000 image analyzer (Fuji PhotoFilm) with the LAS3000-pro software, to detect protein signal. Signal intensities were quantified with Fiji Software. Relative protein levels were calculated using α-tubulin levels as loading controls.

Table MM.5 Properties and working dilutions of the primary antibodies used in this work.

Primary antibody	Host	Dilution	Commercial brand
DYRK1A	Mouse	1:500	Santa Cruz (RR.7; sc-100376)
DYRK1A	Rabbit	1:1000	Sigma (D1694)
HA	Mouse	1:2000	BioLegend (901501)
GFP	Mouse	1:20000	Clontech (632380)
α-Tubulin	Mouse	1:10000	Sigma (T6199)

Table MM.6 Properties and working dilutions of the secondary antibodies used in this work.

Secondary antibody	Host	Dilution	Commercial brand
Anti-Mouse	Rabbit	1:2000	Dako (P0260)
Anti-Rabbit	Goat	1:2000	Dako (P0448)

4.3. Immunoprecipitation assay

Immunoprecipitations (IP) were carried out using magnetic beads coupled to Protein G or Protein A, depending on the host of the antibody used (Protein G for mouse antibodies and Protein A for rabbit antibodies). Beads were incubated with the specific antibody or control immunoglobulins G (IgGs) (Table MM.7) for 1 h at room temperature. Extracts were incubated with antibody-bead complexes for 3 h at room temperature or overnight at 4ºC. The beads were then washed 3 times with a washing buffer (50 mM HEPES pH 7.4, 150 mM NaCl, 2 mM EDTA, 1% NP-40); a last wash was performed without detergent. The immunoprecipitated proteins were finally resuspended in 2x loading buffer (100 mM Tris-HCl pH 6.8, 200 mM DTT, 4% SDS, 20% glycerol, 0.2% bromophenol blue) and boiled 10 min at 98ºC for WB assays or used for *in vitro* kinase assays.

Table MM.7 Properties and working dilutions of the antibodies used for IP.

Antibody	Host	Amount	Commercial brand
Anti-HA	Mouse	1 µg	Biolegend (901501)
Anti-DYRK1A	Rabbit	3 µg	Abcam (69811)
Anti-DYRK1A	Rabbit	3 µg	Sigma (D1694)
IgGs	Rabbit	3 µg	Cell Signaling (2729)

4.4. *In vitro* kinase assay

In vitro kinase (IVK) assays were carried out using either endogenous or ectopically expressed DYRK1A immunoprecipitated from cell lines as source of enzyme. After the IP washes, the beads were split 1:2. Thus, an aliquot was resuspended in loading buffer 2x and analyzed by WB to assess the relative amount of immunoprecipitated kinase. The second half was resuspended in kinase buffer (12.5 mM HEPES, pH 7.4, 2.5 mM $MgCl_2$, 2.5 mM $MnCl_2$, 0.25 mM DTT) and 50 µM ATP in the presence of 2.5 µCi [γ^{32}P]-ATP (3000 Ci/mmol, Perkin Elmer) and 200 µM of the "DYRKtide" substrate, an optimal substrate peptide for DYRK kinases (Himpel et al., 2000). This reaction mix was incubated for 20 min at 30ºC. The reaction was then dotted in triplicates onto P81 Whatmann cellulose papers and washed 4 times with 5% (v/v) orthophosphoric acid to eliminate non-incorporated [γ^{32}P]-ATP. The ^{32}P incorporated on DYRKtide molecules was measured using a scintillation counter, and the signal, given as counts per minutes (cpms), was normalized to the immunoprecipitated kinase levels evaluated by WB.

To evaluate DYRK1A autophosphorylation, the enzyme molecules were eluted from the beads in loading buffer 2x, denatured at 98ºC for 10 min, and fractionated by SDS-PAGE. The gel was then dried for 1 h at 80ºC and exposed to a film or Phosphoimager screen (revealed using

the GE Typhoon Trio imager). The signal was normalized to the kinase amounts evaluated by WB.

4.5. Mass spectrometry analysis

Label-free quantitative mass spectrometry (MS) was used to define and compare the whole proteome and phospho-proteome of the HEC59 parental cell line and the CRISPR-derived clones. Cells were seeded in p100 plates and lysed in Urea buffer (6 M urea-100 mM ammonium bicarbonate [ABC]). The protein amount was quantified with the BCA kit and lysates were diluted with Urea buffer in order to obtain the concentration corresponding to $4x10^6$ cells/ml. Sample preparation and MS analysis were performed at the CRG/UPF Proteomics Unit.

4.5.1. Sample preparation

Four independent samples for each cell line were used. Samples ($4x10^6$ cells, ~1 mg) were reduced with DTT, alkylated with iodocetamide, and digested with trypsin (Promega) and Lys-C (Wako) proteases. Tryptic peptide mixtures were desalted using C18 Hypersep columns (Thermo Fisher Scientific). Phosphorylated peptides were enriched using an immobilized metal-affinity TiO_2 protocol, as described (Sebe-Pedros et al., 2016).

4.5.2. Chromatographic and MS analysis

Samples were analyzed by liquid chromatography (LC)-MS/MS using a LTQ Orbitrap Fusion Lumos mass spectrometer (Thermo Fisher Scientific) coupled to EASY-nLC 1000 (Thermo Fisher Scientific, Proxeon). Peptides were separated by reversed-phase chromatography using a 50-cm column with an inner diameter of 75 µm, packed with 2 µm C18 particles spectrometer (Thermo Scientific). Chromatographic gradients started at 95% buffer A (0.1% formic acid in H_2O) and 5% buffer B (0.1% formic acid in acetonitrile) with a flow rate of 300 nl/min for 5 min and gradually increased to 22% buffer B and 78% A in 79 min and then to 35% buffer B and 65% A in 11 min. After each analysis, the column was washed for 10 min with 10% buffer A and 90% buffer B.

The mass spectrometer was operated in positive ionization mode with nanospray voltage set at 2.4 kV and source temperature at 275°C. Ultramark 1621 was used for external calibration of the FT mass analyzer prior the analyses, and an internal calibration was performed using the background polysiloxane ion signal at m/z 445.1200. The acquisition was performed in data-dependent acquisition mode and full MS scans with 1 micro scans at resolution of 120,000 were used over a mass range of m/z 350-1500. Auto gain control (AGC) was set to 1E5 and charge state filtering disqualifying singly charged peptides was activated. In each cycle of data-dependent acquisition analysis, following each survey scan, the most intense ions above a threshold ion count of 10,000 were selected for fragmentation. The number of selected precursor ions for fragmentation was determined by the "Top Speed" acquisition algorithm and a dynamic exclusion of 60 seconds. Fragment ion spectra were produced via high-energy collision dissociation at normalized collision energy of 28% and they were acquired in the ion trap mass analyzer. AGC was set to 1E4, and an isolation window of 1.6 m/z and a maximum injection time of 200 ms were used. All data were acquired with Xcalibur software v4.1.31.9.

Digested bovine serum albumin (New England Biolabs) was analyzed between each sample to avoid sample carryover and to assure stability of the instrument; QCloud (Chiva et al., 2018) was used to control instrument longitudinal performance during the project.

5. Techniques for RNA analysis

5.1. RNA purification and reverse transcription

Total RNA was extracted using the QIAGEN RNeasy extraction kit (Qiagen) or the TRIzol reagent (Ambion), depending on the purpose of the experiment, and following manufacturer's instructions. Samples were treated with DNase I (Ambion, 2 U/µl) for 30 min at 37ºC to

eliminate the remaining genomic DNA, and RNA samples were quantified with NanoDrop.

For reverse transcription, cDNA was generated by incubating 0.5-1 µg RNA with Superscript II Reverse Transcriptase (Invitrogen) and random primers as recommended by the manufacturer's instructions. Total cDNA from EN and HEC59 cells was used to check the expression of *DYRK1A* wild type (wt) and mutant alleles.

5.2. RNA-Seq

Libraries for RNA-Seq were prepared at the CRG Genomics Unit. Only RNA with RNA integrity number values over 8 was used. Libraries were prepared using the TruSeq Stranded mRNA Sample Prep Kit v2 according to the CRG Genomics Unit internal protocols. Briefly, poly(A)-mRNA selection was carried out on 1 µg of total RNA using streptavidin-coated magnetic beads; the selected RNA was subsequently fragmented to approximately 300 bp. cDNA was synthesized using Superscript II RT (Invitrogen) and random primers. For the synthesis of the second strand of the cDNA, dUTP was used in place of dTTP. and dsDNA was subjected to A-tailing and ligation of the barcoded Truseq adapters. Library amplification was performed by PCR using the primer cocktail supplied in the kit. All purification steps were performed using AMPure XP beads (Beckman).

The libraries were analyzed using Agilent DNA 1000 chip to estimate the quantity and check size distribution, and quantified by qPCR using the KAPA Library Quantification Kit (Kapa Biosystems) before amplification with Illumina's cBot. Libraries were sequenced on an Illumina GAIIx sequencer (HiSeq sequencing v4 chemistry) to a length of 50 bp single-ended. Around 4-6x10^7 reads were obtained for each library with more than 97% aligned reads in all cases, and biological triplicates were used for the analysis.

6. CRISPR-Cas9-based genome editing

6.1. Oligonucleotides and reagents

CRISPR-Cas9 technology was used to target *DYRK1A*-mutant sites in the HEC59 and EN cell lines and revert them to wt. The design, cloning and T7 test of specific sgRNAs was performed in collaboration with Carlo Carolis (CRG Protein Technologies Unit).

For the nucleotide-specific editing, a combination of sgRNAs for targeting and single strand oligonucleotides as templates was used (Bialk et al., 2015). Three sgRNAs targeting the EN mutant site and two sgRNAs targeting the HEC59 mutant site were designed and cloned into PX458 vector (Table MM.2). In addition, two specific 120-mer ssODN were designed by C. Carolis and purchased from Integrated DNA Technologies (Table MM.8). Later on, a new ssODN was designed to optimize the technique. The new ssODN harbored phosphorothioate bonds at the 5' and 3' ends, a CRISPR/Cas-blocking mutation targeting the PAM sequence (Paquet et al., 2016), and additional single-nucleotide mutations to allow screening of the clones by restriction digestion (Table MM.8). The RS-1 reagent (Sigma) was kindly gifted by Valeria Di Giacomo (ZeClinics), and it was used to enhance CRISPR genome editing efficiency.

Table MM.8 ssODNs used for genome editing of EN and HEC59 cell lines.

ssODN name	ssODN sequence
ssODN-EN	5'-AATTTCTATTTAATTCACAAGTTCTGAAATAATACTTACCC-TCTGCCCCAACTGACA**AGA**ACTGCCAAAGTCAACTATCTTG-ATTGCACTGCGTTTGGGGTTACAAAGAAGGATATTTTC-3'
ssODN-HEC59	5'-CCGAGGGACCACATATCAATGGCAAGGTCATAAGGCATTC-CCAGTAGCACCTCTGGAGA**CCG**ATAAAAGCGACTCTGAATAT-ACTGGTATATCTGAAATATATTTCAAAATAGTATTACT-3'
ssODN-HEC59_new	5'-C*CGAGGGACCACATATCAATGGCAAGGTCATAAGGCATT-CCCAGTAGCAC**t**TCTGG**t**GA**CCG**ATAAAAGCGACTCTGAAT-ATACTGGTATATCTGAAATATATTTCAAAATAGTATTAC*T-3'

The target codon is highlighted in bold. *, indicates a phosphorothioate bond. Additional mutations in ssODN-HEC59_new are indicated in lowercase.

6.2. sgRNAs T7 test

The sgRNAs were tested for their efficiency to promote Cas9 cleavage on DYRK1A mutant site by the T7 assay (Guschin et al., 2010). EN and HEC59 cells were transfected with their respective sgRNA-expressing plasmids and GFP+ cells were sorted and grown as single cell clones. A PCR reaction was performed on gDNA to amplify the fragment containing the target site (Table MM.9 for primer sequences), and the PCR products were digested with T7 endonuclease I (New England BioLabs, M0302), following manufacturer's instructions. Digestion products were resolved by 1% agarose gel electrophoresis and sgRNAs efficiency was determined by quantification of the cleaved product *vs* the PCR fragment bands (Figure MM.1).

Table MM.9. Primers for target site amplification PCR.

Primer	Sequence
EN_FW	5'-ACAAGGCATTTTGGTAGCACTG-3'
EN_RV	5'-ATAAGCATCCTGTAATTGCCTCTA-3'
HEC59_FW	5'-ACGCTGAGAAATACATTGTTTGGG-3'
HEC59_RV	5'-GTAGACATCTTTGCCTAAAAACAACT-3'

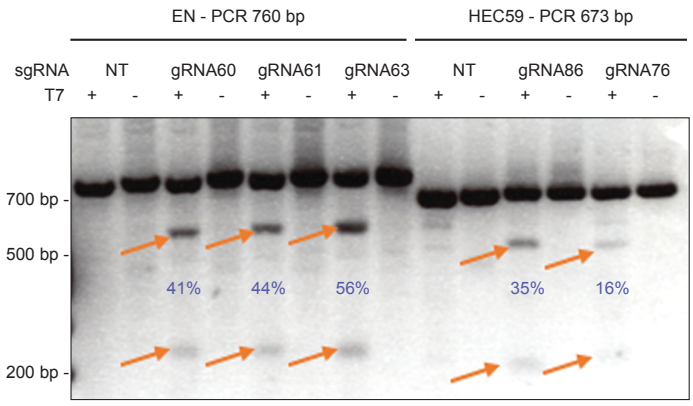

Figure MM.1 T7 test. PCR products from gDNA were digested and fractionated with their respective digestion controls (no T7). Orange arrows point to the bands produced by the T7 cut. Percentages of targeting efficiency are included. NT: non transfected.

Based on the T7 test results, sgRNA63 was selected for EN genome editing. For HEC59, sgRNA86 was initially selected, but later replaced by sgRNA76, since sgRNA76 showed mutant allele-specificity during additional tests, which probably explains the reduced efficiency observed in the T7 assays.

6.3. Clone screen

Clones were initially screened by gDNA extraction, PCR and sequencing. For a second round of reverted clone identification, a new strategy was designed to screen HEC59 clones by using restriction enzymes. After gDNA extraction, amplification of the fragment carrying the target site was performed with HEC59_FW and HEC59_RV primers (Table MM.9). The PCR products were then digested with two restriction enzymes, BcoDI and BstEII (Figure MM.2A-B). The digested PCR products were separated in 1% agarose gels and the band profile was analyzed to distinguish among the different possible editing events, as illustrated in Figure MM.2C. A reverted clone should lose the BcoDI restriction site and gain a BstEII site. Clones that showed a “no event” profile were then digested with BsaI, to avoid losing false negatives, result of a reverted *wt/wt* genotype without a BstEII site gain (Figure MM.2C). The reliability of the strategy was demonstrated by digesting two PCR products from different sources of gDNA with the three enzymes: parental HEC59 (*wt/mut*) and EN (*wt/wt* for the considered gDNA fragment) (Figure MM.2D). Finally, a positive control for BstEII digestion was needed and therefore, a genomic fragment on the *DYRK1A* locus, containing a BstEII recognition site, was identified and amplified by PCR (primers in Table MM.10; Figure MM.2E).

Table MM.10 Primers for BstEII recognition site amplification PCR.

Primer	Sequence
BstEII D1A site_FW	5’-CCCTGGATATGTGTTATAGATGC-3’
BstEII D1A site_RV	5’-TCCCTATGCTTTCATTGTGATTT-3’

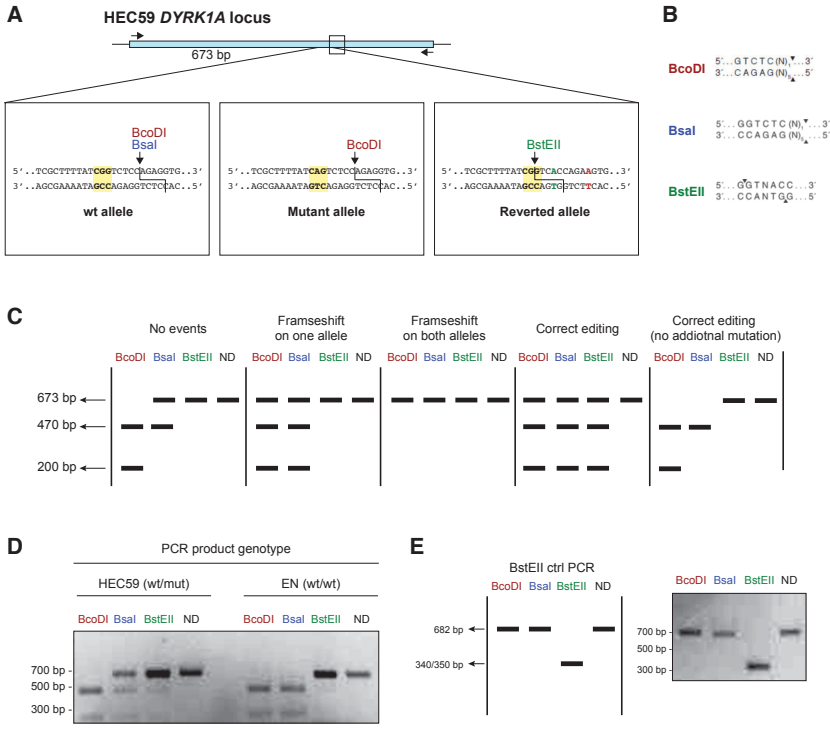

Figure MM.2 Screen strategy for HEC59 CRISPR-clones. A) Differential activity of BcoDI, BsaI and BstEII on wt, mutant and a potential reverted allele on the *DYRK1A* target site. **B)** Recognition sites of BcoDI, BsaI and BstEII. **C)** Predicted digestion profiles of BcoDI, BsaI, BstEII and not digested (ND), considering all possible editing events. **D)** Screen test using PCR products obtained from HEC59 gDNA and EN gDNA, which correspond to the genomic scenarios indicated. **E)** BstEII positive control profile and digestion test.

7. Computational analysis

7.1. Analysis of open-access tumor sequencing data

Bioinformatic analysis of publicly available data from cancer patients was mainly performed by Carlota Rubio Pérez (Nuria López Bigas's group, Institut de Recerca Biomédica-IRB, Barcelona; previously at the Research Unit of Biomedical Informatics, IMIM-UPF), as a part of a collaboration started at the beginning of this thesis project. All tumor sequencing data, including somatic mutations, copy-number alterations

(CNAs) and gene expression (from RNA-Seq RSEM gene-normalized), belonging to the TCGA project was considered. Sequencing data was downloaded from the most recent version of FireBrowse server (firebrowse.org; 2016_01_28 version). Additionally, tumor sequencing data from the IntOGen platform (www.intogen.org, (Gonzalez-Perez et al., 2013)) was also considered for the somatic mutation analysis.

To identify differences in the expression of DYRK genes in tumor samples, the expression levels of DYRK genes transcripts were compared with the ones in paired healthy tissue samples. Of note, the number of cancer types with sequenced paired healthy tissue samples in TCGA was limited, and therefore only cancer type cohorts with at least 10 paired samples sequenced were considered. A gene was considered to be significantly differentially expressed in tumors if Wilcoxon test showed an adjusted *p*-value < 0.05. P-values were adjusted according to Benjamini-Hoechberg correction.

To investigate CNAs in DYRK genes, the FireBrowse portal was used to download outputs of TCGA exome sequencing and whole genome sequencing data computed with the GISTIC2 module (Mermel et al., 2011). Differential gene expression analysis was also performed to assess whether DYRK CNAs were associated to changes in gene expression. Groups were set as GISTIC = 2 (multiple amplification) or GISTIC = -2 (homozygous deletion), and GISTIC = 0 (diploids) tumors were used as control group. Only cancer types cohorts with at least 10 genes in samples per group were considered. A gene was considered to be significantly differentially expressed in tumors if Mann-Whitney U test showed an adjusted *p*-value < 0.05 and a log2-fold change (log2FC) with values: Log2FC < -1 or Log2FC > 1.

The profile of somatic mutations of DYRK tumor samples was dissected to assess whether DYRK genes carry signals of positive selection; the analysis aimed to determine if the mutational patterns deviated from what is expected by chance following described methodology (Rubio-

Perez et al., 2015). Thus, we searched for complementary signals of positive selection in the somatic mutational patterns of DYRK genes, across each cancer type cohort, by employing three different methods:

- OncodriveFM: the score given by this method is based on the bias towards the accumulation of mutation with high predicted functional impact (Gonzalez-Perez and Lopez-Bigas, 2012).
- OncodriveCLUST: the score is based on the bias towards regional clustering of mutations (Tamborero et al., 2013).
- MutSigCV: the score is based on the overall mutation rate, compared with a background model (Lawrence et al., 2013).

7.2. Analysis of the RNA-Seq data

RNA-Seq data analysis was performed in collaboration with Chiara Di Vona. Sequences obtained from each sample were mapped against the human genome (hg38 genome assembly version) using STAR (Dobin et al., 2013). Reads that could not be mapped as unique regions were discarded. Differential gene expression was determined by normalizing data using the trimmed mean of Mvalues normalization method (Robinson and Oshlack, 2010), and filtering genes that had >10 average normalized counts per million with the DEseq2 package (Love et al., 2014). Statistical analysis was performed in RStudio by fitting an exact test with the negative binomial distribution for each set of conditions and testing for differential gene expression utilizing the DEseq2 package (Love, et al., 2014).

7.3. Analysis of the proteomics data

Proteome and phospho-proteome acquired data were analyzed in collaboration with CRG/UPF Proteomics Unit and Chiara Di Vona. MaxQuant v1.6.1.0 was used for peptide identification and quantification. Raw data was searched with Andromeda (Cox et al., 2011) against SwissProt human database (as in October 2018) with the most common contaminants as defined in MaxQuant. A precursor ion mass tolerance of 4.5 ppm at the MS1 level was used, and up to three miscleavages for trypsin were allowed. The fragment ion mass

tolerance was set to 0.5 Da. Carbamidomethylation on Cys was set as fix modification; oxidation of methionine and protein acetylation at the N-terminal were defined as variable modification, and in the case of the phospho-enriched samples, phosphorylation on serine, threonine and tyrosine were also considered as variable modifications. Data was filtered using a false discovery rate (FDR) < 5% threshold at the peptide spectrum match and protein levels.

Proteins abundances were estimated using MaxQuant LFQ (Cox et al., 2014) and phosphosite quantification data was retrieved from the corresponding precursor ion intensities, log2 transformed and normalized. The protein and phosphosite quantitative values were used to calculate fold-changes and their corresponding adjusted *p*-values (q-values) with the Storey method (Storey and Tibshirani, 2003). Significant differences were considered for an adjusted *p*-value < 0.01 for both the proteome and phospho-proteome analysis. For protein differential expression analysis, we considered a log2FC < -0.7 or > 0.7, including also proteins identified in only one condition. To alleviate the "missing value" problem (NAs), in the case of the phospho-proteome analysis, we filtered for peptides identified in at least two replicates for parental HEC59 data and the DYRK1A reverted clone; in the case of the DYRK1A$^{-/-}$ knockout clone, we also consider phosphorylation events that were completely absent in this condition.

7.3. Other computational tools and databases

Principal component analysis (PCA) and heatmaps were generated in collaboration with Chiara Di Vona. PCA of RNA-Seq data was performed using the integrated function of DESeq2 (Love, et al., 2014), whereas heatmaps were generated using the package ComplexHetmap in R (Gu et al., 2016). For RNA-Seq data, log-normalized counts were z-scored, while in the case of phospho-events, we used the already log-transformed intensity values. In both cases k-means clustering was performed and NAs values were treated as explained in the previous section.

The algorithm FoldX (Guerois et al., 2002; Schymkowitz et al., 2005) was used in collaboration with Javier Delgado (Luis Serrano's group, CRG) to predict the impact of DYRK1A cancer mutations on the free energy potential (ΔG) and thus on the stability of the protein. The YASARA simulator platform was used to easily perform FoldX commands; the file 2VX3 containing information on DYRK1A crystal structure was downloaded from the Protein Data Bank (www.rcsb.org).

Gene ontology (GO) were performed using EnrichR (amp.pharm.mssm.edu/Enrichr; (Kuleshov et al., 2016)) web server. Heatmaps of RNA-Seq and MS data were generated using R.

Additional sources of cancer data used in this thesis work were: COSMIC (cancer.sanger.ac.uk/cosmic; (Tate et al., 2019)), cBioPortal (www.cbioportal.org; (Cerami et al., 2012; Gao et al., 2013)), and ICGC (International Cancer Genome et al., 2010). The Cancer Cell Line Encyclopedia (CCLE) (portals.broadinstitute.org/ccle; (Barretina et al., 2012)) was interrogated to identify and obtain information about cancer cell lines mutated in the *DYRK1A* gene.

In addition to cancer databases, other sources of public data were used in this work. Gene expression data of DYRK family members in human tissues was obtained from the GTEx portal (www.gtexportal.org). Protein and DNA sequences were searched and analyzed by using public databases of the National Centre for Biotechnology Information (NCBI, www.ncbi.nlm.nih.gov) and Ensembl (ensembl.org). Bibliography references were queried with the database PubMed from NCBI. The Exome Aggregation Consortium (ExAC, exac.broadinstitue.org; (Lek et al., 2016)), was used to review *DYRK1A* mutations found in the normal population and to compare ExAC *DYRK1A* mutation profile with the one obtained from cancer databases.

8. Statistical analysis

Box-plots and scatter plots were generated using R Studio software and the R package ggplot2 (Wickham, 2009). For box plots, the bottom and top of the box represent the first and third quartiles, and the line inside the box is the second quartile (the median). The ends of the whiskers represent the lowest datum still within 1.5 interquartile range (IQR) of the lower quartile, and the highest datum still within 1.5 IQR of the upper quartile. Any data not included between the whiskers is plotted as an outlier with a dot. Medians comparison was computed through either a two-tailed unpaired Student's t-test, or a two-tailed Mann-Whitney test. Scatter plots were used for correlation analysis, where regression lines and equation were indicated. Significant correlation was assessed with a Spearman test.

Bar graphs were generated with Microsoft Excel v19.01. Statistical significance was calculated with a two-tailed unpaired Student's t-test (Microsoft Excel v15.33). The data in the graphs represent the mean ± standard deviation (SD) of independent experiments. A p-value<0.05 was considered significant (*p<0.05; **p<0.01; ***p<0.001), with some exceptions (sometimes a p<0.01 was considered necessary for significance). All experiments were performed independently at least two times, with an n ≥ 3 for most of the experiments.

Results

1. DYRK1A is a potential tumor driver

1.1. *In silico* analysis of TCGA data

To understand to what extent, and in which cellular context, alterations in DYRK genes contribute to carcinogenesis and tumor progression, a systematic *in silico* analysis was performed, in collaboration with Carlota Rubio Pérez (Nuria López Bigas' group, IRB, Barcelona).

Publicly available data from TCGA were interrogated to define the profile of DYRK genes in tumor samples, considering different layers of gene alterations: differential gene expression, CNAs and somatic mutations (Figure R.1). An initial analysis was performed on the TCGA release available on 2015, which included a smaller number of tumor samples than the current one (n = 4,068 covering 16 tumor types (Cancer Genome Atlas Research et al., 2013; Rubio-Perez et al., 2015)). This analysis gave indications of alterations in DYRK genes. The results presented in this Thesis work correspond to a second analysis performed using the last TCGA release (Pan-Cancer Atlas, April 2018), containing information extracted from more than 10,000 tumor samples included in 33 different tumor types (Hoadley et al., 2018). Moreover, the list of somatic mutations was obtained from the former TCGA dataset (August 2014), plus 2,724 additional samples derived from other large sequencing cancer projects, including the ICGC cohort, covering 28 tumor types and obtained from Intogen (see Materials and Methods section).

For the purpose of this thesis work only the last analysis will be presented, since it gave a wider profile of DYRK genes status in cancer (more tumor types included) and more robust results (increased number of samples). The cancer types considered in this study and their respective TCGA symbol are listed in Table R.1.

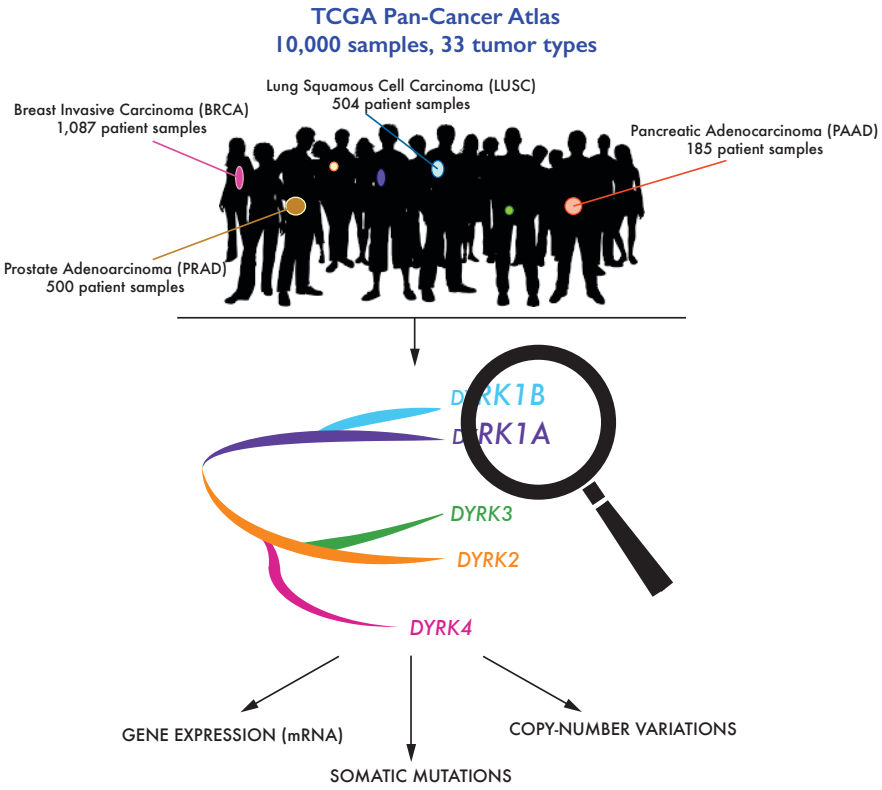

Figure R.1 Overview of the *in silico* analysis of DYRK genes in tumor samples. TCGA data from the Pan-Cancer Atlas project were analyzed, focusing on DYRK family of genes. The study aimed to understand whether any of the members of DYRK family could represent a potential tumor driver, by interrogating gene expression data, CNAs and somatic mutations.

1.2. DYRK genes are differentially expressed in cancer

Differential gene expression at the mRNA level was assessed by analyzing TCGA RNA-Seq data from those tumor types with at least 10 available paired healthy-tumor samples. This filter reduced the number of tumor types to be analyzed to 15 (Table R.1 and Figure R.2). DYRK genes were found either down-regulated or up-regulated, depending on the tumor type, with members of the family showing a conserved pan-cancer trend. Indeed, *DYRK1A* was found to be down-regulated in most of the tumor types analyzed (Figure R.2A), whereas its closest paralogue *DYRK1B* was found mainly up-regulated (Figure R.2B). The class II member *DYRK2* showed the same tendency, having increased

expression levels in most of the tumor types considered in the study (Figure R.2C). On the contrary, *DYRK3* and *DYRK4* did not follow any particular trend (Figure R.2D-E). Therefore, the analysis indicated that the expression of DYRK family members is altered in tumors at the mRNA level.

Table R.1 TCGA cancer types. A total of 32 cancer types from the TCGA Pan-Cancer project and their respective symbols. Colon adenocarcinoma (COAD) and rectal adenocarcinoma (READ) cohorts were considered as a unique tumor type (COADREAD).

TCGA Symbol	Tumor type	DE*
LAML	Acute myeloid leukemia	
DLBC	Lymphoyd neoplasm diffuse large B cell lymphoma	
THYM	Thymoma	
OV	Ovarian cancer	
UCEC	Uterine corpus endometrial carcinoma	22
CESC	Cervical squamous cell and endocervical adenocarcinoma	
UCS	Uterine carcinosarcoma	
BRCA	Breast invasive carcinoma	112
PRAD	Prostate adenocarcinoma	51
TGCT	Testicular germcell tumors	
BLCA	Bladder carcinoma	19
KIRC	Kidney renal clear cell carcinoma	71
KIHC	Kidney chromophobe	24
KIRP	Kidney renal papillary cell carcinoma	32
ESCA	Esophageal carcinoma	10
STAD	Stomach adenocarcinoma	31
COADREAD	Colorectal adenocarcinoma	29
LIHC	Liver hepatocellular carcinoma	50
PAAD	Pancreatic ductal adenocarcinoma	
CHOL	Cholangiocarcinoma	
LUAD	Lung adenocarcinoma	56
LUSC	Lung squamous cell carcinoma	50
MESO	Mesothelioma	
GBM	Glioblastoma multiforme	
LGG	Brain lower-grade glioma	
SKCM	Skin cutaneous melanoma	
UVM	Uveal melanoma	
HNSC	Head and neck squamous cell carcinoma	43
SARC	Sarcoma	
PCPG	Pheochromocytoma and paraganglioma	
THCA	Thyroid carcinoma	59
ACC	Adrenocortical carcinoma	

Hematologic and lymphatic
Gynecologic
Urologic
Gastrointestinal
Thoracic
Central nervous system
Melanomas
Others

*tumor types used for the DE (differential expression) analysis; the number of samples with paired healthy/tumor tissue is indicated.

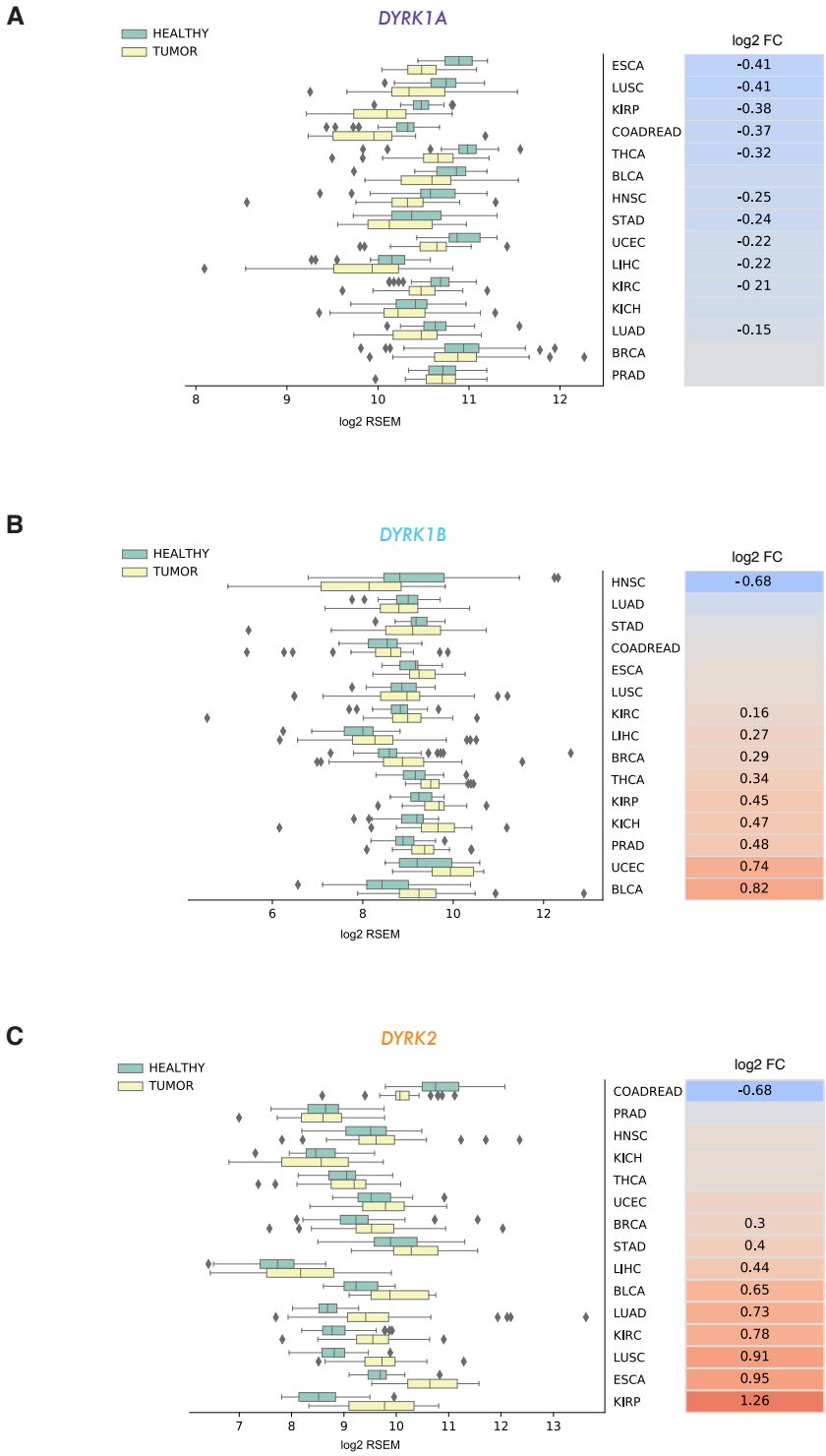
A
DYRK1A
HEALTHY
TUMOR
log2 FC
ESCA -0.41
LUSC -0.41
KIRP -0.38
COADREAD -0.37
THCA -0.32
BLCA
HNSC -0.25
STAD -0.24
UCEC -0.22
LIHC -0.22
KIRC -0 21
KICH
LUAD -0.15
BRCA
PRAD
8 9 10 11 12
log2 RSEM
B
DYRK1B
HEALTHY
TUMOR
log2 FC
HNSC -0.68
LUAD
STAD
COADREAD
ESCA
LUSC
KIRC 0.16
LIHC 0.27
BRCA 0.29
THCA 0.34
KIRP 0.45
KICH 0.47
PRAD 0.48
UCEC 0.74
BLCA 0.82
6 8 10 12
log2 RSEM
C
DYRK2
HEALTHY
TUMOR
log2 FC
COADREAD -0.68
PRAD
HNSC
KICH
THCA
UCEC
BRCA 0.3
STAD 0.4
LIHC 0.44
BLCA 0.65
LUAD 0.73
KIRC 0.78
LUSC 0.91
ESCA 0.95
KIRP 1.26
7 8 9 10 11 12 13
log2 RSEM

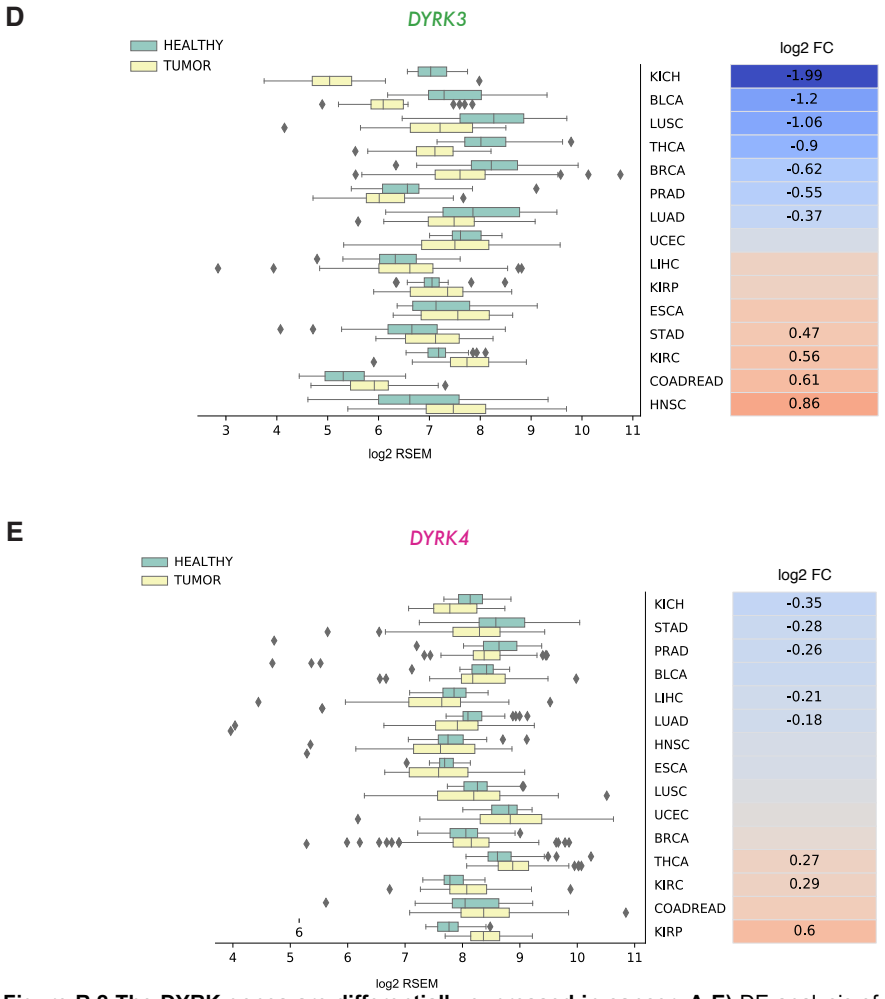

Figure R.2 The DYRK genes are differentially expressed in cancer. A-E) DE analysis of *DYRK1A* (**A**), *DYRK1B* (**B**), *DYRK2* (**C**), *DYRK3* (**D**) and *DYRK4* (**E**) genes using RNA-Seq data obtained from TCGA paired healthy/tumor samples (see Table 1 for the number of samples used for each tumor type). Tumor types are ranked following log2FC values, which are indicated when significant (Wilcoxon test, adjusted *p*-value < 0.05).

1.3. DYRKs copy number alterations (CNAs)

Changes in gene expression can arise as the consequence of deregulated transcriptional *cis*- or *trans*- mechanisms or they might result from alterations at the genomic DNA sequence. Among the somatic alterations occurring in tumor cells, copy number alteration (CNAs) are defined as big modifications of genomic DNA (> 1 kb) generated by amplification or deletion events (Krijgsman et al., 2014; Yi and Ju, 2018).

CNAs, in particular, gene amplification, are relatively frequent events in cancer genomes (Santarius et al., 2010). Analysis of TCGA data with the GISTIC method (Mermel et al., 2011) indicated that DYRK genomic regions appear amplified/deleted in tumor cohorts (Figure R.3). To better define the driver potential of DYRK family genes, we next aimed to determine whether DYRK CNAs correlate with changes in gene expression. The analysis is based on the assumption that gene amplifications/deletions occurring in tumor driver genes will be associated to coherent expression changes, and, in fact, the integration of gene expression and CNA data has been used to identify potential tumor drivers (Ohshima et al., 2017; Rubio-Perez, et al., 2015; Santarius, et al., 2010). Therefore, a DE analysis was carried out on tumor samples with amplifications (GISTIC = 2) or homozygous deletions (GISTIC = -2) in each of the DYRK genes, using tumor samples diploid for each of the genes (no CNAs, GISTIC = 0) as control groups.

Coherent with the results described in the previous section, analysis of DYRK CNAs pointed at the class I member *DYRK1B* and the class II member *DYRK2* as frequently amplified-overexpressed in specific tumor cohorts (Figure R.3B-C), suggesting a possible role as tumor drivers in these specific cancer types. In particular, *DYRK1B* and *DYRK2* were found significantly amplified respectively in 7 and 9 TCGA cohorts. No significant CNAs-derived expression changes were observed for *DYRK1A* (Figure R.3A); while, *DYRK3* and *DYRK4* showed alterations in 1 and 2 TCGA cohorts, respectively (Figure R.3D-E). These results only partially explain the upregulation of *DYRK1B* and *DYRK2* expression observed in tumors since only 2 out of 9 *DYRK1B*-overexpressing (BRCA and BLCA) and 5 out of 10 DYRK2-overexpressing cancer types (BRCA, BLCA, LUSC, LUAD and HNSC) showed also multiple amplifications. Therefore, alternative mechanisms such as promoter methylation or altered activity of transcription factors might be responsible for the differential expression observed for those tumors in which *DYRK1B* and *DYRK2* are not amplified, and of course for *DYRK1A*, *DYRK3* and *DYRK4*.

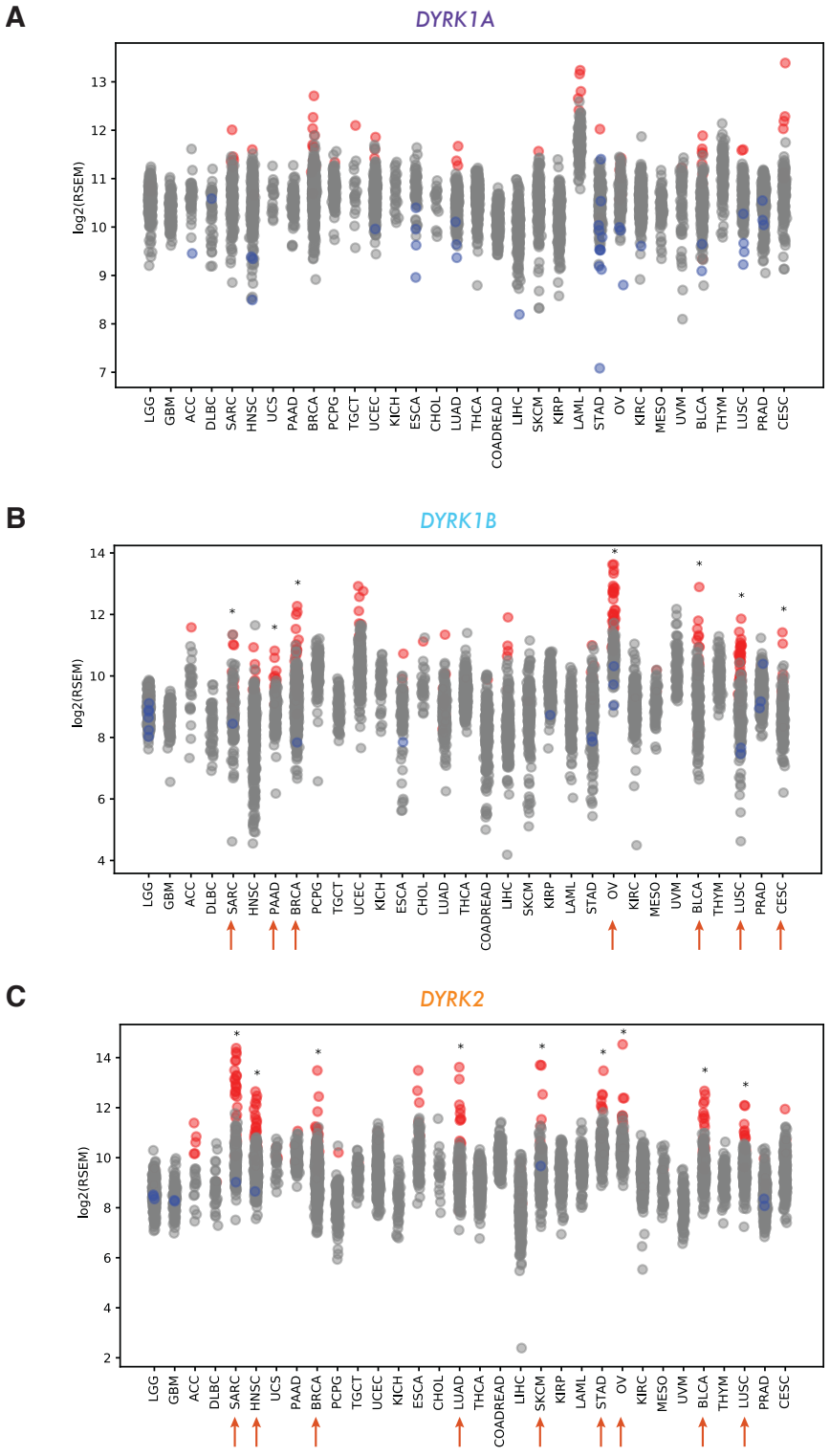
A
DYRK1A
log2(RSEM)
B
DYRK1B
log2(RSEM)
C
DYRK2
log2(RSEM)
LGG GBM ACC DLBC SARC HNSC UCS PAAD BRCA PCPG TGCT UCEC KICH ESCA CHOL LUAD THCA COADREAD LIHC SKCM KIRP LAML STAD OV KIRC MESO UVM BLCA THYM LUSC PRAD CESC

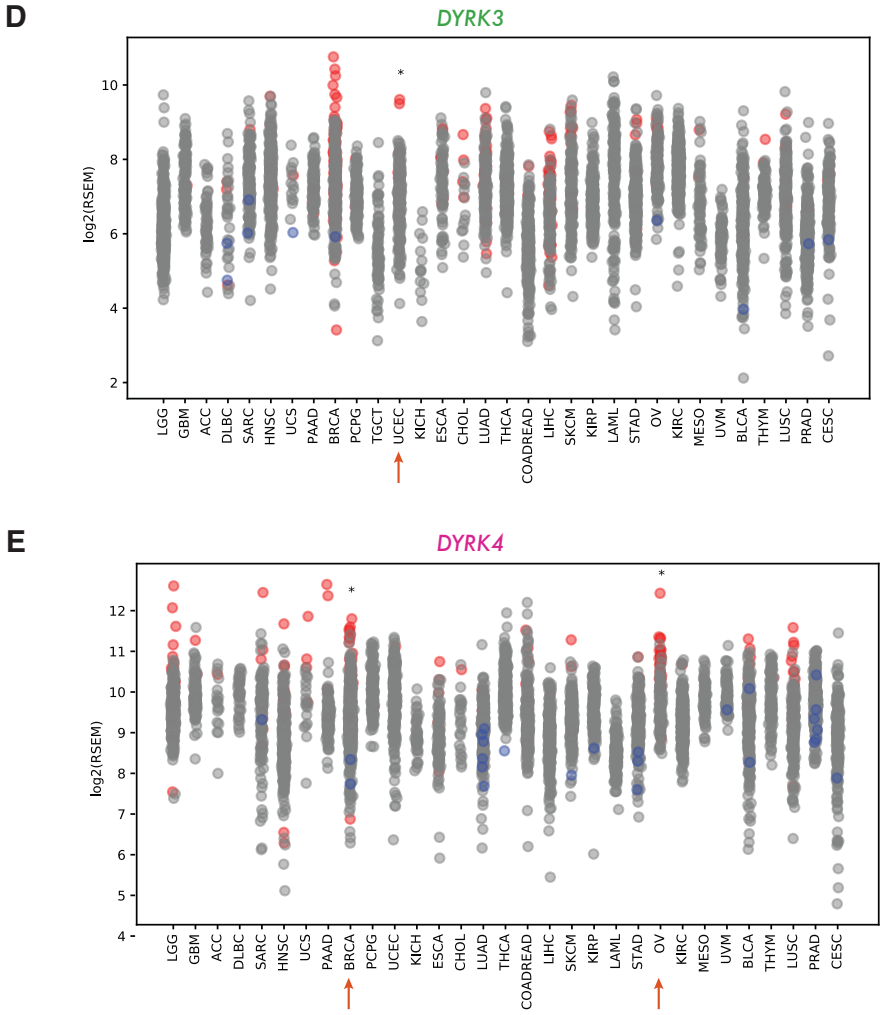

Figure R.3 DYRK family members CNAs in cancer samples *vs* gene expression. *DYRK1A* (**A**), *DYRK1B* (**B**), *DYRK2* (**C**), *DYRK3* (**D**) and *DYRK4* (**E**) gene expression values are plotted for each tumor type. Each dot represents a tumor sample. Multiple amplification (GISTIC = 2) and homozygous deletions (GISTIC = -2) are represented as red and blue dots, respectively. Only tumors with RNA-seq data and CNA values in each cohort were used. DE analysis was performed using diploid samples (grey dots) as controls. Cohorts with significant coherent expression changes are indicated with arrows (Mann-Whitney test, adjusted *p*-value < 0.05; Log2FC < -1; Log2FC > 1).

1.4. DYRK1A shows signals of positive selection

To better evaluate if any of the DYRK genes is a tumor driver, we also analyzed the profiles of somatic mutations in tumor samples, following approaches previously described (Rubio-Perez, et al., 2015; Tamborero et al., 2013). These studies, and others, consider that a gene is a cancer driver if it bears signals of positive selection. Signals of positive selection are identified by means of the study of the pattern of accumulation of somatic mutations (including single-nucleotide variations [SNV] and small insertions/deletions [indels]) and how they deviate from models of expected random distribution of mutations. These methods are based on the assumption that mutations occurring in tumor driver genes provide survival advantages and are thus positively selected during carcinogenesis. Hence, this selection leaves "signals" that can be traced in tumor cohorts. Here, we used three different methods to reveal signals of positive selection to identify driver genes, following the pipeline used in (Rubio-Perez, et al., 2015) (Figure R.4A): OncodriveFM (Gonzalez-Perez and Lopez-Bigas, 2012), OncodriveCLUST (Tamborero et al., 2013) and MutSigCV (Lawrence et al., 2013). However, none of the DYRK family members had a mutation profile that could be computed with OncodriveCLUST in any cohort, since no recurring variant was found in any tumor type.

Among all the members of the family, *DYRK1A* was the only gene scoring for signals of positive selection (Figure R.4B). In particular, we obtained a significant score with OncodriveFM in three cohorts, corresponding to three different tumor types: liver hepatocellular carcinoma (LIHC), uterine corpus endometrial carcinoma (UCEC) and esophageal carcinoma (ESCA). Moreover, we found a further signal given by MutSigCV in UCEC (Figure R.4B)

The profile of somatic mutations provides also information on the putative function played by the tumor driver genes. In particular, oncogenes are often characterized by activating mutations clustering in specific residue positions (hotspots). On the contrary, tumor suppressor genes frequently

show a strong incidence of LoF mutations (frameshifts and nonsense), and they lack hotspots, with mutations more randomly distributed across the gene sequence (Davoli et al., 2013). As mentioned above, the analysis identifies the class I member DYRK1A as a putative tumor driver and furthermore, the profile of somatic mutations (Figure R.4C) indicates a potential tumor-suppressive role. This hypothesis is also supported by the DE results, which rendered a very clear trend for DYRK1A towards downregulation in tumor samples (Figure R.2A).

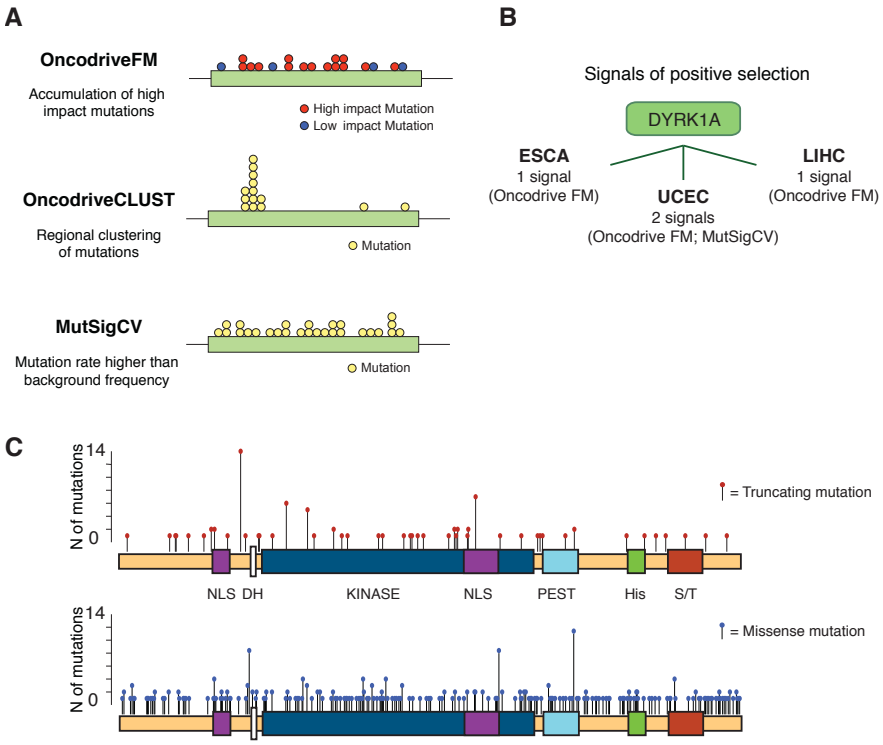

Figure R.4 DYRK1A shows signals of positive selection. A) Schematic description of the three methods used to detect signals of positive selection (see Materials and Methods). Adapted from (Tamborero, et al., 2013). **B**) DYRK1A showed signals of positive selection in three TCGA cohorts: liver hepatocellular carcinoma (LIHC), esophageal carcinoma (ESCA) and uterine corpus endometrial carcinoma (UCEC). **C**) Distribution of LoF mutations (upper scheme) and missense mutations (lower scheme) in DYRK1A reported in cBioPortal (April, 2019). Protein domains are indicated (see Figure I.2).

2. DYRK1A mutations identified in tumors are LoF

2.1 Generation of DYRK1A cancer variants for functional analysis

The outcome of the analysis of TCGA data suggested that loss of DYRK1A, by either down-regulation of at the mRNA level or gene mutation, is positively selected in cancer. However, no functional data on the DYRK1A somatic mutations was available, so the question was whether the amino acid changes negatively or positively affect DYRK1A activity.

We first looked at the mutations described at that moment and found that the proportion of LoF in DYRK1A was higher than expected. The number of DYRK1A somatic mutations has increased since then, and at the time of writing this Thesis manuscript, we manually curated a comprehensive list of DYRK1A cancer missense mutations by reviewing different cancer repositories and additional public data generated by cancer genomic studies. The list has been included in the manuscript as Annex II. Somatic mutations in DYRK1A gene include missense (77%), nonsense (12.5%) and indels resulting in frameshifting (8.8%). In the latter cases, most of the mutations are located before the end of the catalytic domain, and therefore they will generate truncated proteins devoid of catalytic activity. For the missense mutations, they are found all along the primary structure, including the non-catalytic N-terminus, the catalytic domain and the non-catalytic C-terminus.

To assess the impact that DYRK1A cancer-associated missense mutations observed in tumor tissues could have on DYRK1A activity, we selected a pool of 27 DYRK1A missense variants from cancer databases to perform functional assays (Table R.2). Most of the variants map in the catalytic domain, with some exceptions (Figure R.5 and Table R.2). In some cases, the mutation is found in several samples (E160K, R467Q, R559C), or the same residue mutated to different amino acids (S311F,

S311P, S311Y). Finally, many of the mutated residues are also mutated in other members of the DYRK family (Table R.2).

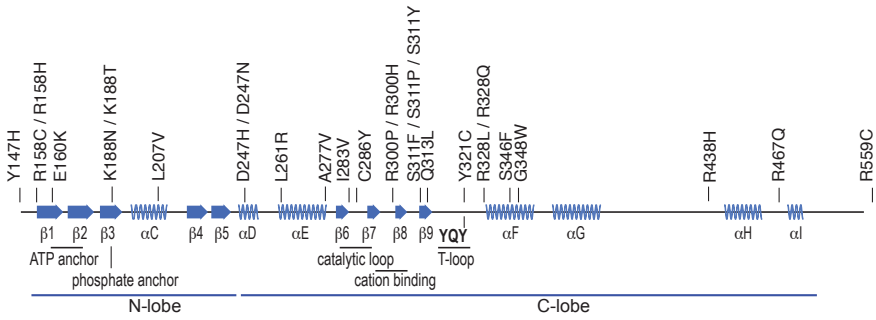

Figure R.5 Distribution of the selected DYRK1A cancer variants. 27 DYRK1A cancer-associated variants were selected among all the mutations found in cancer databases. Their distribution along the catalytic domain is shown. The scheme shows the secondary structure of the catalytic domain based on Protein Data Bank accession 2WO6.

Table R.2a Description of the selected DYRK1A cancer-associated variants.

DYRK1A Cancer Variants selected for functional screens				
Variant	**Cancer Tissue**	**Sample ID**	**Domain**	**Other DYRKs**
Y147H	Endometrium	TCGA-D1-A103	DH box	DYRK1A Y147C (2x) DYRK3 Y197C
R158H*	Ovary (cell line) Large intestine	TOV21 TCGA-AG-A002-01	Catalytic: beta 1	DYRK1B R110H (2x)
R158C	Stomach	TCGA-BR-8680		DYRK2 R221S
E160K	Large Intestine (5x) Bladder Endometrium (2x)	TCGA-AA-A00N DFCI_3549 Genentech 587376 TCGA-AG-A002-01 587376 TCGA-DK-A6AW-01 TCGA-A5-A2K5 TCGA-AX-A05S	Catalytic: beta 1	DYRK1A E160Q DYRK1B E112K (3x) DYRK3 E210K
K188N	Lung	MU11199963	Catalytic: ATP binding	DYRK1B K140T
K188T	Large intestine Large intestine (cell line)	DFCI_3010 HT115		DYRK3 K238N
L207V	Lung	TCGA-33-4533	Catalytic: alpha C	DYRK1A L207P/L207I
D247H	Endometrium	TCGA-FI-A2EW	Catalytic: alpha D	DYRK1B D199Y
D247N	Upper aerodigestive	TCGA-CR-5248		
L261R	Hematopoietic and Lymphoid	Broad_CLL007	Catalytic: alpha E	DYRK3 L311S
A277V	Ovary	OV207	Catalytic: alpha E	DYRK1A A277P DYRK1B A229S
I283V*	Ovary	TCGA-04-1338	Catalytic: beta 6	-
C286Y	Lung	TCGA-33-4586	Catalytic: catalytic-loop	DYRK1A C286F DYRK1B C238Y
R300H	Stomach	TCGA-HF-7132	Catalytic: beta 8	DYRK1A R300C (3x) DYRK1B R252H (3x)
R300P	Hematopoietic and Lymphoid	Broad_CLL045		DYRK3 R348C*/R348H (2x)
S311F	Skin	CSS-35-T	Catalytic: beta 9	DYRK1B S263Q
S311P	Endometrium (cell line)	EN		DYRK2 S372R
S311Y	Endometrium	TCGA-B5-A0JY		

DYRK1A Cancer Variants selected for functional screens				
Variant	**Cancer Tissue**	**Sample ID**	**Domain**	**Other DYRKs**
Q313L	Lung	TCGA-85-8070	Catalytic: beta 9	-
Y321C	Lung	Broad_LUAD-5V8LT	Catalytic: T-Loop	-
R328L	Endometrium	TCGA-A5-A0GH	Catalytic: P+1 Loop	DYRK1B R280H (2x)*
R328Q	Endometrium (3x)	TCGA-BS-A0UA-01 TCGA-A5-A0G1 TCGA-AP-A059		
	Endometrium (cell line)	HEC-59		
S346F	Large Intestine (cell line)	MDST8	Catalytic: alpha F	DYRK2 S407C
G348W	Skin	Broad_MEL-Ma-Mel-55	Catalytic: alpha F	DYRK1A G348R (2x)
	Lung	TCGA-05-4396		
R438H	Stomach	STC291	Catalytic: CMGC insert	DYRK1A R438C (2x)
R467Q	Large intestine (cell line)	HT115	Catalytic (Alpha I)	DYRK1B R419H
	Large intestine (2x)	T3024		
		DFCI_3024		DYRK2 R523C (2x)
	Endometrium (4x)	TCGA-BK-A6W3		
		TCGA-EO-A3AY		DYRK2 R523H (4x)*
		TCGA-EY-A1GD		
		TCGA-AP-A1E0		DYRK3 R510C*
	Hematopoietic and Lymphoid	DLBCL-RICOVER_174		
	Breast	MBCProject-ErfKfjto-Tumor-SM-AZ5GM		DYRK3 R510H*
	Upper aerodigestive	HKNPC-098-Tumor-SM-7CKA4		
R559C*	Large intestine (3x)	TCGA-AA-A010-01	Putative RanBPM BS	DYRK1A R559H*
		DFCI_335135		
		Genentech 587256		
	Large intestine (cell line) (2x)	LS180		
		SNUC2B		
	Brain	TCGA-06-5416-01		
	Urinary tract (3x)	WCM060_2		DYRK1B P508L
		WCM077_2		
		WCM231_2		
	Stomach	TCGA-VQ-A924		

*ExAC variant (exac.broadinstitue.org; (Lek et al., 2016))

Each of the 27 DYRK1A cancer variants were introduced into a vector to express HA-tagged DYRK1A by site-directed mutagenesis, to generate expression plasmids in mammalian cells that allow to screen them for their impact on protein functionality.

2.2. DYRK1A cancer variants negatively affect the enzymatic activity

Since DYRK1A is a protein kinase, the first functional screen aimed to determine the impact of the mutation on the enzymatic activity. Thus, HEK-293T cells were used as hosts for transient expression of DYRK1A WT and the cancer variants. The enzymatic activity was measured in anti-HA IPs used for IVK assays, and two different aspects were investigated in these assays. On the one hand, the ability to phosphorylate a substrate

peptide with a specific consensus sequence for DYRK kinases ("DYRKtide" (Himpel et al., 2000)) was assessed (Figure R.6A). On the other hand, the capacity of the DYRK1A mutants to autophosphorylate, either in *cis* or in *trans*, was also analyzed although to a smaller set of mutants (22 mutants) (Figure R.6A). In the former case, the amount of phosphorylated peptide was assessed by measuring the incorporated radioactive ATP using a scintillation counter (Figure R.6B), whereas autophosphorylated DYRK1A proteins were detected by SDS-PAGE and autoradiography (Figure R.6C). As shown in Figure R.6D, the experiments revealed a partial or total loss of enzymatic activity caused by most of the DYRK1A cancer variants screened; moreover, none of the mutants analyzed led to significant increased activity. Some of the variants presented an enzymatic activity close to that of the WT protein, as it was the case of R158H or R559C, which we later found to be variants present in the human population as they are collected in the ExAC database (Lek, et al., 2016). A correlation analysis showed that there was a positive correlation between the two types of enzymatic activity (Figure R.6E), suggesting that when the catalytic activity is altered, both aspects are affected in the same manner. Given the model of DYRK1A activation, the results might also indicate that the mutations affect the activation of the kinase preventing the authophosphorylation in the T-loop. Therefore, activity on substrate was chosen as the main assay to describe the whole group of DYRK1A variants.

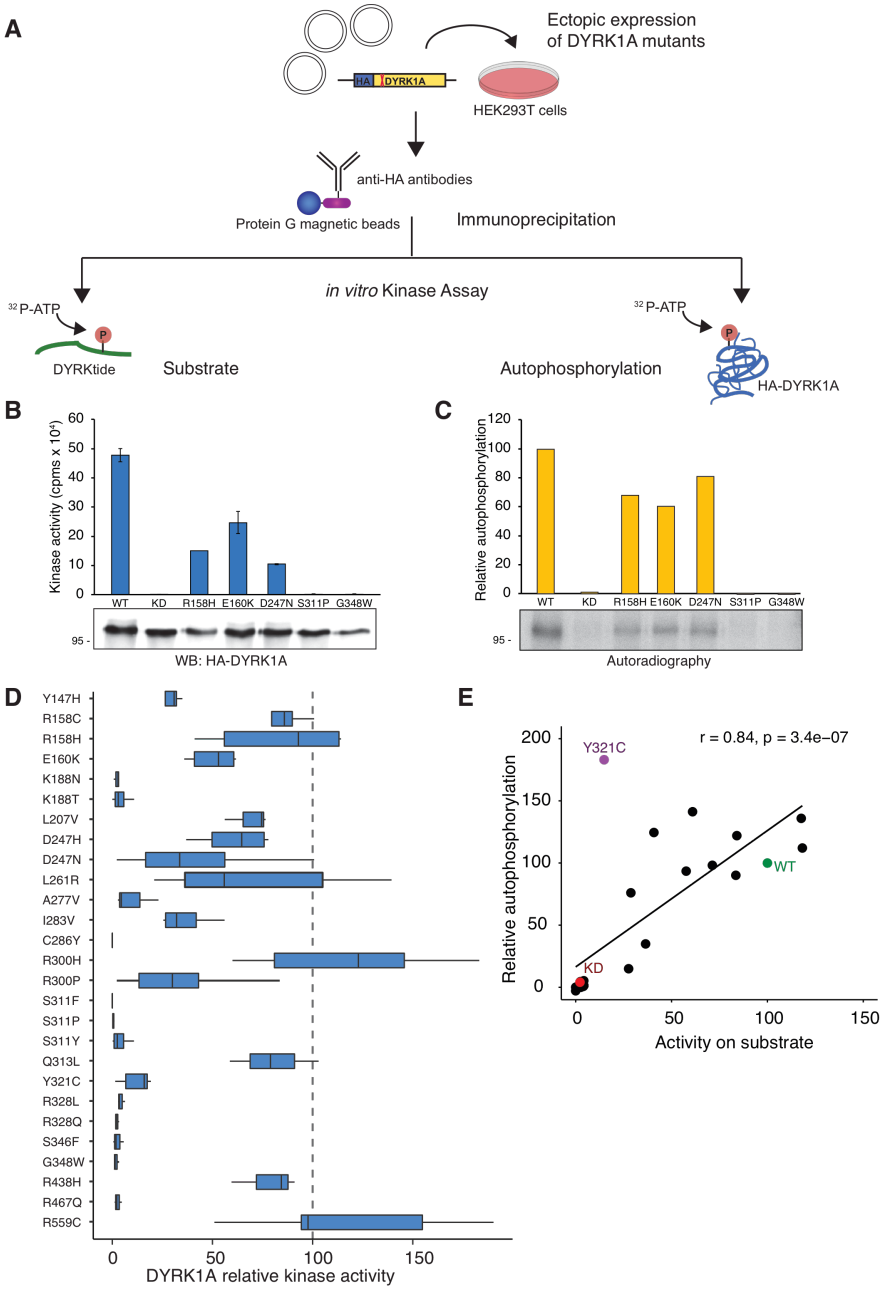
A
Ectopic expression
of DYRK1A mutants
HA
DYRK1A
HEK293T cells
anti-HA antibodies
Protein G magnetic beads
Immunoprecipitation
in vitro Kinase Assay
32 P-ATP
DYRKtide
Substrate
32 P-ATP
Autophosphorylation
HA-DYRK1A
B
Kinase activity (cpms x 10³)
WT KD R158H E160K D247N S311P G348W
95 -
WB: HA-DYRK1A
C
Relative autophosphorylation
WT KD R158H E160K D247N S311P G348W
95 -
Autoradiography
D
Y147H
R158C
R158H
E160K
K188N
K188T
L207V
D247H
D247N
L261R
A277V
I283V
C286Y
R300H
R300P
S311F
S311P
S311Y
Q313L
Y321C
R328L
R328Q
S346F
G348W
R438H
R467Q
R559C
DYRK1A relative kinase activity
E
r = 0.84, p = 3.4e−07
Y321C
WT
KD
Relative autophosphorylation
Activity on substrate

Figure R.6 DYRK1A cancer variants show partial or total loss of activity. A) Schematic representation of the screen. **B)** Substrate phosphorylation showing the results of a representative experiment, in which DYRK1A WT protein and a mutant in the ATP binding site (K188R, KD) are included. The plot shows radioactivity incorporation (cpms) into DYRKtide (mean ± SD of technical replicates). The amount of DYRK1A IP assessed by WB is shown in the lower panel. **C)** DYRK1A autophosphorylation showing the results of a representative experiment. The densitometric values of the autoradiography are plotted as percentages of the WT protein value, set as 100. **D)** Summary of the characterization of the DYRK1A catalytic activity on the DYRKtide substrate for each mutant: the radioactivity signals were normalized to the amount of DYRK1A detected in the IPs by anti-HA WB and plotted as a the percentage of the WT protein value, set as 100 (the dashed line marks this value). The box-plot represents the distribution of activity values from at least 3 independent experiments. **E)** Correlation between the relative values from the substrate phosphorylation assays and autosphosphorylation levels, normalized by setting the WT values as 100. The Spearman correlation coefficient and the *p*-value are shown. The values for DYRK1A WT, the kinase inactive mutant KD and the mutant Y321C are shown in colors.

The mutant Y321C deserves a special mention, since it was the only outlier, with a strong autophosphorylation rate, despite of a low activity on the exogenous substrate (Figure R.6E). As explained in the Introduction, Y321 is the residue of the activation loop that is autophosphorylated during the protein synthesis, and this event is required for full kinase activation (Himpel et al., 2001). Even though the retention of *in vitro* enzymatic activity for certain Y321 mutants (Y321H or Y321Q in contrast to the death kinase mutant Y321F) has already been shown (Adayev et al., 2007), it was quite surprising to observe such enhanced radioactive signal in the autophosphorylation assay (almost 2-fold of the WT protein). One possible interpretation of these results is that the substitution has altered the substrate specificity, and the kinase does not longer phosphorylate efficiently DYRKTide but it is able to phosphorylate other residues when it uses itself as substrate. Alternatively, the change might promote autophosphorylation events instead of the use of an exogenously substrate. Further experiments are required to explore the nature of the high autophosphorylation activity of the mutant Y321C and what happens to the kinase, from a biochemical point of view, when Y321 is mutated to different residues.

2.3. DYRK1A cancer variants negatively affect protein stability

Another important aspect to explore in order to determine whether DYRK1A cancer variants affect protein function is represented by the stability of the protein. Protein accumulation levels in live cells depend on many factors, including the rate of protein degradation and the intrinsic stability of the folded protein structure. This feature acquires special significance in the case of DYRK1A, which it is a dosage-sensitive gene, and little fluctuations in protein amounts strongly affect cell behavior (see Introduction).

To explore how the cancer variants affected the stability of the protein, the HA-tagged versions were expressed in HEK-293T cells together with a GFP-expressing vector to correct for transfection efficiency. The protein accumulation levels depend on the balance between protein synthesis and degradation rate. Given that the DYRK1A variants were ectopically expressed using the same vector and under the same experimental conditions, we attributed any change in the protein accumulation levels to variation in protein stability.

Total cell lysates were prepared 48 h post-transfection by resuspending the cell pellets in loading buffer to avoid interferences with changes in protein solubility, and the DYRK1A and GFP protein levels were assessed by WB (Figure R.7A and B). The results shown in Figure R.7C indicated that the mutations affect the stability of DYRK1A to different extent, but compared to DYRK1A WT, lower levels of protein accumulation were observed for most of the DYRK1A cancer mutants screened (Figure R.7C).

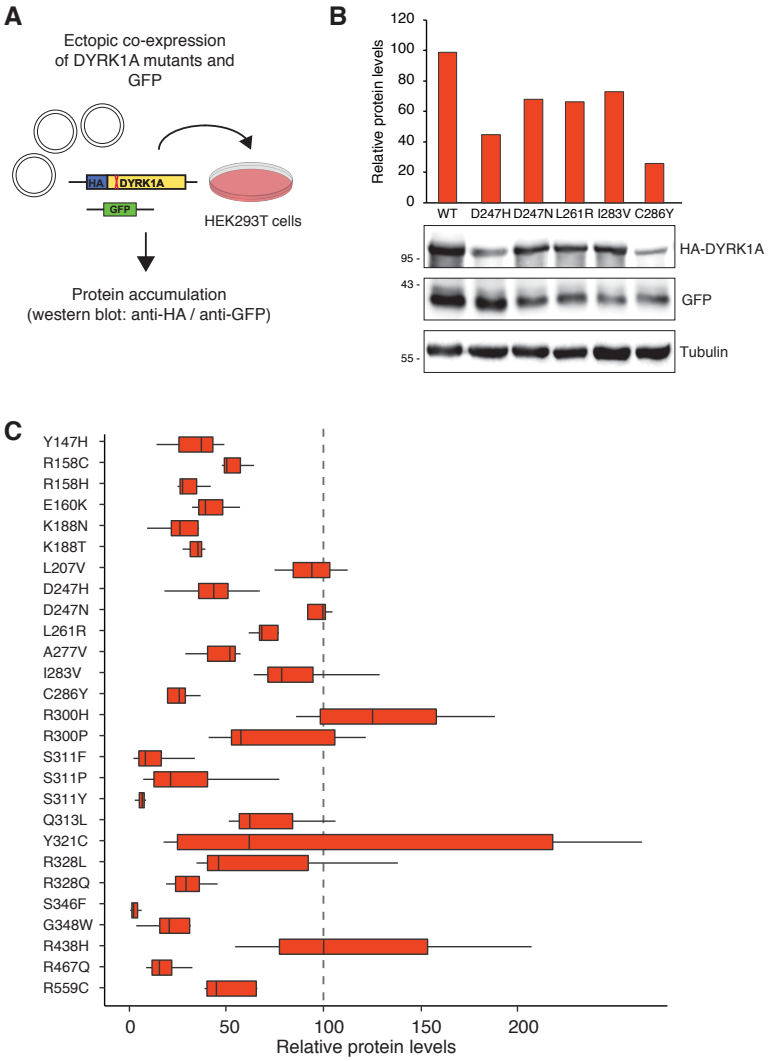

Figure R.7 DYRK1A cancer variants show reduced stability. A) Schematic representation of the screen. **B)** Results of a representative experiment: the values generated with the densitometric analysis of the anti-HA signals in the WB were corrected for transfection efficiency (anti-GFP WB) and plotted as percentages of the WT protein, set as 100. **C)** Summary of the characterization of the protein stability for each mutant: the accumulation levels were plotted as the percentage of the WT protein value, set as 100 (marked with a dashed line). The box-plot represents the distribution of activity values from at least 3 independent experiments

2.4. Changes in DYRK1A stability caused by cancer mutations are linked to aberrant folding and loss of activity

Missense mutations can lead to a switch in the thermodynamic properties of a protein and thus impair normal folding during protein synthesis. Misfolded proteins are more susceptible to degradation, thanks to cellular proteolytic systems that are sensitive to aberrant folding (reviewed in (Waters, 2001). To gain more insight about the thermodynamic contribution to the stability loss for DYRK1A cancer variants, we decided to use the FoldX program (foldxsuite.crg.eu/about). FoldX is a force field algorithm based on the calculation of free energy (ΔG) of macromolecules with a high-resolution 3D structure, which can be used to predict the impact of mutations in the folding and stability of proteins and nucleic acids (Guerois et al., 2002; Schymkowitz et al., 2005). Such effect is defined by the differential ΔG (ΔΔG); thus, negative values are associated with a gain in stability, whereas positive values mean a loss of stability.

Using available information on the DYRK1A crystal structure (Soundararajan et al., 2013), ΔΔG values were calculated using FoldX for DYRK1A cancer-associated variants and compared with the levels of protein accumulation obtained through the functional screens described above. The free energy variations for Y321C and R559C could not be computed because Y321 phosphorylation in the PDB file interfered with FoldX calculation, and because R559C was not included in the DYRK1A 3D structure (aa 127-485). A significant correlation between the FoldX-predicted values and the experimental ones was found (Figure R.8A; Spearman's test, *p*-value < 0.001), suggesting that FoldX represents a useful tool to predict the impact of DYRK1A cancer-associated mutations on DYRK1A protein stability. However, FoldX did not predict a high variation in free energy value for some of the low-stability variants (6 of the 17 examined). These findings could indicate that other factors might control DYRK1A stability, and the autophosphorylation of specific residues could be one of them since phosphorylation has a regulatory role in targeting proteins to ubiquitin-mediated degradation (Swaney et al.,

2013). In fact, DYRK1A autophosphorylation on S97 has been shown to regulate DYRK1A protein stability (Kii et al., 2016). In line with these results, we observed a positive correlation between kinase activity and protein accumulation for DYRK1A cancer-associated variants (Figure R.8B), supporting the hypothesis that DYRK1A activity and stability are functionally linked. It should be mentioned that such positive correlation has been also shown by our group when analyzing missense mutants identified in patients with DYRK1A haploinsufficiency syndrome (Arranz et al., 2019).

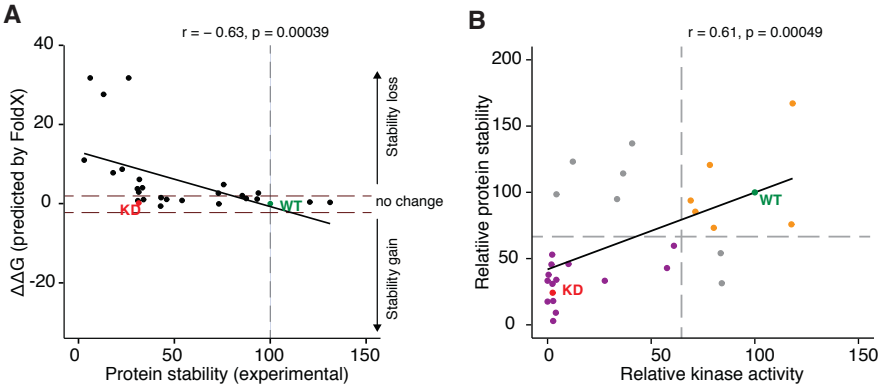

Figure R.8 The lower stability of DYRK1A cancer variants is linked to misfolding and loss of activity. A) Correlation analysis between the stability values obtained in the experimental tests and FoldX-predicted ΔΔG values. ΔΔG ≤ -1.5: gain of stability; ΔΔG ≥ 1.5: loss of stability; -1.5 < ΔΔG < 1.5: no effect. **B**) Correlation analysis between the kinase activity of the variants and their stability values. Three groups can be distinguished, WT-like mutants (orange dots) with activity and stability values close to 100%, LoF mutants (purple dots) with low activity and stability values, and mutants whose activity and stability do not correlate (grey dots). In **A** and **B**, the Spearman correlation coefficient and the *p*-value are shown.

In conclusion, these functional studies suggested that DYRK1A cancer mutations are LoF mutations, since most of the variants analyzed (21/27) led to impaired catalytic activity and/or reduced protein stability (Figure 9 and Table 3).

Table R.3 Summary of DYRK1A cancer variants activity and stability. LoF parameters set as: activity < 70% of WT, *p*-value < 0.01 and/or stability < 50% of WT, *p*-value < 0.01 (n ≥ 3 independent experiments, Student's *t*-test).

DYRK1A variant	Catalytic Activity		Protein Stability		LOF
	Mean (%)	*p*-value	Mean (%)	*p*-value	
WT	100	-	100	-	-
Y147H	28	4.98E-06	33	2.91E-03	YES
R158C	84	8.87E-02	54	8.77E-04	NO
R158H	84	0.275	31	2.08E-04	YES
E160K	58	1.83E-03	43	1.49E-03	YES
K188N	2	2.89E-08	31	8.71E-04	YES
K188T	4	1.53E-08	34	4.51E-05	YES
L207V	69	8.85E-03	94	0.598	YES
D247H	61	6.74E-03	43	1.31E-03	YES
D247N	41	2.40E-03	93	0.441	YES
L261R	71	0.289	85	0.321	NO
A277V	10	1.57E-04	46	3.46E-03	YES
I283V	36	1.03E-04	87	0.417	YES
C286Y	0	7.40E-18	23	3.50E-05	YES
R300H	118	0.369	131	0.226	NO
R300P	33	2.51E-04	76	0.167	YES
S311F	0	7.40E-18	13	1.81E-05	YES
S311P	0	4.52E-10	32	4.96E-03	YES
S311Y	4	1.64E-08	6	3.87E-10	YES
Q313L	80	0.197	73	0.185	NO
Y321C	12	8.65E-08	117	0.167	YES
R328L	4	8.94E-08	73	0.456	YES
R328Q	2	8.37E-09	31	1.88-05	YES
S346F	3	3.97E-07	3	6.38E-07	YES
G348W	2	2.33E-08	26	8.46E-04	YES
R438H	78	8.63E-02	121	0.672	NO
R467Q	3	8.73E-08	18	4.20E-06	YES
R559C	118	0.546	63	4.74E-02	NO

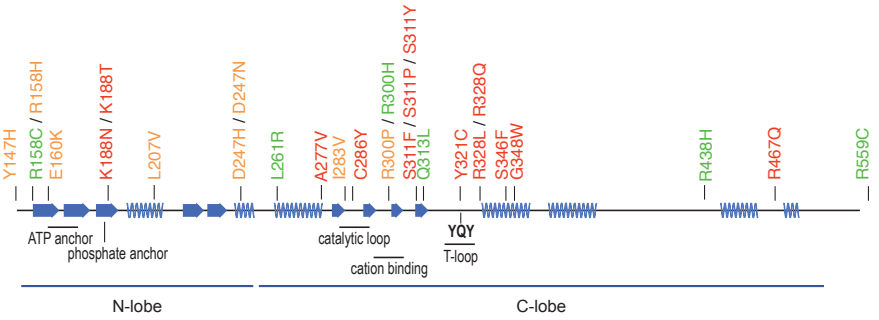

Figure R.9 DYRK1A cancer variants are LoF. Schematic representation of the results obtained in the functional screens. Color code: green = no significant effect; orange = partial effect on activity/stability; red = strong effect on activity/stability and total loss of enzymatic activity.

3. DYRK1A acts as a tumor suppressor in endometrial cancer cell lines

3.1. HEC59 and EN are heterozygous *DYRK1A*-mutated cell lines of endometrial carcinoma

According to the results obtained analyzing the TCGA data, DYRK1A emerged as a potential tumor driver. Among the three TCGA tumor types in which signals for positive selection were detected, Uterine Corpus Endometrial Carcinoma (UCEC) was the only set revealing two independent signals (Figure R.4B), and DYRK1A also showed reduced expression in UCEC tumor samples compared with paired healthy samples (Figure R.2A). In addition, by manually reviewing all DYRK1A mutations in cancer samples annotated in distinct cancer databases (Annex II), we provided additional clues supporting a role for this kinase as tumor driver in endometrial cancer. First, endometrial cancer shows the higher percentage of truncating mutations (nonsense and indels causing frameshift; Figure R.10), with all of them appearing before the end of the catalytic domain. Additionally, while DYRK1A missense mutations seem to map in equal proportion to the catalytic domain and the non-catalytic N- and C-terminal regions in cancer tissues (205 vs 192, 410 aa vs 403 aa), uterine cancer samples show a trend towards accumulation in the catalytic domain (38 vs 18). Finally, applying the

FoldX method to all the DYRK1A cancer variants mapping in the crystal structure of the kinase, we observed an enrichment of destabilizing mutations in uterine tumors, when compared with the tendency observed in the Pan-Cancer cohort (Table R.4).

Table R.4 DYRK1A missense mutations in cancer tissues. DYRK1A missense mutations reported in cancer databases where manually reviewed (Annex II). Numbers are indicated for each category. For the stability analysis, ΔΔG ≤ -1.5: gain of stability (GoS); ΔΔG ≥ 1.5: loss of stability (LoS); -1.5 < ΔΔG < 1.5: no effect.

Cancer Tissue	TOTAL	Domain		FoldX prediction		
		Catalytic	Non-Catalytic	LoS	No effect	GoS
PanCancer	397	205	192	47	64	1
Blood	25	16	9	5	9	0
Brain	12	4	8	2	2	0
Breast	19	6	13	2	4	0
Cervix	11	5	6	1	3	1
Kidney	4	2	2	1	1	0
Large Intestine	51	28	23	6	19	0
Liver	36	20	16	11	5	0
Lung	28	17	11	7	9	0
Ovary	5	3	2	1	2	0
Pancreas	7	2	5	1	2	0
Prostate	9	5	4	1	3	0
Skin	54	17	37	7	10	0
Stomach	26	19	7	10	8	0
Thyroid	3	0	3	0	0	0
Upper aero-dig	21	12	9	3	8	0
Urinary tract	20	8	12	4	3	0
Uterus	56	**38**	18	**23**	14	0
Others	10	3	7	3	0	0

Therefore, all this evidence pointed out endometrial cancer as a suitable model to investigate whether DYRK1A drives tumor formation and/or progression. To this purpose, we interrogated the CCLE (portals.broadinstitute.org/ccle; (Barretina et al., 2012)) and identified two endometrial cancer cell lines, HEC59 and EN, harboring missense mutations in the *DYRK1A* gene, which could be used as cellular models (Figure R.11).

HEC59 and EN are two cell lines isolated from the biopsies of two advanced, poorly differentiated, endometrioid adenocarcinomas taken from Japanese patients (Isaka et al., 2003). EN and HEC59 are heterozygous for *DYRK1A* point mutations that result in the protein variants S311P and R328Q, respectively. Both variants were included in the functional screens described in the previous section and both of them were LoF, with a complete loss of kinase activity (Figure R.6D).

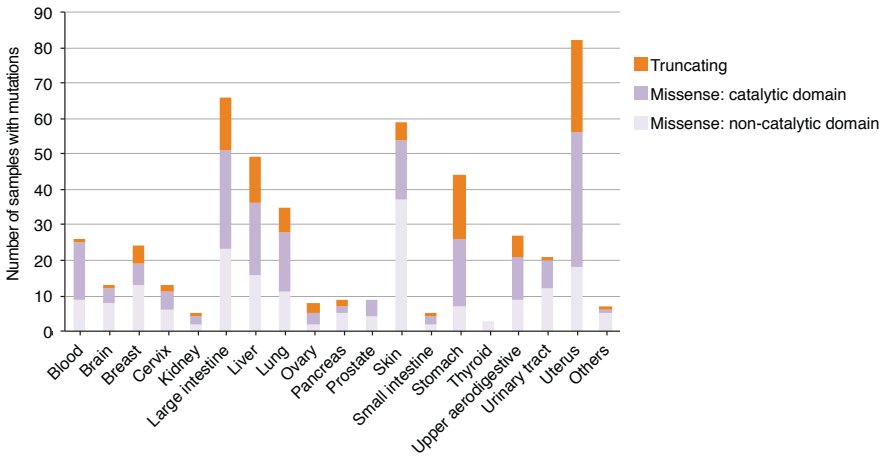

Figure. R.10 Distribution of *DYRK1A* cancer mutations across tissues. Number of cancer missense and truncating mutations collected across different cancer browsers (Annex II), across different tissues. Boundaries for the DYRK1A catalytic domain were set to aa 140-500, based on the results of kinase assays using truncated DYRK1A variants obtained by our laboratory and other groups (Arranz, et al., 2019; Himpel, et al., 2001)

The *DYRK1A* genotype was confirmed by sequencing the mutation site in the genomic DNA of both cell lines (Figure R.12A, upper panels). The expression of both alleles at mRNA, wt and mutated, was also confirmed by sequencing of the transcript (Figure R.12A, lower panels), and DYRK1A was expressed at the protein level, with its characteristic pattern of 3 bands (Figure R.12B). Finally, in order to confirm loss of function, IVK assays were performed on immunoprecipitated endogenous DYRK1A, which showed that the DYRK1A protein pool isolated from both HEC59 and EN cell lines had almost 50% of the catalytic activity when compared with HeLa cells, a *DYRK1A*$^{wt/wt}$ cervical carcinoma cell line (Figure R.12C), compatible with only the protein produced by the WT allele

having kinase activity. Thus, these results demonstrate that the alterations observed at the gene and transcript levels result in a LoF phenotype.

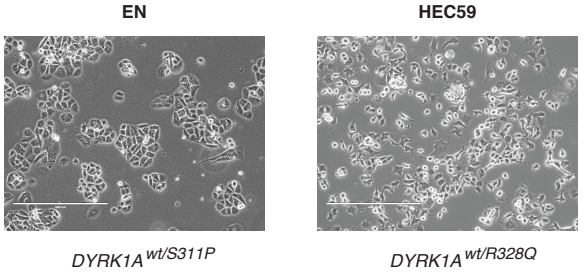

Figure R.11 EN and HEC59 are two DYRK1A-mutated endometrial carcinoma cell lines. Phase contrast photographs of EN and HEC59, two heterozygous *DYRK1A*-mutated endometrial carcinoma cell lines, carrying the missense mutations S311P and R328Q, respectively. Scale bar, 400 µm.

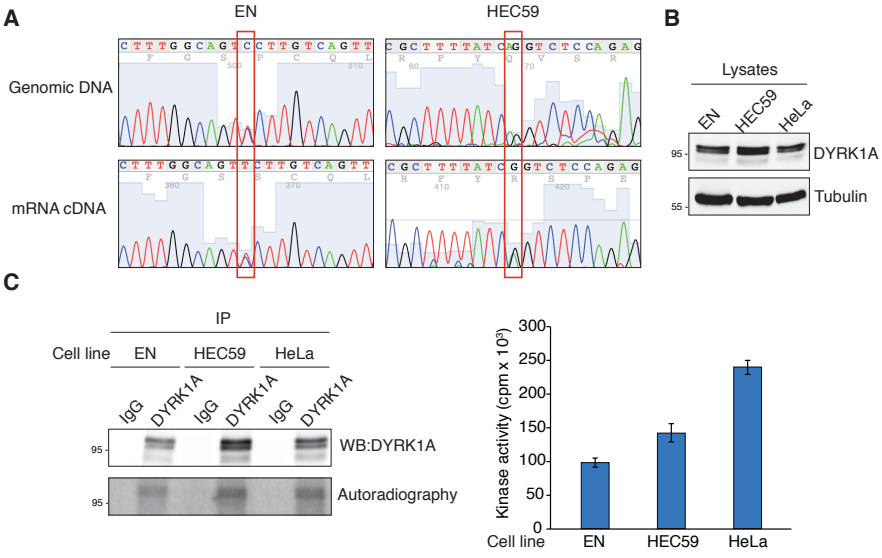

Figure R.12 Characterization of the endometrial cancer cell lines with mutations in *DYRK1A*. A) The *DYRK1A* mutation loci of EN and HEC59 cell lines were PCR-amplified using genomic DNA (upper panels) and total cDNA (lower panels) as templates, and sequenced. The heterozygous sequences are visible as two overlapping peaks, highlighted with a red square. **B)** The expression of DYRK1A in EN and HEC59 was assessed by WB. **C)** Functional validation of DYRK1A-functional loss in HEC59 and EN cell lines. Endogenous DYRK1A was IP and evaluated using IVK assays. HeLa cells were used as a *DYRK1A*$^{wt/wt}$ control cell line. Both the levels of authophosphorylation (left panel) and the ability to phosphorylate DYRKtide (right panel) were evaluated.

3.2. DYRK1A overexpression impairs proliferation of EN and HEC59 cells

After confirming that EN and HEC59 cells were *bona fide* DYRK1A-dysfunctional cancer models, the next experiments were aimed to investigate whether this loss of functional DYRK1A was responsible, or at least contribute, for the malignant phenotype in the two cell lines. To address this question, DYRK1A was ectopically expressed as a gain of function experiment. Cells were transduced with lentiviral vectors to express GFP-DYRK1A, to allow for selection of the DYRK1A expressing cells based on GFP detection. Thus, cells were FACS-sorted and screened in colony formation assays to assess for cell self-renewal ability (Figure R.13A). The expression of GFP-DYRK1A was confirmed by DYRK1A immunoblotting, using pre-sorted cell lysates (Figure R.13B). The experiments showed that overexpression of DYRK1A reduced colony formation in both HEC59 and EN compared with control cells (Figure R.13C-D).

3.3. A HEC59-derived *DYRK1A wt/wt* "reverted" clone shows reduced proliferation

3.3.1. CRISPR-based genome editing in endometrial cancer cell lines

Given that DYRK1A overexpression led to a strong reduction in the clonogenic capabilities of the two endometrial cancer cell lines, this could mean that restoring functional DYRK1A protein amounts led to an impairment in their proliferative ability. However, such effect could be the consequence of cell cycle perturbations due to a massive DYRK1A expression as described in other cell types, and based on a G1-arrest induced by DYRK1A-dependent degradation of Cyclin D1 (Chen et al., 2013). Therefore, another approach was explored. The strategy consisted in "correcting" the mutation on the *DYRK1A* gene to the WT sequence by targeted CRISPR/Cas9-mediated genome editing (Figure R.14A), restoring thereby a $DYRK1A^{wt/wt}$ genotype.

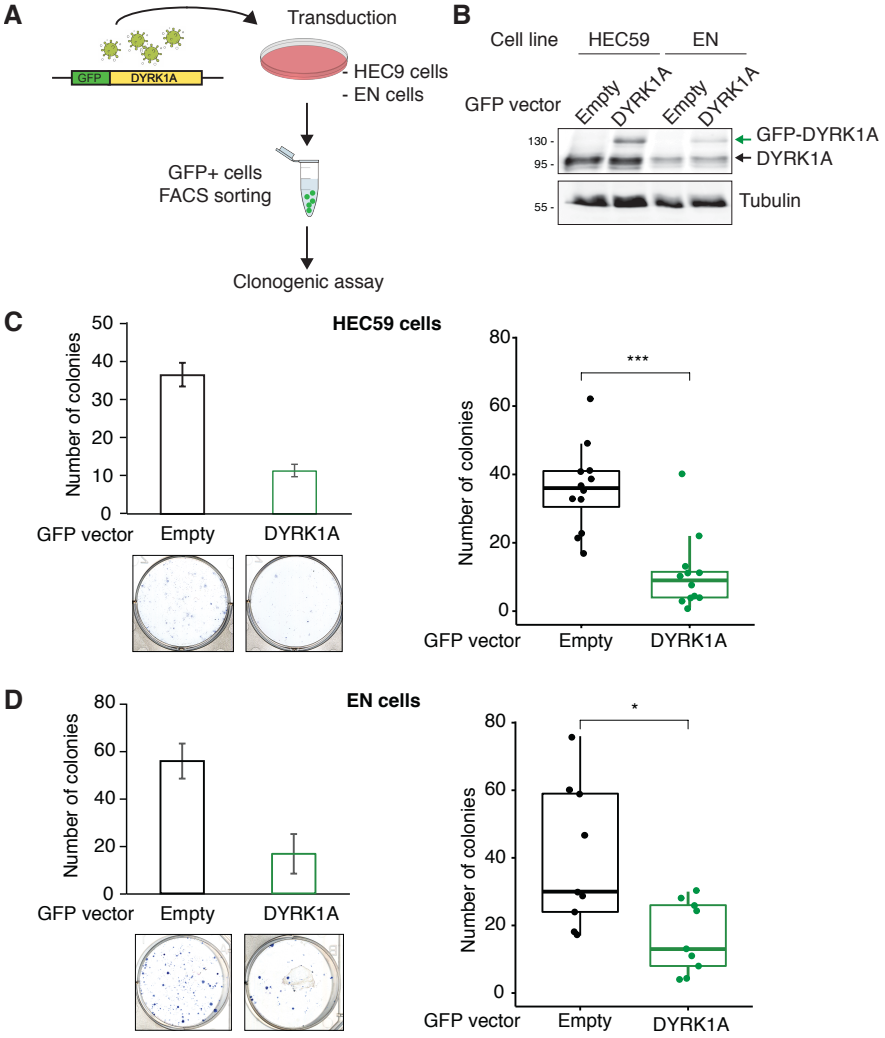

Figure R.13 DYRK1A overexpression reduces HEC59 and EN clonogenic capacity. A) Schematic representation of the experiment: HEC59 and EN cells were transduced with lentiviral particles to express a GFP-DYRK1A fusion protein or with a bicistronic lentivector to express DYRK1A and GFP. GFP+ cells were FACS-sorted and seeded for clonogenic assays. **B)** WB of total lysates of the transduced cells to check DYRK1A overexpression prior to sorting. A 130 kDa band corresponding to the molecular weight of the GFP-DYRK1A fusion protein appears in both EN and HEC59 extracts, confirming ectopic expression. **C, D)** Colony formation assays for HEC59 (**C**) and EN (**D**). The barplots (left) show quantification of a representative experiment (mean ± SD of experimental triplicates). Boxplots (right) were generated by plotting results from n = 3 independent experiments. The medians were compared with a two-tailed unpaired Mann-Whitney test (*, $p \leq 0.05$; ***, $p \leq 0.001$).

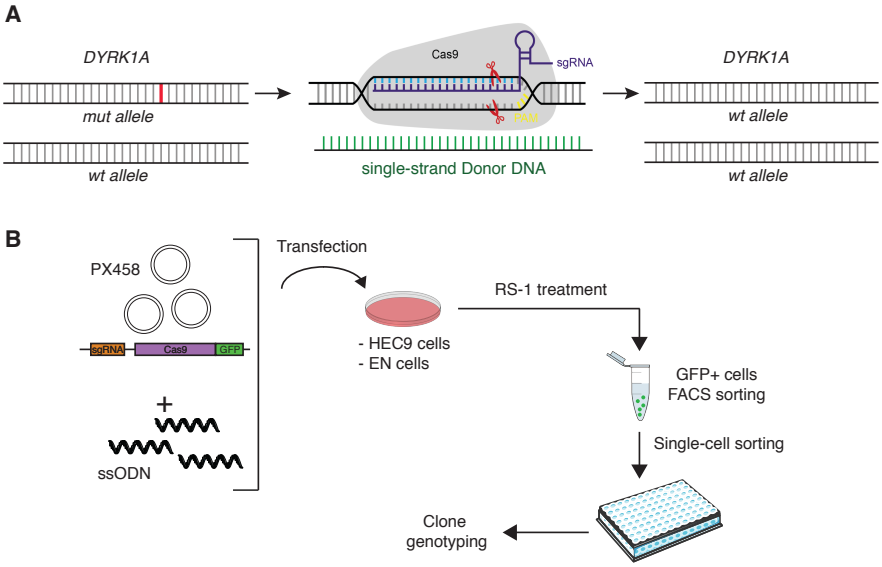

Figure R.14 Genome "correction" to *DYRK1A*$^{wt/wt}$ in endometrial cancer cell lines. **A)** Design of the CRISPR/Cas9-based strategy to revert DYRK1A-mutated alleles to wt in HEC59 ad EN cell lines. **B)** Scheme for the experimental procedure: HEC59 and EN cells were transfected with sgRNA-Cas9-GFP expressing vectors and a specific ssODN. GFP-expressing cells were FACS-sorted in MW96 plates at single-cell density. After colony growth, the clones were genotyped.

EN and HEC59 cells were transfected with a sgRNA-Cas9 vector and the ssODN (see Materials and Methods for details). The RS-1 drug is a RAD51 stimulator (Jayathilaka et al., 2008), and it was added to the cells to increase the frequency of homologous recombination events (Song et al., 2016). Next, GFP+ cells were sorted and clones were grown individually and screened to identify positive "reverted" clones with a *DYRK1A*$^{wt/wt}$ genotype (Figure R.14B).

After the first unsuccessful screens, the procedure was improved trying to increase the knock-in efficiency and also to set up a faster and easier screening protocol. Furthermore, HEC59 was selected as the only cell model for genome editing, since EN cells resulted very difficult to manipulate, due to their slow growth and the low percentage of clone recovering after cell sorting and single-cell plating. Thus, a new ssODN was designed for HEC59 *DYRK1A* gene editing with several modifications. First, phophorothioate bonds were introduced at both

boundaries, to increase the knock-in efficiency and precision (Renaud et al., 2016). Second, additional sequence modifications were introduced aimed to introduce silent mutations in the HEC59 genome to: i) disrupt the PAM sequence, therefore preventing further cleavage events after correct editing, and ii) change the restriction profile of the genome locus, which allowed clone screening by restriction digestion (Figure R.15A-B; details are found in the Materials and Methods section). Figure R.15B shows an example of one of the screens to identify positive clones. One of the clones (#123.B2) showed a restriction pattern that suggested the occurrence of a correct knock-in (Figure R.15B). Hence, we proceeded to further validation through genomic DNA locus sequencing and functional assays.

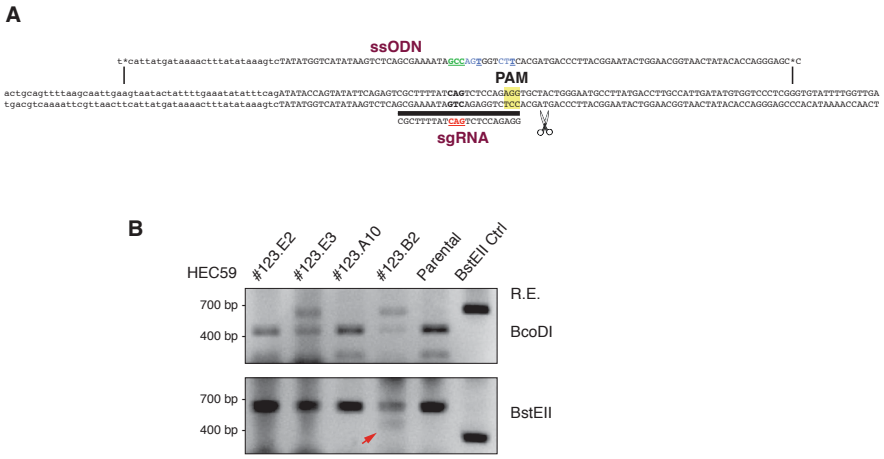

Figure R.15 Modification of the CRISPR-cas9 genome editing to increase precise knock-in efficiency and speed up the screening step. A) Structure of the new ssODN for precise HEC59 genome-editing. The sgRNA mapping on the *DYRK1A*-mutated allele is represented and the target PAM is also highlighted. The WT codon sequence is shown in green and additional mutations are indicated in blue. **B)** Example of a screening with BcoDI and BstEII restriction enzymes. The mutation site was amplified with PCR and the digested product with the indicated enzymes are loaded in 1% agarose gel. The parental HEC59 cell line and a BstEII positive control are also loaded. The #123.B2 clone shows the expected profile of a positive-reverted clone (the cleavage by BstEII enzyme generated the fragment indicated with the red arrow).

3.3.2. The HEC59-derived clone #123.B2 is a *DYRK1A*$^{wt/wt}$ reverted clone

Correct genome editing and a restored *DYRK1A*$^{wt/wt}$ genotype in the HEC59-derived clone #123.B2, with the incorporation of the additional silent mutations included in the ssODN, was confirmed by genomic DNA and transcript sequencing (Figure R.16A). Next, to determine if the reverted genotype was linked to a gain in DYRK1A activity, an IVK assay was performed on immunoprecipitated endogenous DYRK1A proteins, which showed that the DYRK1A protein obtained from #123.B2 presented a 2-fold increase in substrate phosphorylation capacity compared with the activity levels of parental HEC59 DYRK1A (Figure R.16B-C), confirming that the reversion was also occurring at the functional level.

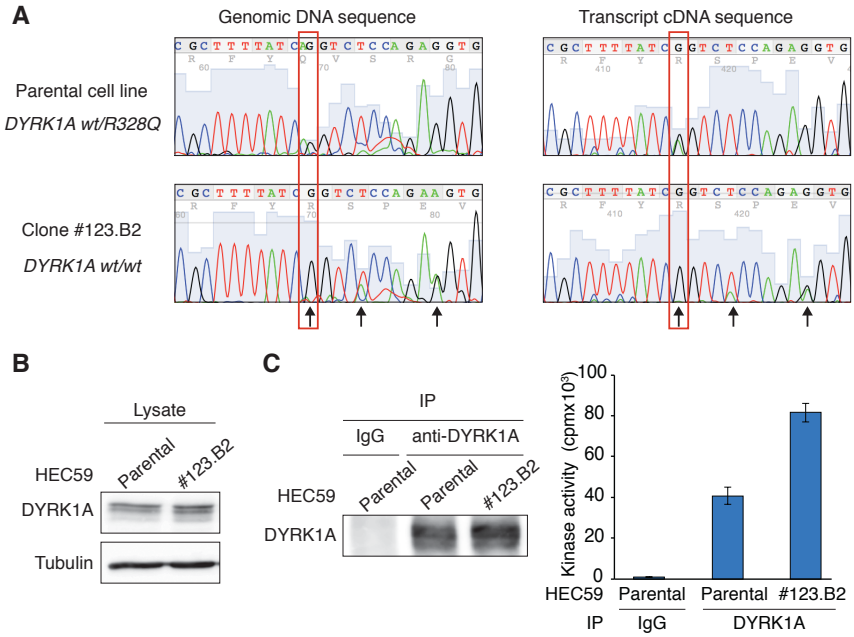

Figure R.16 HEC59-derived clone #123.B2 is a positive, functionally restored, *DYRK1A wt/wt* clone. A) Genomic and cDNA sequencing of the mutation site of HEC59 #123.B2 clone confirms the reverted *DYRK1A*$^{wt/wt}$ genotype (the reverted nucleotide is indicated in the red square). Additional mutations incorporated through the engineered ssODN are indicated with black arrows. **B)** Expression analysis of DYRK1A by WB in the indicated clones. **C)** Functional validation of the activity gain in the reverted clone: the IVK was performed using immunoprecipitated DYRK1A from HEC59 parental cells and its derived clone #123.B2 on DYRKtide. The bar graph shows a representative experiment (mean ± SD of triplicates).

3.3.3. The HEC59 reverted clone exhibits reduced proliferation

Next, we aimed to assess whether restoring a *DYRK1A*$^{wt/wt}$ genotype caused any changes in the behavior of HEC59 cancer cells, focusing on their proliferation ability. Clonogenic assays revealed that the HEC59 #123.B2 clone had a diminished clonogenicity, compared with the parental HEC59 cells, with a 7-fold reduction in colony formation (Figure R.17A). The reduced proliferation rate was also observed in cumulative growth experiments, although to a less extent (Figure R.17B). These results indicate that the gain of the full DYRK1A content has a negative impact on the proliferation of the tumor cells.

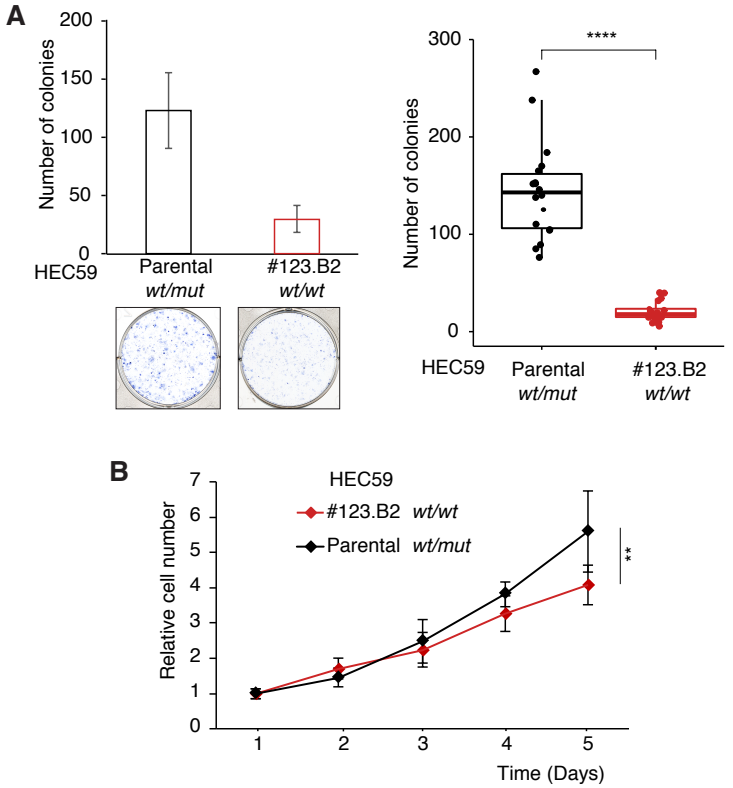

Figure R.17 HEC59-derived *DYRK1A*$^{wt/wt}$ clone shows reduced proliferation. A) Colony formation assay using parental HEC59 and its derived #123.B2 clone: the bar-plot (left) shows colony quantification from a representative experiment (mean ± SD of experimental triplicates); the box-plot (right) was generated with results from n = 6 independent experiments in triplicates (****, p ≤ 0.0001, Mann-Whitney test). **B)** Cumulative growth curve of parental HEC59 and its derived #123.B2 clone: the cell numbers at day 1 were set to 1 (mean ± SD, n = 3 independent experiments; **, p ≤ 0.01, Student's *t*-test, only comparisons at day 5 are shown).

3.3.4. Non-edited HEC59-derived CRISPR clones do not show differences in proliferation

To reinforce the proposal that reduced proliferation was specifically due to functional DYRK1A gain in HEC59-derived clone #123.B2, another clone, which did not undergo genome editing in the *DYRK1A* locus (parental-like), was isolated and characterized. As shown in Figure R.18, the *DYRK1A* genotype of the HEC59-derived clone #123.D5 was the same as the parental cell line (Figure R.18A), and in agreement, no changes were observed in the kinase activity levels associated to the endogenous protein (Figure R.18B).

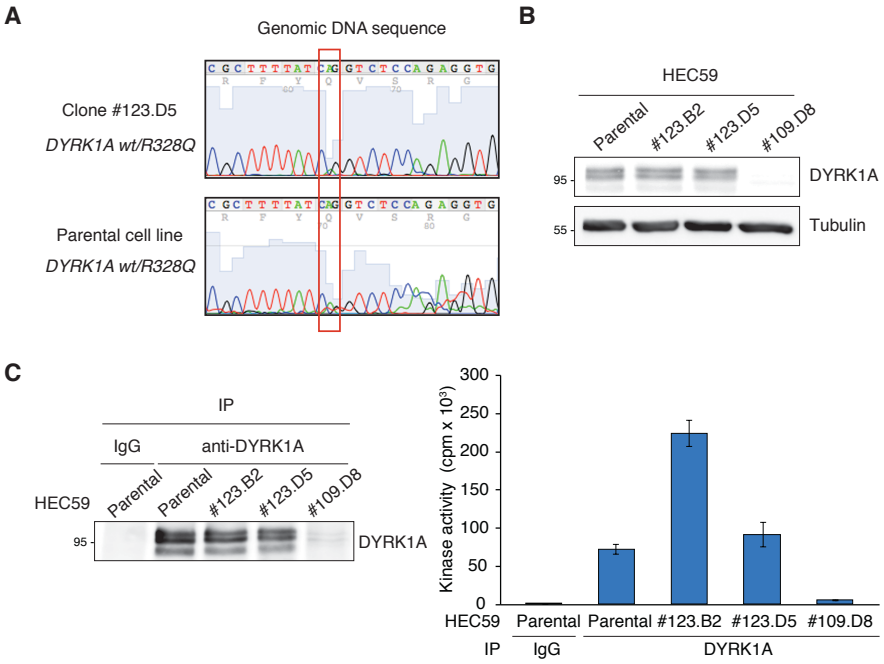

Figure R.18 Characterization of HEC59-derived CRISPR/Cas9 clones. A) Genomic and cDNA sequencing of the parental HEC59 cell line and the parental-like clone #123.D5 (*DYRK1A*$^{wt/R328Q}$). **B)** Expression analysis of DYRK1A by WB in the indicated HEC59-derived clones: #123.B2, *DYRK1A*$^{wt/wt}$; #123.D5, *DYRK1A*$^{wt/R328Q}$; #123.D8, *DYRK1A*$^{mur/R328Q}$. **C)** Functional validation of HEC59 CRISPR clones. Endogenous DYRK1A was immunoprecipitated and assessed by Western blot (left) and IVK assays on DYRKtide (right). The bar graph shows a representative experiment (mean ± SD of triplicates).

The characterization of HEC59 clone #123.D5 showed that it displayed a significant increase in colony formation capacity compared with the parental cell line in clonogenic assays (Figure R.19A), with no significant differences in cumulative growth assays (Figure R.19B).

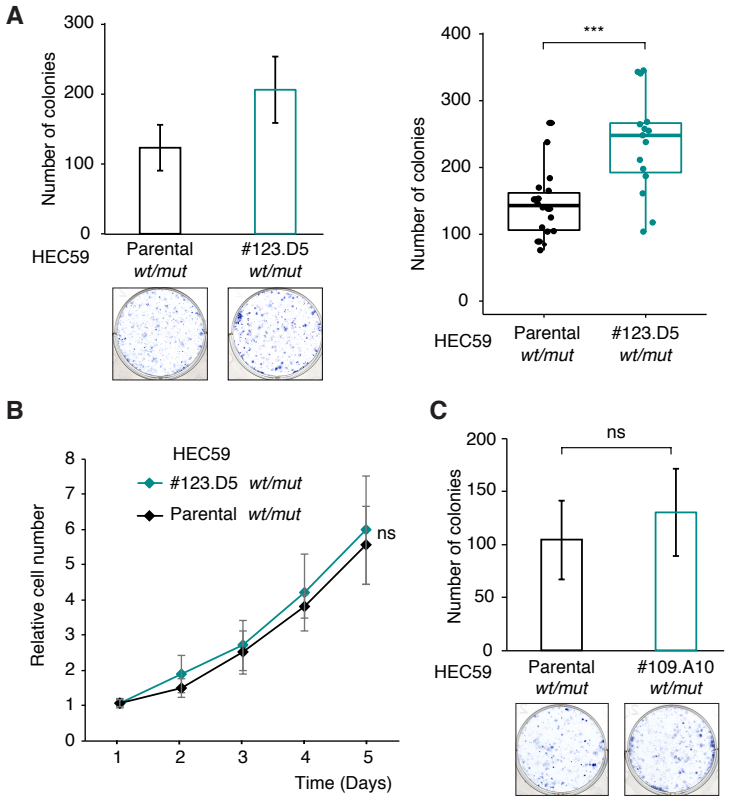

Figure R.19 Proliferation capabilities of HEC59 parental-like clones (*DYRK1A*$^{wt/R328Q}$). **A)** Colony formation assay using parental HEC59 and its derived clone #123.D5. The bar-plot (left) shows colony quantification from a representative experiment (mean ± SD of triplicates); the box-plot (right) was generated with results from n = 5 independent experiments, in triplicates (***p ≤ 0.001, Mann-Whitney test). **B)** Cumulative growth curve of parental HEC59 and its derived #123.D5 clone, in which the cell numbers at day 1 were set to 1 (mean ± SD of n = 3 independent experiments; ns = not significant, Student's t-test, only comparisons at day 5 are shown). **C)** Colony formation assay using parental HEC59 and its derived clone #109.A10. The bar-plot was generated with results from n = 2 independent experiments, in triplicates (ns = not significant, Mann-Whitney test).

Cancer cell lines are heterogeneous biological systems. Their behavior is therefore the result of each cell contribution, which is closely linked to the genetic and epigenetic changes accumulated during cell culture and

manipulation. Such variance can never be completely recapitulated by single clones isolated from the cell line itself. Hence, we argued that the small difference observed in colony formation capacity between the parental HEC59 cell line and the parental-like clone #123.D5 might be clone-specific. To confirm this hypothesis, we isolated an alternative parental-like clone from the CRISPR screen to perform additional clonogenic assays. The clone #109.A10 did not show any sequence modification on the mutated *DYRK1A* locus and kinase assays confirmed a parental-like enzymatic potential (data not shown). When assayed in clonogenic assays, this parental-like clone showed a proliferative capacity similar to the parental HEC59 (Figure R.19C), suggesting that the differences observed in clone #123.D5 could either be due to HEC59 cellular heterogeneity or to off-target effects induced by the CRISPR procedure. Nevertheless, we think that the fact that "parental-like" clones did not show diminished clonogenic capabilities provide robust evidence supporting that the proliferative deficiency displayed by the reverted clone is actually due to the restored *DYRK1A*$^{wt/wt}$ genotype.

3.3.5. HEC59-derived clones deficient for DYRK1A show increased clonogenicity

As shown by the genomic analysis, HEC59 cells are heterozygous for the LoF mutation R328Q. The data deposited in several cancer databases consulted indicate that heterozygosity is a recurrent condition in DYRK1A-mutated cancer samples, and we did not find any case indicative of loss of heterozygosity. Our working hypothesis is that DYRK1A haploinsufficiency is sufficient to promote tumor progression. The absence of tumor samples with total depletion of DYRK1A could mean that retention of functional DYRK1A, albeit reduced, is essential for the cancer cell viability; alternatively, total DYRK1A depletion might not provide further advantage to cancer cells and it does not undergo positive selection. To explore these possibilities, we posed to characterize the behavior of homozygous, DYRK1A functional knock-out (KO) cells. Thus, we isolated HEC59-derived clones that went through "incorrect" editing

events on both alleles during the CRISPR screen, mostly due to Non-Homologous-End-Joining (NHEJ) DNA repair activity, which is error-prone and tends to generate frameshifts (Ceccaldi et al., 2016).

Two independent clones were isolated, #109.D8 and #109.G5, and their genomic identity confirmed by sequencing of the mutated locus (data not shown), which indicated that they were homozygous for truncating mutations. These results were in agreement with the lack of detectable DYRK1A protein expression or associated-kinase activity (Figure R.18B-C, for #109.D8). The two clones showed increased clonogenic capabilities in comparison with the parental HEC59 cells (Figure R.20A and C), although no significant differences were observed in cumulative growth curves (Figure R.20B for #109.D8). These results suggested that total loss of DYRK1A enhances the proliferative/survival capacity of HEC59, when assayed in single-cell colony formation, but it does not affect global proliferation rate.

The outcome of these experiments do not explain why DYRK1A homozygous mutations or LOH events have not been found in cancer samples, which is the expectation by considering the strong increase in clonogenic capacity. These findings thus raise the interesting possibility that the loss of DYRK1A in tumors has distinct effects than those observed in tumor cell models, and further suggest that DYRK1A depletion may affect the behavior of the neoplastic cells in the tumor niche.

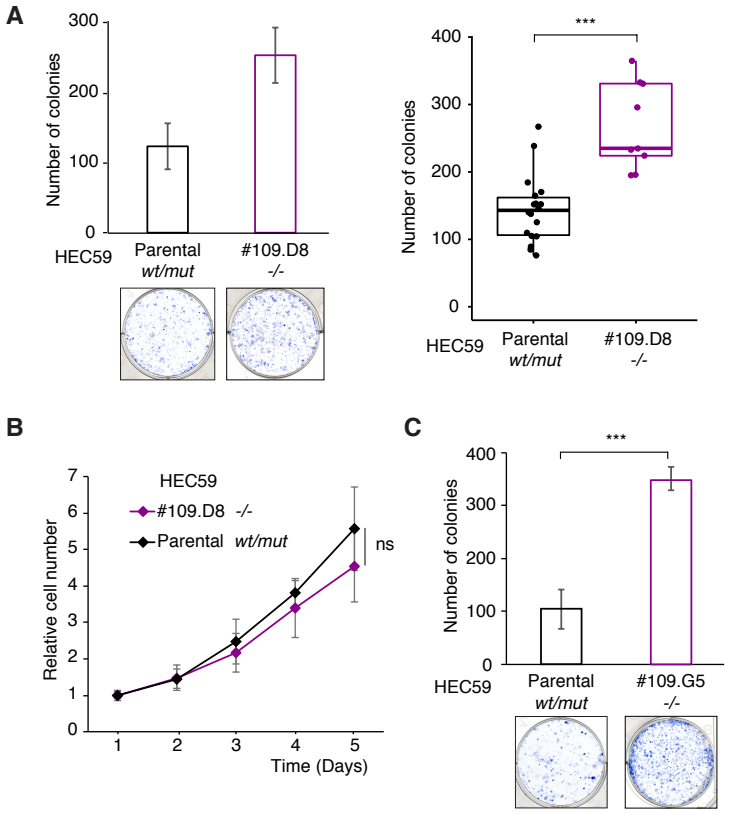

Figure R.20 Characterization of HEC59-derived DYRK1A KO (*DYRK1A*$^{-/-}$) clones. A) Colony formation assay using parental HEC59 and its derived clone #109.D8. The bar-plot (left) shows colony quantification from a representative experiment (mean ± SD of triplicates); the box-plot (right) was generated with results from n = 3 independent experiments, in triplicates (***p ≤ 0.001, Mann-Whitney test). **B)** Cumulative growth curve of parental HEC59 and its derived #109.D8 clone, in which the cell numbers at day 1 were set to 1 (n = 2 independent experiments; ns = not significant, Student's t-test, only comparisons at day 5 are shown). **C)** Colony formation assay using parental HEC59 and its derived clone #109.G5. The bar-plot was generated with results from n = 2 independent experiments, in triplicates (***p ≤ 0.001, Mann-Whitney test).

3.4. The HEC59-derived DYRK1A reverted clone shows increased sub-G1 cell population

Activated cell cycle progression and repressed apoptotic program are hallmarks of cancer cells. Among the cellular factors that have been found phosphorylated and thereby modulated by DYRK1A, are critical regulators of both processes, such as p53, Cyclin D1, p27^{Kip1} or Caspase 9 (Chen, et al., 2013; Park et al., 2010; Seifert et al., 2008; Soppa et al.,

2014). In this regard, the results shown in Figure R.17 indicated that reversion of DYRK1A to a WT status induced a reduction in clonogenic assays and, to a lesser extent, in cumulative growth. These effects could be the result of alterations in cell proliferation and/or survival. To test this hypothesis, the cell cycle profile of the HEC59-derived *DYRK1A*$^{wt/wt}$ clone was monitored and compared with that of parental HEC59 cells. The flow cytometric analysis showed no significant differences in any of the phases of the cell cycle (Figure R.21A), suggesting that the DYRK1A reversion does not causes major changes in cell cycle progression in this cellular context. Therefore, we speculated that reduction in the cell numbers could be due to decreased cell viability. This possibility was assessed by measuring the sub-G1 population by FACs analysis. As shown in Figure R.21B, the DYRK1A$^{wt/wt}$ cells (#123.B2) showed a significant increment in the sub-G1 population when compared with the parental HEC59 cells, indicating that restoring normal DYRK1A levels led to increased cell death. Interestingly, the HEC59-derived clone deficient in DYRK1A (#109.D89) displayed an opposite trend, with a reduction in cell death (Figure R.21B). Of note, this type of assay does not allow to discriminate between different types of cellular death; thus, we cannot ascribe the differences in the sub-G1 population to alterations in the apoptotic program or necrotic processes. Together, these data suggest that restoring a normal functional DYRK1A protein dosage in the endometroid carcinoma HEC59 cells either enhanced the response to programmed cell death or reduced the overall cell fitness, leading to an increment in the non-viable cell fraction. Notably, this effect appears to correlate with variations in the DYRK1A dosage, with the total loss of DYRK1A having a protective effect. The alteration in the survival potential in response to the DYRK1A dosage would explain, at least in part, the results of the clonogenic assays with the different clones.

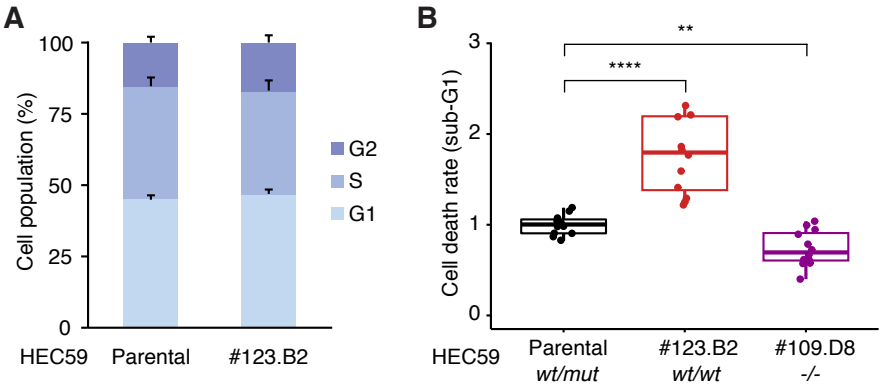

Figure R.21 The HEC59-derived clones with DYRK1A dosage modifications show differences in cell death rate. **A)** Flow cytometry analysis of cell cycle phases in parental HEC59 and the reverted *DYRK1A*$^{wt/wt}$ #123.B2 clone. The graph shows mean ± SD of n = 2 independent experiments. **B**) Flow cytometry analysis of the sub-G1 population in parental HEC59, the reverted #123.B2 clone and the KO #109.D8 clone. The percentage of the sub-G1 values was normalized to the values of the parental cell line set as 1. The graph shows the results of 3 independent experiments performed in triplicate.

3.5. Alteration of DYRK1A dosage in endometroid tumor cells affects tumor growth *in vivo*

The results obtained so far with the endometrial cancer cellular models suggest that restoring functional DYRK1A expression in DYRK1A-deficient endometrial cancer cell lines leads to impaired proliferative capacity (Figure R.17) most likely linked to decreased cell survival (Figure R.21), suggesting a role for DYRK1A as tumor suppressor in this biological context. To evaluate DYRK1A contribution to tumor formation and progression, we decided to analyze the behavior of the HEC59-derived cell lines with different dosage of DYRK1A in mouse xenografts. Although we are aware of the limitations of tumor xenograft models by using immunocompromised animals and the growth of the cells outside the proper tumor environment, we thought that this type of experiments might provide information beyond the tumor cell itself growing in controlled tissue culture conditions. The HEC59 parental cell line and the genome-edited clones were inoculated subcutaneously into the flanks of nude mice, and the tumor growth followed. Tumors generated by the polyclonal HEC59 cells behaved similarly to the tumors derived from the

parental-like clone #123.D5. On the contrary, xenografts of the HEC59-derived clone with the reversion in DYRK1A showed a clear growth delay and a strong reduction in the size of the tumors at the experiment end-point (Figure R.22A-C, clone #123.B2). Strikingly, and in contrast to the phenotype observed in the cell cultures assays, xenografts derived from the clone deficient in *DYRK1A* showed a slower tumor growth compared to the parental cell line (Figure R.22A-C, clone #123.D8), indicating that the total loss of DYRK1A in the tumor cells represents an unfavorable condition for the tumor proliferation in animal hosts, and further suggesting defects in the cross-talk of these cells with the tumor microenvironment.

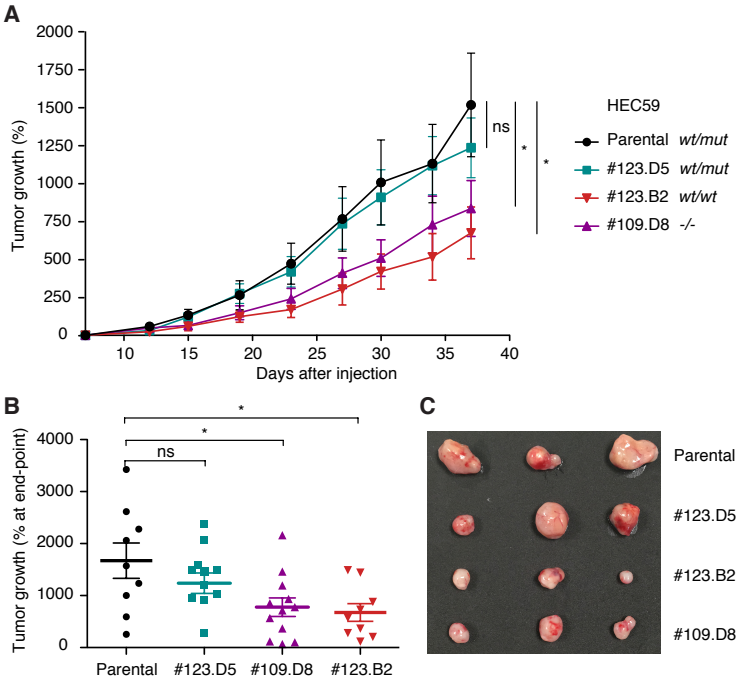

Figure R.22 Characterization of the tumor growth of HEC59 and its derived clones with different dosages of DYRK1A. **A)** Follow-up of tumor growth after subcutaneous inoculation in nude mice of the HEC59 parental cell line and its derived clones. The tumor volumes were measured and normalized by the first-point value (set as 0). The graph shows mean ± SEM of n = 12 tumors per group. For the statistical analysis only comparisons at day 35 are shown (*p ≤ 0.05, ns = not significant, Mann-Whitney test). **B)** Plot representing relative tumor growth values at end-point (day 35). The graph shows mean ± SEM of n=12 (*p≤0.05, ns= not significant, Mann-Whitney test). **C)** Photographs showing three representative tumors for each clone taken after sacrifice and tumor removal.

4. An integrated proteomic-transcriptomic analysis reveals enhanced STAT1 activation and an interferon signaling pathway signature in the HEC59-derived DYRK1A-WT clone

4.1. Proteome profiling of *DYRK1A*$^{wt/wt}$ and *DYRK1A*$^{-/-}$ HEC59 clones reveals a DYRK1A dose-dependent enrichment in type I Interferon (IFN-I) response factors

To gain further insight on the molecular changes provoked by the restoration of DYRK1A-WT in the HEC59-derived #123.B2 clone, we implemented a proteomic approach based on free-label quantitative MS to evaluate whether differential protein expression could provide some clues on the biological mechanisms responsible for the observed changes in phenotype. The HEC59-derived DYRK1A-KO clone #109.D8 was also included in the analysis to monitor changes in global proteome linked to a complete loss of DYRK1A. Total protein extracts were prepared in quadruplicates and all samples were analyzed by LC-MS/MS. A total of 4,525 proteins were identified in the experiment, including DYRK1A, which was absent in the DYRK1A-KO clone. PCA revealed that the proteome of each clone cluster tightly and is distinct from the others (Figure R.23A), indicating that each clone possesses a unique proteome signature. The analysis rendered a total number of 259 proteins that were up-regulated or down-regulated in the HEC59-derived clones when compared with the parental protein profile (Figure R.23B). GO enrichment analysis showed no particular enrichment for the downregulated proteins in the DYRK1A-WT clone or the upregulated ones in the DYRK1A-KO clone. However, enrichment in Type I Interferon (IFN-I) signaling-related GO terms in the upregulated group in the DYRK1A WT cells and the downregulated group in the DYRK1A-KO cells when compared with the parental HEC59 cells was observed (Figure R.23C), which includes downstream targets of the pathway such as MX1, OAS2, OAS3, or

ISG15. IFN signaling has been extensively described as a master regulatory network modulating immune cells, mostly in response to microbial and viral infection, stimulating anti-proliferative transcriptional programs (Gonzalez-Navajas et al., 2012). IFNs exhibit important antineoplastic effects, reflecting both direct antiproliferative responses mediated by IFN receptors expressed on malignant cells, as well as indirect immunomodulatory effects (Borden, 2019; Dunn et al., 2006; Fish and Platanias, 2014). Lack of several key effectors of the IFN signaling cascade has been observed in different type of tumors, which has led to the proposal that loss of responsiveness to IFNs may be a critical component of the host response to tumors (Cheon et al., 2014).

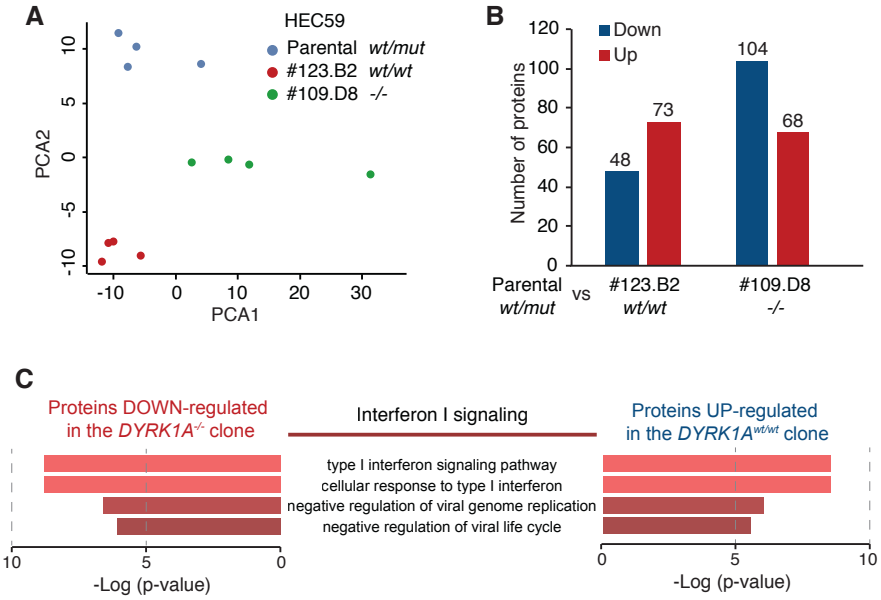

Figure R.23 Proteomic analysis of HEC59 parental cells and its derived *DYRK1A*-edited clones. A) Principal component analysis of the proteomic data. Four replicates for each condition were used. **B)** Number of differentially expressed proteins in the *DYRK1A*-edited clones in comparison to the HEC59 parental cells. Threshold: log2FC ≤ -0.7 (downregulated) or log2FC ≥ 0.7 (upregulated) and adjusted *p*-value < 0.01. The proteins detected in one of the clones but absent in the parental cells (or *vice versa*) were also included. **C)** GO term analysis of the differentially abundant protein indicated in the *DYRK1A*-edited clones, ranked by *p*-values according to the Enrich-R software (Kuleshov et al., 2016).

Therefore, the results obtained with the proteome analysis defined the protein expression profiles of the HEC59 DYRK1A-edited clones and provided new hints on molecular changes caused by variations in functional DYRK1A protein abundance, as it is the case of proteins encoded by IFN-responsive genes (Figure R.23C).

4.2. DYRK1A gain drives STAT1 activation and coherent IFN-response gene expression in HEC59 cells

The changes observed at the protein level could be due to gene expression changes, to post-transcriptional regulatory mechanisms, or both. To explore these possibilities, we generated a phospho-proteomic profile to identify gain/loss of phosphorylation events in the DYRK1A-modified HEC59 clones. The analysis yielded more than 6,000 unique phosphosites identified, mapping to 2,441 proteins.

Hierarchical cluster analysis highlighted different groups of unique phosphorylation events, with distinct patterns across the three different conditions (Figure R.24A). To better understand which groups of phospho-events could be directly or indirectly boosted by DYRK1A activity, we focused the analysis on those clusters whose intensity changed following a “DYRK1A-increasing-dosage” (DID) pattern, i.e. showing increased phosphorylation from the DYRK1A (-) null condition (KO clone) to the normal DYRK1A amount (+/+) condition, represented by the reverted clone, with the parental HEC59 cells serving as an intermediate (+/-) state (Figure R.24A). The phosphorylation of S727 of Signal transducer and activator of transcription 1 (STAT1) was identified as one of these events (Figure R.24B). STAT proteins are the ultimate effectors of IFN and other crucial signaling pathways, getting activated through phosphorylation, which in turn allows their translocation to the nucleus and the promotion of the transcription of specific gene signatures (Ivashkiv and Donlin, 2014; Majoros et al., 2017). STAT1 is phosphorylated by different upstream kinases, in response to several types of extracellular signals; multiple phosphorylation sites have been identified, but phosphorylation of Y701 represents the key activation event

and phosphorylation of S727 is also required for full transcriptional activity (Horvath, 2000; Wen et al., 1995).

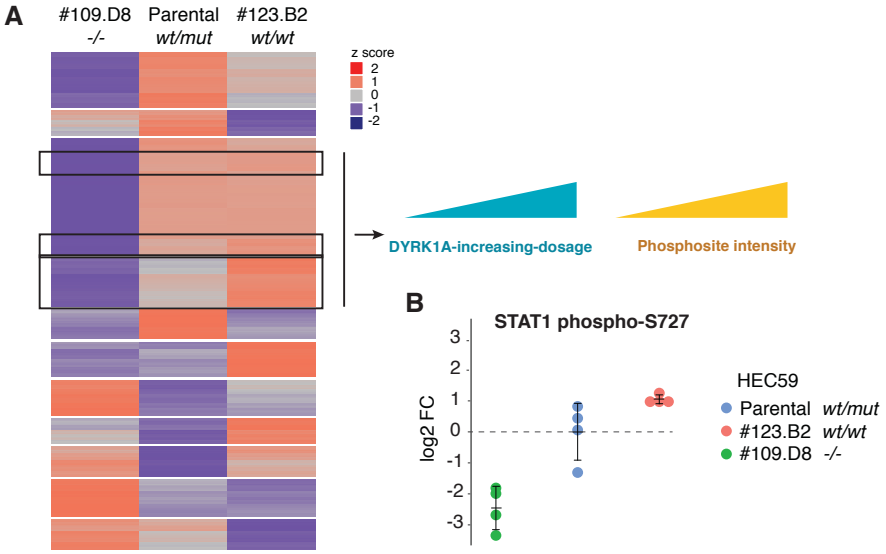

Figure R.24 Phospho-proteome profiling of HEC59 *DYRK1A*-edited clones. A) Hierarchical cluster analysis of unique phosphorylation events (peptides); only peptides detected in at least two of the four replicates in both parental and reverted clone were used. The median intensity of the replicates in each condition was z-scored and coloured as shown in the scale bar. The cluster responding to DYRK1A dosage is marked with squares. **B)** STAT1 p-Ser727 log2(FC) in reverted #123.B2clone, Parental cells and KO #109.D8 clone, normalized to parental values (mean of parental condition replicates set as 1). The graph also includes the mean ± SD for each group.

To assess whether the changes in activated STAT1 had consequences at the transcriptional level, we integrated the proteomic and phospho-proteomic data with RNA-Seq data. The analysis showed that the DYRK1A-WT and -KO clones had profound changes in transcript abundances when compared with HEC59 parental cells. Intriguingly, total loss of DYRK1A led to more dramatic gene expression rewiring than that associated to the gain in DYRK1A (Figure R.25A). Following the same criteria as for the phospho-proteomic analysis, we zoomed into those genes that appeared to have a DID-like behavior (increasing from DYRK1A-KO clone to DYRK1A-WT clone) to determine which transcriptional programs were boosted by increased DYRK1A dosage (Figure R.25B). Notably, ChEA analysis indicated that the DID-cluster is

indeed enriched in STAT1 and STAT2 targets (Figure R.25C, upper panel). In agreement, GO terms analysis unveiled a significant enrichment for IFN signaling-associated genes (Figure R.25C, lower panel), providing additional robustness to our results.

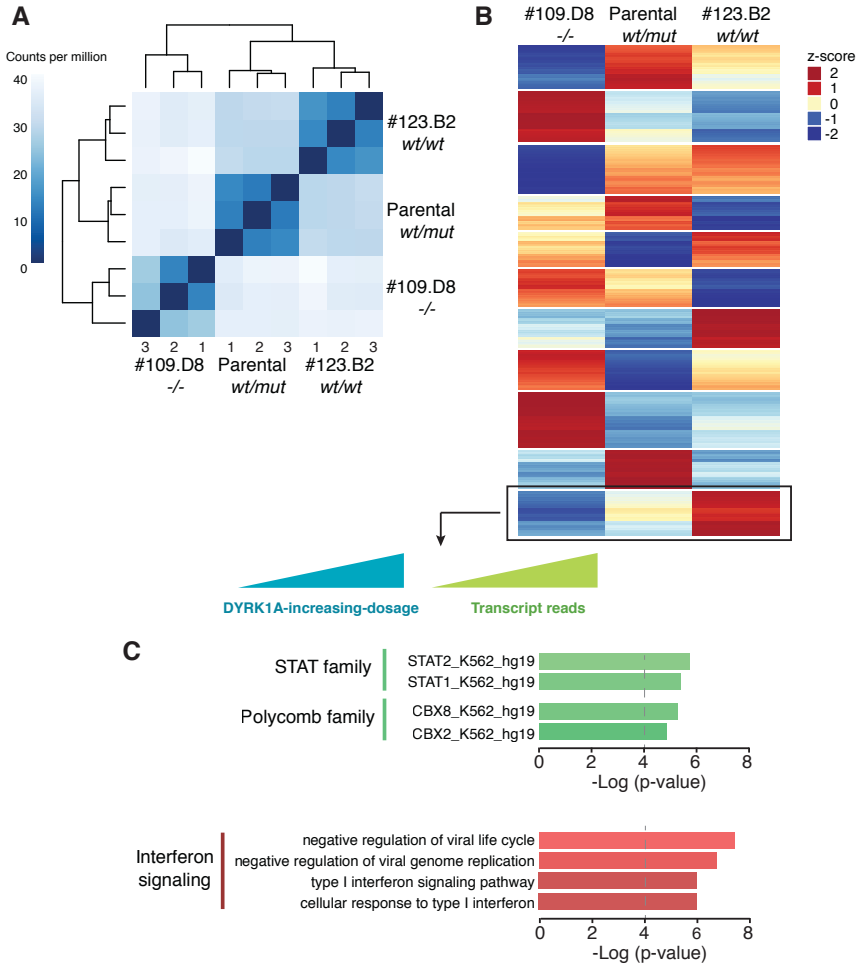

Figure R.25 Gene expression analysis of HEC59 *DYRK1A*-edited clones. A) Correlation heatmap of the different biological replicates used for the RNA-seq analysis. Euclidean distance was calculated across replicates; this analysis gives an overview over similarities and dissimilarities between samples. **B**) Genes were grouped into eleven clusters on the basis of the similarity of expression (clustering type: K-means clustering). The DYRK1A-increasing dosage (DID) cluster is marked with a square. The median intensity of the three biological replicates in each condition was z-scored and coloured as shown in the scale bar. **C**) Analysis of the transcription factor enrichment based on ENCODE ChIP-seq data (upper panel) and of GO Terms Biological Processes enrichment (lower panel) of the genes extracted from the DID cluster, filtered for those showed adjusted *p*-value < 0.01. The EnrichR web browser was used.

In summary, the integrated transciptomic/proteomic/phospho-proteomic study performed on the HEC59 parental cell line and the *DYRK1A*-edited derived clones has uncovered multiple molecular changes, generated by the sole *DYRK1A* gene correction/deletion. Moreover, we identified a DYRK1A dosage-dependent event affecting IFN-I signaling, which is most likely mediated by STAT1 activation. The link between DYRK1A gain/loss and the IFN signaling response and whether this interplay is responsible for the observed anti-proliferative effect caused by functional DYRK1A restoration in HEC59 cells, remain to be elucidated.

Discussion

1. Identification of DYRK family members as potential tumor drivers

The aim of this Thesis project was to dissect the potential of DYRK protein kinases as molecular tumor drivers in specific tumor contexts. Although isolated reports had revealed altered expression of single DYRK members in tumors, this study represents the first comprehensive research effort of multi-type alterations of the whole DYRK family of kinases in cancer samples.

As a parallel project of my PhD, I also carried out a study in collaboration with Cristina Fillat's group (IDIBAPS, Barcelona), where we investigated the role of DYRK1A and DYRK1B in pancreatic cancer. The article, published in *Gut* journal in October 2018, has been included in this manuscript as Annex I, and it will be discussed in-depth in the following sections.

Although the Thesis work focused on DYRK1A, we also provide initial evidence that other two members of the DYRK family of kinases, DYRK1B and DYRK2, may function as tumor drivers in several cancer types. More specifically, they show a tendency towards gene amplification and overexpression in specific tumor types, indicating a potential role for these two kinases as oncogenic factors.

1.1. DYRK1B is amplified in tumors and plays pro-tumorigenic functions in pancreatic cancer

By looking at the tumor/healthy DE analysis, *DYRK1B* turned out to be overexpressed in BLCA, UCEC, PRAD, KICH, KIRP, THCA, BRCA, LIHC and KIRC (Figure R.2B). Amplification of the *DYRK1B* genomic region with coherent overexpression was observed in BLCA, BRCA, LUSC, SARC, CESC, OV and PAAD (Figure R.3B). The last 4 tumor cohorts were not in the DE analysis, since the number of paired healthy-tumor samples did not pass the threshold used, so no correlations could be established; however, the results indicate that overexpression in BRCA and BLCA could be due to gene amplification

(Figure R.3B-C). Our analysis confirms previously reported *DYRK1B* amplification/overexpression in ovarian cancer (Gao et al., 2009) and pancreatic cancer (Deng et al., 2006), and *DYRK1B* upregulation in breast tumor tissues (Chen et al., 2017). Moreover, we provide additional information on a potential oncogenic role played by *DYRK1B* in other tumor tissue types such as uterus (UCEC), bladder (BLCA), kidney (KICH, KIRP and KIRC), liver (LIHC) and thyroid (THCA). However, experimental work is needed to confirm *DYRK1B* overexpression in independent cohorts and to study how it contributes to tumorigenesis in these biological contexts. In the case of pancreatic ductal adenocarcinoma (PDAC), we provide further experimental data by using the cell line PANC-1, which presents 19q13.2 amplification (Kuuselo et al., 2007; Miwa et al., 1996), and overexpresses DYRK1B (Deng, et al., 2006). We demonstrate that *DYRK1B* knockdown drastically reduced cell proliferation, motility and invasion in this cell line (Luna et al., 2018)(Annex I). These results suggest that targeting DYRK1B in *DYRK1B*-overexpressing pancreatic tumors might represent a good therapeutic strategy. We also show that treatment of PANC-1 with the DYRK inhibitor harmine strongly reduced cell proliferation and tumor growth in the *Ela-myc* PDAC mouse model (Luna, et al., 2018)(Annex I). Given that harmine targets both DYRK1A and DYRK1B (Bain et al., 2007), the inhibitor-dependent antitumor effects could be the consequence of DYRK1A inhibition, DYRK1B inhibition, or both. Although specific DYRK1B inhibitors not targeting DYRK1A, or *vice versa*, would be needed to evaluate the independent effects of each kinase, the dual targeting ability could be also envisaged as an advantage for treating tumors with overexpression of the two class I kinases.

1.2. DYRK2 is a potential oncogene

Another member of the DYRK family that deserves additional consideration is DYRK2. Compared with the respective healthy tissues, we found *DYRK2* overexpressed in 8 tumor cohorts: BRCA, STAD,

LIHC, BLCA, KIRC, LUAD, LUSC, ESCA and KIRP (Figure R.2C). Analysis of CNAs demonstrated that the up-regulation is associated with gene amplification in BRCA, LUAD, LUSC, BLCA and STAD. Significant *DYRK2*-overexpression was also observed in OV, SKCN, SARC and HNSC (Figure R.3C). As for *DYRK1B*, the results of the analysis of the TCGA cohorts are consistent with previous reports that showed *DYRK2* amplification/overexpression in different cohorts of esophageal carcinoma, lung adenocarcinoma (Miller et al., 2003) and gastric adenocarcinoma (Gorringe et al., 2005). The BRCA cohort is included among the TCGA cohorts where *DYRK2* is found upregulated (Fig R.2C); of note, several publications have studied the role played by DYRK2 in breast cancer with conflicting results. Our results may indicate that *DYRK2* amplification/overexpression is positively selected in breast cancer cells. This hypothesis would be in agreement with the pro-tumorigenic role proposed by previous studies, which showed that DYRK2 inhibition impaired cell proliferation and breast tumor growth (Banerjee et al., 2018; Guo et al., 2016). However, no evidence of increased *DYRK2* expression was provided in these works. On the contrary, Taira and colleagues reported decreased protein expression levels in tissue microarrays of several tumor types, including breast, even though no statistical analysis is provided, and increased tumorigenic potential when *DYRK2* was silenced. These authors did show significant correlation between low levels of DYRK2 expression and tumor aggressiveness (Taira et al., 2012). These results are not necessarily in discordancy with our findings, since we did not consider differences in tumor stages or grade of malignancy in the analysis of the TCGA data; moreover, we analyzed exclusively RNA-Seq data, which could mean that transcript levels might be not recapitulated by protein staining. Finally, although the research works mentioned above showed opposite outputs of *DYRK2* silencing, it should be observed that different cell lines were used, thus suggesting that DYRK2 oncogenic or tumor suppressive function in breast cancer may depend on the genetic background of the breast cancer cells.

Further lines of investigation are required to study in-depth how DYRK1B and DYRK2 participate in cancer-promoting processes.

2. DYRK1A cancer-associated mutations are LoF

DYRK1A was identified as a putative tumor driver with multiple methods of analysis of somatic mutation patterns (Figure R.4B), and it was found downregulated at the transcript level in most of the TCGA tumor cohorts considered (Figure R.2A). These results suggest that the loss of DYRK1A either by inactivating mutations or by reduction in expression could be selected in tumor cells. In this regard, it is worth noticing that *DYRK1A* belongs to a class of genes defined as LoF-intolerant by the ExAC large-scale study, which collected and reviewed exome and whole sequencing data from more than 60,000 human samples (Lek et al., 2016). The result is extremely interesting, since it may indicate that different genetic and molecular landscapes create the conditions that allow a higher mutation burden on *DYRK1A* gene in cancer cells. In other words, while DYRK1A LoF is poorly tolerated at the germline level, it may be not only well tolerated in tumor cells but positively selected, as indicated by the results obtained with computational methods (Figure R.4C). Indeed, by comparing the profile of DYRK1A missense variants obtained from the ExAC browser and the pattern of DYRK1A cancer-associated variants, it is evident that the overall mutation frequency is lower in the normal population and the distribution of the variants in the coding sequence is different (Figure D.1). Amino acid changes reported in ExAC are localized mainly in the non-catalytic C-terminal part of the protein, with fewer changes mapping in the catalytic domain (Figure D.1), indicating that most residues in this domain are important for protein functionality. Of note, the only variant annotated as LoF is a change affecting a splice donor site (not included in the figure), which would affect the splicing of the last coding exon. On the contrary, nonsense mutations and frameshit indels in tumor samples are accumulated within the N-terminus and the

kinase domain (Figure R.4C), suggesting positive selection for truncation-causing changes, whereas missense mutations are distributed quite homogeneously along the protein sequence (Figure D.1).

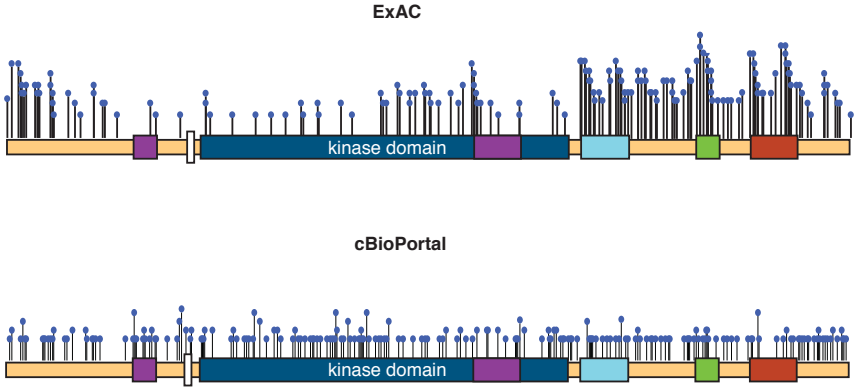

Figure D.1. Distribution of DYRK1A mutations in normal and cancer samples. All DYRK1A missense mutations listed in ExAC browser (upper panel) and cBioPortal cancer browser (lower panel) are mapped along the primary structure of the DYRK1A protein. The height of the sticks does not reproduce the allelic frequency, and varies only for illustrative reasons. Indeed, the Figure does not intend to compare allele frequencies since the number of individuals analyzed in each study is very different. DYRK1A protein domains are as described in Figure I.2.

All these observations fit with our speculation that DYRK1A somatic alterations are positively selected in tumors. Indeed, the results obtained in this Thesis work provide experimental evidence for this hypothesis, because the majority of the representative group of tumor somatic missense variants analyzed for functional impact (21 out of 27) dramatically affect protein function and stability, and they are therefore LoF mutations (Figure R.9 and Table R.3). Of note, the ExAC study was published after the choice of the DYRK1A missense cancer variants, and we noticed that 3 of them were also found in the normal population, R158H, I283V and R559C (Table R.2). In agreement with the LoF intolerance of DYRK1A in normal population, none of these mutants shows total loss of activity and R559C is functionally a WT protein (Table R.3). Therefore, they might represent passenger mutations in the tumor samples.

The results generated by our functional analysis resemble what has been shown for the protein kinase C family of kinases, where a an extensive functional characterization of PKC cancer-associated mutations was performed, showing that most are LoF (Antal et al., 2015), thus questioning the assumption that cancer mutations in kinase genes previously described to act as oncogenes are activating mutations.

Despite these observations, DYRK1A inactivation through LoF mutations remains a low-frequency-event, in the vast landscape of tumor genetic alterations. In this sense, we speculate that loss of DYRK1A function is positively selected only under specific circumstances. As discussed by many authors, the low-penetrance genes, although harder to identify, might represent determinants of intratumor and intertumor heterogeneity (Garraway and Lander, 2013; Wood et al., 2007), and a source of tumor-specific targets to be exploited for personalized therapies. Thus, uncovering the “addiction” of low-penetrance tumor driver genes to specific molecular context is a very important aspect in current cancer research; this aspect will be further discussed in chapter 4.

2.1. Recurrence of LoF mutations in cancer and in DHS

The relevance of DYRK1A in neuronal development and in the regulation of basic cellular processes in multiple adult cell lineages has been extensively proved (Arbones et al., 2019). It was not then surprising, the scarceness of *DYRK1A* non-silent mutations in the general population reported by the ExAC study (Figure D.1 and associated text). Normal levels of DYRK1A active protein are required for proper developmental processes and, in fact, heterozygous *de novo* mutations in DYRK1A gene have been associated to a specific ASD syndromic form, the *DYRK1A* haploinsufficiency syndrome (DHS), or MRD7 (OMIM:614104) (van Bon et al., 2016). While for truncating mutations DYRK1A LoF is easily predictable, no information about the effect on DYRK1A function was provided. A first study filled the gap by

screening a small group of these variants (Widowati et al., 2018). Additionally, our group and collaborators published a comprehensive biochemical screen on the whole list of *DYRK1A de novo* missense mutations reported to date to confer functional significance to these changes and give proper information to ascribe those cases as DHS (Arranz et al., 2019). Figure D.2 shows all mutations assayed in our screens, the cancer group included in this Thesis work and the group associated to DHS. Both functional screens examined the functional impact of the mutations following the same procedure, that is by assessing catalytic activity and protein accumulation levels. Interestingly, many of the residues mutated in DHS are also found in cancer samples, in some cases with the same amino acid change, suggesting the existence of LoF-hotspots in the DYRK1A sequence. Moreover, several of the detected indels are also shared by the two situations (data not shown), further pointing to the existence of hotspots. Germline mutations in tumor suppressor genes are often associated to proliferative disorders, which are characterized by an increased risk of developing specific types of cancers (Payne and Kemp, 2005). DHS individuals are young in age so no information on tumor burden is available, but these results might point to an increase risk of suffering cancer in the adulthood.

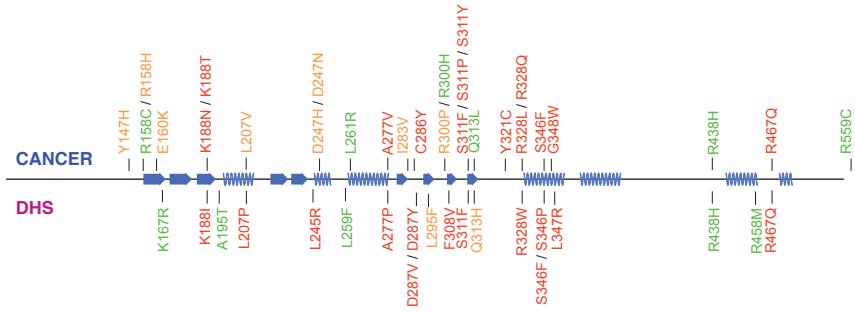

Figure D.2. DYRK1A pathological mutations. Comparison of the functional impact indicated with a color code (see Figure R.9) of reported DYRK1A missense variants in cancer and DHS. Data for DHS has been taken from (Arranz et al., 2019).

2.2. Hints on DYRK1A biochemistry: the activity-stability link

To assess the impact of cancer somatic mutations on DYRK1A function, we analyzed two very important features of a cellular enzyme: the intrinsic catalytic activity and stability *in vivo*, interpreted as levels of protein accumulation. Given the strong dosage-dependence of DYRK1A, the last feature could be also very relevant. We found that most of the screened mutations had profound effects on both DYRK1A kinase activity (Figure R.6) and protein accumulation, which we assumed to depend almost entirely on protein degradation rates (Figure R.7). Notably, the functional characterization of DYRK1A cancer variants also provided information about the biochemical connection between DYRK1A activity and stability (Figure R.8B). Inactivating mutations are not destabilizing *per se*, as demonstrated by other studies characterizing cancer-related mutations on other cellular enzymes (Gaboriau et al., 2015; Kugel et al., 2015; Li et al., 2016), but in the case of DYRK1A we found a significant correlation between stability and activity (Figure R.8B). This outcome has been confirmed also by the functional analysis of DHS *de novo* mutations (Arranz, et al., 2019), indicating that it is a DYRK1A specific property regardless of the pathological context. Thus, we argue that regulatory mechanisms might exist by which dysfunctional DYRK1A proteins are detected and degraded faster by the cells. We show that the DYRK1A inactive mutants are unable to phosphorylate a substrate and also lack autophosphorylation activity. It is therefore possible that some of the autocatalytic events might be responsible for preventing proteasome-targeted degradation. In this regard, and as previously mentioned, autophosphorylation of S97 by a catalytic active intermediate during protein synthesis has been proposed as a crucial step hampering DYRK1A degradation (Kii et al., 2016).

We noticed that some of the variants escaped the linear correlation activity/stability. Among them, the mutant Y321C in the activation loop-tyrosine was especially interesting, since it showed a dramatic

decrease in kinase activity on substrate but retained high autophosphorylation activity; the protein accumulation levels of this mutant were highly variable levels, although close to the WT-level median (Figure R.6D and R.7C). This higher autophosphorylation activity would produce a more complex autophosphorylation profile, which might explain the high variability in stability assays. These observations suggest that there could be unique biochemical features *in vitro*, with unforeseen consequences *in vivo*, for DYRK1A mutations that deserve further exploration. We should also mention that the biochemical characterization of the DYRK1A variants was restricted to those variants appearing in the catalytic domain. It is therefore possible that other cancer-associated variants outside this domain might also impact DYRK1A properties (subcellular localization, substrate choice, etc.,) rendering them LoF from a biological viewpoint. The lack of knowledge on key sequences determining these features has limited further exploration.

3. Good or evil? The dual role of the dual-specificity kinase DYRK1A as tumor driver

The word “dual” has never been more appropriate for the kinase DYRK1A. Beyond its dual substrate residue-specificity, DYRK1A seems to play a dual role as tumor driver. Indeed, our results suggest that DYRK1A function in tumor cells is context-dependent, in agreement with previous reports.

As previously mentioned, our results support the hypothesis that loss of DYRK1A expression or function is positively selected in cancer. Indeed, our DE analysis showed significant DYRK1A downregulation in 11 out of the 15 tumor types considered: ESCA, LUSC, KIRP, COADREAD, THCA, HNSC, STAD, UCEC, LIHC, KIRC and LUAD (Figure R.2A). No upregulation was detected in any tumor cohort. Lower DYRK1A mRNA levels have been found by other group in AML samples (not included in

our DE analysis), which was more apparent in relapsed patient samples (Liu et al., 2014). DYRK1A downregulation was also reported in the BRCA TCGA cohort (Kim et al., 2016), a result that we could not reproduce (Figure R.2A), probably due to the use of different statistical analysis (paired Wilcoxon test in this work vs unpaired Student's t-test in Kim et al., 2006). Distinct molecular mechanisms could be responsible for DYRK1A downregulation in tumor cells. First, alterations in the activity/levels of the transcription factors already described to promote DYRK1A expression (Kim, et al., 2016; Lee et al., 2009; Lu et al., 2011; Maenz et al., 2008), or of unknown transcriptional regulators in the tumor cells. Second, epigenetic changes at the promoter locus, or at other regulatory regions, might occur; this aspect could be explored by crossing DNA methylation data with gene expression data in TCGA samples. Finally, post-transcriptional mechanisms affecting steady-state mRNA levels by miRNAs or RNA binding proteins might be involved as well.

In addition to reduced DYRK1A expression in tumors, the analysis of somatic mutations revealed signals of positive selection in three cancer types, LIHC, ESCA and UCEC, and we provide experimental prove that DYRK1A cancer missense mutations, including several found in these tumor types, are *bona fide* LoF mutations.

Despite these results, our work on pancreatic cancer, together with data from others, suggest that the role of DYRK1A in cancer is much more complex. Thus, contrary to the general trend observed in DE analysis of TCGA data, we found that DYRK1A was upregulated in PDAC samples at the mRNA level in 3 independent cohorts (Luna, et al., 2018)(Annex I). Similar behavior was reported in glioblastoma and in head and neck squamous cell carcinoma (Pozo et al., 2013; Radhakrishnan et al., 2016). Of note, the PAAD (pancreatic adenocarcinoma) and the GBM (glioblastoma) TCGA cohorts were not included in our DE analysis for not reaching the minimum number of paired samples. However, we did observe downregulation of DYRK1A in the HNSC TCGA samples

(Figure R.2A). These contradictory results could be due to the use of different cohorts in the two studies; alternatively, the fact that DYRK1A overexpression was observed at the protein level (Radhakrishnan, et al., 2016) could mean that the increase is caused by post-transcriptional mechanisms, despite a slight but significant downregulation at the mRNA level (as detected in the TCGA cohort).

In the next sections, I will discuss the controversial role of DYRK1A in cancer using the results from the two tumor models studied in this work: pancreatic adenocarnicoma and endometrial carcinoma.

3.1. DYRK1A plays oncogenic functions and promotes tumor growth in pancreatic adenocarcinoma

Pancreatic cancer is not among the most recurrent cancer types, but it certainly represents one of the worse malignancies in terms of prognosis and increasing incidence, which make this disease the fourth leading cause of cancer-related death in United States and prediction to become the second by 2030 (Rahib et al., 2014; Siegel et al., 2018). The disease groups several cancer types, but PDAC accounts for almost 90% of all cases (Feldmann et al., 2007). Environmental risk factors are strongly related with lifestyle, smoking, alcohol consumption and obesity among the modifiable risk factors (McGuigan et al., 2018), which would explain why its incidence is increasing mostly in developed countries. Poor outcomes are mainly due to late diagnosis, with most patients presenting advanced stages and proximal or distant metastases. Current therapeutic opportunities are limited; surgical resection with adjuvant chemotherapy represents the only potential curative procedure, but in 80% of cases is not applicable due to the advanced stage of the disease at time of presentation (Ilic and Ilic, 2016). The treatment for advanced, metastatic PDAC consists of palliative chemotherapy, with the FOLFIRONOX regime the most widely accepted protocol (McGuigan, et al., 2018). Therefore, the high grade of malignancy and the narrow window of intervention for PDAC patients

highlight a strong need for prevention, new strategies for early detection and alternative treatment approaches.

By using the PDAC cell line model PANC-1, we showed that *DYRK1A* silencing with specific shRNAs led to impaired PANC-1 cell growth, migration and invasion (Figure 2A and 2C-E in Annex I). Similar results were obtained using harmine, which strongly hindered PANC-1 proliferation (Figure 2B in Annex I). Mechanistically, DYRK1A depletion led to decreased stability of c-MET (Figure 7 in Annex I), a well-described RTK with key functions in development and organ repair, whose overexpression or hyperactivation had already been associated with different types of cancer, including PDAC. Indeed, targeting MET or its ligand HGF has been proposed as a potential therapeutic strategy for PDAC and both HGF and MET inhibitors are under evaluation in clinical trials (Modica et al., 2018; Rizwani et al., 2015). Notably, PDAC was poorly represented in the list of DYRK1A mutations in cancer samples (3 variants in the catalytic domain and only 1 appears to be destabilizing according to FoldX; Table R.4 and Annex II), which concurs with a need for PDAC cells to preserve DYRK1A activity.

This work thus revealed a pro-tumorigenic role for DYRK1A in PDAC, at least, by increasing c-MET stability. It is also possible that additional mechanisms exist by which DYRK1A promotes PDAC tumor growth, and preliminary results from the analysis of differentially expressed genes in DYRK1A silenced PANC-1 cells suggest that the secretion of molecules important for the cross-talk between the neoplastic cells and other cells in the tumor niche is also affected (data not shown). Coupling harmine treatment with c-MET inhibitors will probably help to unveil eventual c-MET-independent DYRK1A oncogenic functions.

Further investigation is required to better elucidate how DYRK1A participates in pancreatic ductal cells transformation and PDAC tumor progression. Nevertheless, our results suggest that DYRK1A can be a potential therapeutic target for treating c-MET “addicted” PDAC tumors.

3.2. DYRK1A represents a novel tumor suppressor in endometrial cancer

Endometrial cancer represents the most common gynecological malignancy in Europe and United States and its incidence is increasing annually (Henley et al., 2018; Siegel, et al., 2018). Among the different histological types of uterine cancers (Bokhman, 1983; Lax and Kurman, 1997), endometrioid adenocarcinoma is the most frequent (almost 70%) (Henley, et al., 2018). This malignancy presents clear symptoms since its onset, and it is thereby diagnosed at early stages in most cases. Indeed, most patients are characterized by good prognosis and a high 5-year survival rate (95.3%) (Henley, et al., 2018; Siegel, et al., 2018). In contrast, patients with advanced or recurrent endometrial carcinoma have poor prognosis and a very low 5-year survival rate (16.2%). Since the mid-1970s, uterine corpus and uterine cervix carcinomas are the only cancer types, among the most common ones, for which survival has not improved (Siegel, et al., 2018). The only approved targeted therapy is represented by hormonal therapy (Sommeijer et al., 2013), whereas current chemotherapeutic treatments are associated with high toxicity and limited efficacy, highlighting a strong need for new therapeutic approaches.

The results obtained in this Thesis work strongly suggest a role for DYRK1A as tumor suppressor in endometrial carcinoma. On the one hand, we found DYRK1A significantly downregulated at the transcript level in the UCEC TCGA cohort (Figure R.2A). Moreover, analysis of somatic mutations in UCEC tumor samples revealed signals of positive selection with two independent methods (Figure R.4B). Finally, DYRK1A deleterious mutations are found more frequently in endometrial cancer specimens than in other cancer types (Figure R.10 and Table R.4; see also Annex II for the full list of DYRK1A somatic mutations). All these findings suggest that endometrial cancer models would be very appropriate to study whether and how DYRK1A mutations drive tumor progression. Fortunately, we found two

endometrioid carcinoma cell lines, EN and HEC59, with LoF mutations in one *DYRK1A* allele, which displayed reduced DYRK1A activity (Figure R.12C), thus representing useful models for gain-of-function experiments.

First, we showed that DYRK1A overexpression impaired the capabilities of both cell lines to form colonies when grown in diluted conditions (Figure R.13C-D). Second, using a more elegant approach, we also showed that restoring the *DYRK1A*$^{wt/wt}$ genotype in HEC59 cells led to a strong reduction in clonogenic assays (Figure R.17A) and in cumulative growth (Figure R.17B), which appears be due to, at least, reduced survival of the reverted cells (Figure R.21B). More importantly, xenograft experiments in mice using the DYRK1A-reverted clone showed delayed tumor growth compared to the parental cell line (Figure R.22), indicating that reverting the DYRK1A mutation negatively affected the ability of HEC59 cells of surviving and/or dividing *in vivo*. Together, these findings point at DYRK1A as a novel tumor suppressor in endometrial cancer and further suggest that DYRK1A mutations in endometrial tumors represent driver mutations. Notably, other endometrial cancer DYRK1A-mutated cell lines are available (HEC251 and SNGM, portals.broadinstitute.org/ccle), and they could be exploited to extend these results by analyzing the behavior of the corresponding reverted clones.

Given the limitations of mouse xenografts as cancer models to properly study the tumor niche, a complementary approach should involve alternative *in vivo* strategies using endometrial cancer mouse transgenic models. Several models have been engineered so far, including the Mitogen-inducible gene 6 (Mig-6) model (Kim et al., 2017), the Pten-inducible KO model (Mirantes et al., 2013) and the Pten/Lkb1-deficient model (Cheng et al., 2014). One smart strategy would be to cross these mice with *Dyrk1a*$^{+/-}$ mice (Fotaki et al., 2002) to study *Dyrk1a*-haploinsufficient mouse models of endometrial carcinoma. A conditional *Dyrk1a* KO model is also available (Thompson et al., 2015),

which would allow to target specific cell types to further dissect the contribution of the cellular components of the tumor microenvironment. Another possible strategy may take advantage from recent CRISPR/Cas9-based methods, which allow multiple genome-editing events to generate specific cancer mouse models (Gargiulo, 2018; Oldrini et al., 2018). Thus, introducing specific *DYRK1A* mutations or allele deletions through sgRNAs delivery directly into the uterus of adult animals might represent an elegant way to mimic a specific DYRK1A somatic mutation event in uterine cells and to investigate how such event affects tumor development in the endometrium.

Finally, we are aware that additional research work would be required to fully support the involvement of DYRK1A in endometrial carcinoma, apart from the already mentioned studies on other DYRK1A mutated cell lines. The experiments should include evaluation of DYRK1A expression changes in alternative, independent cohorts of endometrial tumor samples and immunohistochemistry analysis on endometrial cancer patient samples to provide evidence that the *DYRK1A* loss observed at the mRNA level is mirrored at the protein level. Identifying the genetic background that favors the selective loss of DYRK1A will also help to stratify endometrial tumors for future therapy approaches.

3.3. A multi-level approach to uncover new DYRK1A-regulated cellular pathways in endometrial cancer cells

To uncover the molecular mechanisms contributing to the modified behavior of DYRK1A reverted HEC59 cells, we have performed a comprehensive analysis aimed at identify changes at multiple molecular levels. The most relevant aspects of the outcome of this study will be discussed in the next sections.

3.3.1. Increased DYRK1A dosage activates STAT1-mediated IFN response

Whole proteome analysis in HEC59 parental cells and CRISPR-derived clones revealed the upregulation of proteins belonging to the IFN-I

signaling pathway in DYRK1A-WT reverted cells, and the downregulation of the same category of genes in DYRK1A-KO cells (Figure R.23C). Binding of the IFN-I family of cytokines to their membrane receptors activate signaling cascades in target cells, which ultimately induce the expression of IFN-stimulated genes (ISG), leading to a multitude of cellular responses that ultimately cause enhanced cellular protection against viral and bacterial infection and activated immunosurveillance (Ng et al., 2016) (Figure D.3). Interestingly, the expression of IFN-I receptor 1 and 2 (IFNAR1-2) and ISGs changes in a stage-dependent manner during menstrual cycle in mammalian uterine cells (Ozaki et al., 2005; Shirozu et al., 2017). Moreover, expression of IFNα is upregulated during embryo implantation (Li et al., 2001), suggesting that IFN signaling may play relevant functions in controlling endometrial physiologic processes and during gestation. In addition, IFN-I signaling drives the immune response to cancer cells, by stimulating immune cells, preventing tumor cells immune escape and inducing cell death and cell cycle arrest in neoplastic cells, although the molecular processes orchestrating this response are not fully understood (Dunn et al., 2006; Musella et al., 2017) (Figure D.3).

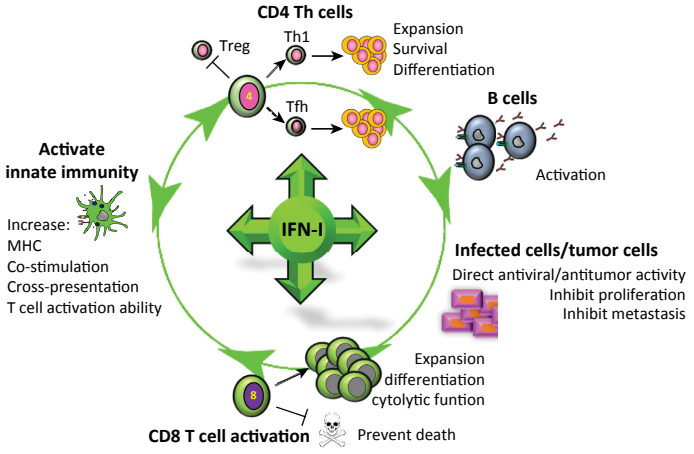

Figure D.3. Type 1 Interferon-modulated processes in response to virus infection and cancer. Activation of I-IFN signaling promotes multiple downstream pathways, in the different cell types within the infection/tumor niche. These events lead to immune response activation and anti-proliferative effects in tumor cells. Adapted from (Snell et al., 2017).

STAT proteins are a family of transcription factors which are activated through phosphorylation in response to many diverse stimuli; once activated they translocate to the nucleus and promote gene expression, thus modulating crucial cellular processes, from cell division to apoptosis and defense against infection (Levy and Darnell, 2002). A few reports have linked DYRK1A and STAT proteins. Thus, phosphorylation of STAT3 by DYRK1A on the activating residue S727 was documented in a screen aimed at identifying STAT3 kinases and confirmed by co-expression in mammalian cells (Matsuo et al., 2001; Wiechmann et al., 2003). Increased STAT3 S727 phosphorylation was observed in neuronal progenitors in the Ts1Cje DS mouse model, which was attributed to elevated DYRK1A levels in this model (Kurabayashi et al., 2015). However, our results showed changes in STAT3 phosphorylation on S727 not depending on the DYRK1A dosage, with a reduction in the phosphosignal by both gain and loss of *DYRK1A* (data not shown). On the other hand, the phosphorylation of STAT1 on S727 was found to gradually increased following DYRK1A dosage differences among the three conditions (Figure R.24B); however, our current data do not allow us to formally probe that STAT1 is a direct substrate of DYRK1A. STAT1 homodimers and heterodimers with STAT2 bind to DNA and activate transcription of a broad panel of genes, affecting many cellular processes (Levy and Darnell, 2002). Importantly, we found coherent expression of IFN-I responsive genes, supporting functional activation of STAT1 (Figure R.25C).

Opposing roles for STAT1 and STAT3 in mediating tumor related processes have been suggested. In particular, STAT3 has been described to promote proliferation and survival in response to different growth signals, whereas STAT1 has been found to mediate anti-proliferative cellular mechanisms and increased immune response against transformed cells (Avalle et al., 2012). The activated IFN response might explain the anti-proliferative behavior of HEC59

DYRK1A-WT reverted cells, and attenuated STAT1/IFN-I signaling due to DYRK1A functional loss could be one of the mechanisms of acquired survival advantage by HEC59 tumor cells. Concurring with this model, previous studies revealed decreased Interferon regulatory factor 1 (IRF1) levels in endometrial carcinoma samples, compared with normal tissue (Giatromanolaki et al., 2004; Kuroboshi et al., 2003). STAT1-mediated tumor suppressive functions have been in part explained by activation of genes encoding for negative regulators of cell cycle checkpoints, such as CDKN1A (p21WAP), CDKN1B (p27KIP), among others (Chin et al., 1996; Levy and Darnell, 2002; Mandal et al., 1998). However, we did not observed changes at the transcript or protein level for most of these genes, which agrees with the lack of effect on the cell cycle profile by DYRK1A dosage changes (Figure R.21A). It is likely that the advantage gained through reduced STAT1 signaling is also linked to tumor niche-related mechanisms, like immunosuppression and immune escape by tumor cells, although these processes cannot contribute to the phenotype we observed in cell culture experiments and immunosuppressed mouse models.

In summary, our analysis discloses a new regulatory axis DYRK1A/STAT1/IFN that could represent an anti-neoplastic pathway in the tumor context under study, and which surely deserves further investigation in other biological contexts.

3.3.2. Additional clues on anti-proliferative molecular mechanisms mediated by DYRK1A

Although the enhanced STAT1/IFN response may contribute to the DYRK1A-dependent tumor suppressive phenotype, it is most likely that additional cellular mechanisms are also involved. In this sense, the DID group of phosphorylated proteins (Figure R.24A) offers an excellent platform for identifying cellular pathways differentially regulated by DYRK1A dosage-dependent events. Although no differences were observed in the cell cycle profile as result of changes in DYRK1A dosage, our results indicate that cell viability is indeed affected. The

increase in the non-viable cell population may be caused by increased programmed cell death, necrosis or any other type of cell death. We have screened our high-throughput data sets searching for putative candidates that could explain the observed phenotype. We did identify changes in S194 phosphorylation in the apoptotic factor Fas associated via Death Domain (FADD), a modification that is involved in cell cycle regulation by FADD rather than apoptosis (Alappat et al., 2003; Tourneur and Chiocchia, 2010). Phosphorylation of FADD S194 was reported to happen during mitosis and to mediate FADD localization at spindle poles (Alappat et al., 2005). Interestingly, we identified other M phase-specific phosphorylation events in the DID group (Figure D.4).

The DNA damage-associated factor p53 binding protein 1 (53BP1) is hyperphosphorylated in response to DNA damage by the kinases ATR and ATM, thus promoting 53BP1 recruitment to damage foci (Anderson et al., 2001; Jowsey et al., 2007). Additionally, phosphorylation events at the C-terminus of 53BP1 during mitosis have been causally linked to the block of DNA repair process that cells use to prevent deleterious events like defective chromosome segregation and telomere fusions (Heijink et al., 2013; Orthwein et al., 2014). Several C-terminal 53BP1 phosphorylated residues are included the DID group (Figure D.4). No functional roles have been associated to any of these sites, so it is difficult to offer further insight, but some of them are SP sites and they might be direct targets of DYRK1A. We also found multiple phosphorylated peptides belonging to Cut homeobox protein 1 (CUX1) (Figure D.4), a transcription factor whose activity is inhibited during M phase through hyperphosphorylation (Sansregret et al., 2010) and to microtubule associated protein 1A, 1B, 1S (MAP1A, MAP1B and MAP1S) (Figure D.4), which have been shown to coordinate microtubule dynamics in several cellular mechanic processes, including mitotic division (Mohan and John, 2015).

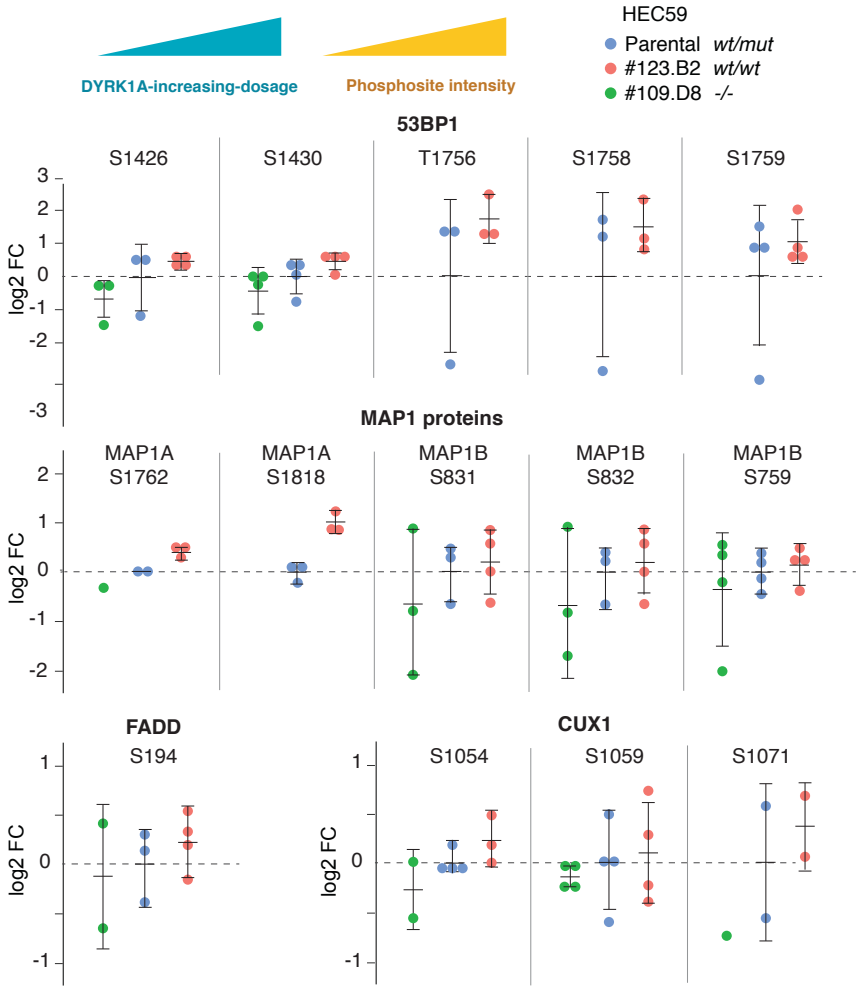

Figure D.4 M phase-associated phospho-events in the DID cluster. Phospho-events of cellular factors for which hyperphosphorylation has been described enriched during mitosis. Log2FC values of phospho-peptide intensities in parental HEC59 cells, reverted DYRK1A-WT and DYRK1A-KO clones, normalized to HEC59-parental values (mean of replicates set as 1) are represented. The graphs also include the mean ± SD for each group. For some events, no peptides were detected in any replicate of the DYRK1A-KO clone.

Phosphorylation dynamics is crucial to orchestrate the complex network of events that occur during cell division (Dephoure et al., 2008). Alterations in this delicate regulation might cause aberrant mitosis and consequently, cell death. This process, known as mitotic catastrophe, is a cellular protective mechanism unrelated to apoptosis (Vitale et al.,

2011). The M-phase associated events described above could point at a prolonged or blocked mitotic process in reverted *DYRK1A*$^{wt/wt}$ cells. We argue that increased frequency of aberrant mitosis might explain the reduction in viable cells proportion caused by DYRK1A increased dosage in HEC59 cells. Although this proposal needs to be experimentally addressed, we find it quite attractive. DNA damage repair processes are strongly altered in cancer cells, as indicated by the hypermutator genetic profile and heterozygous LoF mutations in crucial DNA repair genes such as *BRCA1* and *TP53BP1* itself (data available on CCLE browser, portals.broadinstitute.org/ccle). In this scenario, mitotic checkpoint inactivation becomes crucial for cancer cells to undergo cell division, regardless of DNA damage status. DYRK1A might be involved in the regulation of mitosis-associated DNA repair signaling and DYRK1A LoF could have equipped endometrial cancer cells with compensatory mechanisms to overcome cell division blockade and escape mitotic catastrophe-cell death program (Figure D.5).

3.4. Targeting DYRK1A: therapeutic opportunities

At this point, it becomes clear that the DYRK1A function in cancer is complex and therefore, it prompts for rigorous research work before designing DYRK1A-targeting strategies. The use of the currently available DYRK1A inhibitors may represent an attractive approach for treating those cases when DYRK1A is overexpressed and/or promote tumorigenic processes, as in the case of PDAC, as we have demonstrated in mouse models of this tumor type (Luna, et al., 2018)(Annex I). Since c-MET has been extensively associated to resistance to chemotherapy, with emerging evidence also in pancreatic cancer (Delitto et al., 2014; Shah et al., 2007), combination of DYRK1A inhibitors and standard adjuvant therapies might represent a good strategy to overcome MET-mediated chemoresistance in PDAC.

In the case of endometrial cancer, or other cancer types where DYRK1A is found to play tumor suppressive functions, the potential

therapeutic opportunities are less obvious. Cancer driver genes have been revealed to be more frequently tumor suppressors than oncogenes (Vogelstein et al., 2013), and in these cases the targeting strategies are more complicated, representing a significant challenge for modern oncology (Liu et al., 2015; Morris and Chan, 2015), as it is illustrated by the fact that none of anticancer agents currently used in clinics target tumor suppressor genes.

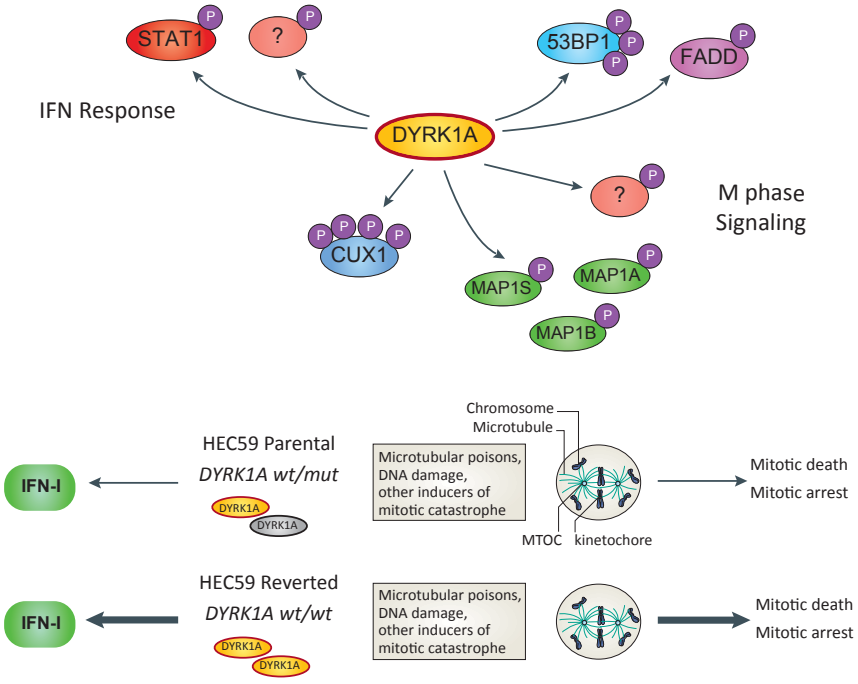

Figure D.5 Model of DYRK1A-mediated tumor suppressive functions in HEC59 reverted DYRK1A-WT clone. Schematic representation of potential tumor suppressive mechanisms mediated, either directly or indirectly, by DYRK1A in HEC59 cells. Increased phosphorylation of STAT1 and other putative factors lead to IFN-I pathway activation; increased phosphorylation of 53BP1, MAP proteins, CUX1 and FADD S194 might be linked to dysregulation of mitotic checkpoints and thus, to increased frequency of mitotic death events in reverted HEC59 DYRK1A-WT cells. Adapted from (Vitale, et al., 2011).

One possibility to target tumors with DYRK1A LoF could be to identify compounds that increase DYRK1A *in vivo* activity or stability. Second,

gene therapy with viral vectors might represent a strategy for targeting DYRK1A-mutated tumors, although only modest results have been achieved so far for other tumor suppressors (Amer, 2014). Alternatively, learning from DYRK1A dosage-sensitivity might help to identify altered intracellular signaling pathways for which inhibitors are available. Finally, our data suggest that DYRK1A inactivation might be effective in DYRK1A-deficient tumors, given that complete loss of DYRK1A led to significantly impaired tumor growth in xenografts (Figure R.22). This phenomenon may be related to the crosstalk between tumor and stromal cells of the tumor microenvironment, since DYRK1A-KO cells performed better than the parental line in tissue culture assays (Figure R.20A and R.20C). In this regard, the pro-angiogenic properties of DYRK1A (Rozen et al., 2018) acquire particular relevance. Of note, the DYRK1A inhibitor EGCG suppresses angiogenic processes during endometriosis (Xu et al., 2011), a common pathological process characterized by proliferation of endometrial cells outside the uterus. In this context, a recent study showed the inhibitory effect of recombinant IFN molecules on endometriotic cells growth and migration (Dicitore et al., 2018). Together, these pieces of research make us proposed a model by which a regulatory IFN-I/DYRK1A axis contributes to maintain a benign state in endometrial cells.

We should not forget that DYRK1A is an essential gene in normal cells. Thus, although cancer cells can tolerate and even being selected for DYRK1A losses, one can speculate that this loss is not for free. Understanding the vulnerabilities that cancer cells experience for maintaining a pool of functional DYRK1A may help to identify specific and hopefully targetable synthetic lethal genes. Synthetic lethality has been extensively studied in genetics, but only recently applied to cancer drug discovery (Nijman, 2011; O'Neil et al., 2017). The most famous case of such application is the use of poly(ADP-ribose) polymerase (PARP) inhibitors for treatment of *BRCA1/2* mutation-carrier breast cancer patients (Sonnenblick et al., 2015). In this regard, results from

our laboratory proposed a role for DYRK1A in regulating the response to DNA damage, by interacting with the ubiquitin ligase ring finger 169 (RNF169) (Roewenstrunk, 2016). Indeed, DYRK1A depletion increased sensitivity to ionizing irradiation, suggesting that DYRK1A-deficient cancer cells might be more sensitive to DNA damage agents. However, we observed no differences in sensitivity to DNA damage-inducing drugs such as doxorubicin and cisplatin between parental HEC59 cells and the reverted DYRK1A-WT clone in preliminary experiments (data not shown).

4. DYRK1A in cancer: still a complex picture

The complexity of the role played by DYRK1A in cancer appears to be, largely related to context-specificity. Indeed, it is currently widely accepted that context, interpreted as the genetic and molecular landscape of the cell of origin where oncogenic events take place, is what really determines whether a gene will contribute to tumor development or not (Schneider et al., 2017). Thanks to the great advances in cancer genomics field, we are not only discovering new drivers, but also obtaining more precise information about tissue-specificity of known cancer genes (Haigis et al., 2019). Although cancer genes often control cellular processes that are considered crucial for homeostasis maintenance, regardless of the cell type, they do not give rise to cancer in every cell of origin when altered. A striking example is represented by germline mutations in *BRCA1* and *BRCA2* genes; as they control genomic stability, they are expected to increase tumor incidence independently of cell type, but they have been associated to higher risk exclusively for breast and ovarian cancer (Miki et al., 1994; Wooster et al., 1995).

Additional aspects that determine the potential of a given gene to exert tumor driver functions might be intrinsic to the genetic alterations of the cancer cells. In this regard, a high-throughput screening aimed at identifying kinase inhibition-vulnerabilities in tumor cell lines revealed

that the most sensitive cell types to DYRK1A inhibition were *RB1*-mutated osteosarcoma cell lines (Campbell et al., 2016), indicating that DYRK1A pro-survival function in this tumor type may be dependent on *RB1* loss.

Tissue-specificity can also be related to differential expression mechanisms, at least for cancer genes whose expression is restricted to specific cell lineages, such as the Estrogen receptor 1, which plays tumorigenic functions only in estrogen-responding tumors. However, even for ubiquitously expressed, dosage-sensitive tumor driver genes, differential expression profiles might affect differently their driver-tissue specificity. Indeed, DYRK1A expression levels in normal tissues might provide clues about the differences in functional DYRK1A dosage necessary to ensure tissue homeostasis. Normal uterus is, the tissue expressing the highest *DYRK1A* transcript levels among the different human tissues analyzed by GeTX (Figure I.3). On the other hand, normal pancreatic *DYRK1A* mRNA levels are the lowest, right after liver (Figure I.3). Given that little fluctuations in DYRK1A dosage have dramatic effects on cellular outcomes, normal expression levels can say a word about which direction will take dysregulation events to perturb cellular homeostasis.

The dual nature of DYRK1A in cancer is not an isolate case at all. Other important cancer drivers have been shown to play both tumor suppressor and oncogenic roles. As already remarked, this duality might strongly depend on the cellular context, as in the case of Notch (Lobry et al., 2014), or the previously described STAT1 (Meissl et al., 2017), or even on gene dosage dynamics, like it has been observed in a very interesting work on the transcription factor E2F1 (Shats et al., 2017).

5. Final remarks

Advances in cancer genomics and increasing research work on cancer-associated alterations are accelerating the discovery of many low-frequency-mutated new driver genes, even though mechanisms and tissue-specificity in eliciting tumor progression still need to be elucidated.

I believe that this work has generated helpful data on alterations in members of the DYRK family of kinases in cancer and additionally, it has contributed to shed light on the role played by the kinase DYRK1A in cancer. Nonetheless, one of the difficulties of this work lies on DYRK1A itself, a critical cellular kinase involved in so many crucial cellular processes, with an increasing list of substrates; this situation makes very difficult to assign a complex phenotype as cancer to a particular or unique function. This also likely affects to the assignment of a unique label as “oncogene” or “tumor suppressor”.

Coming back to our dilemma: DYRK1A in cancer, is it good or evil? Maybe it is a naïve question and, as I have discussed, the current situation pictures a very complex scenario. To make a “humanistic” parallelism, if we hardly trace a marked line to separate good and dark sides of a person, we should not do it in cell biology neither, being aware that every protein has to be put into context. We have just started to shed light on the role played by DYRK1A in cancer and to explore the biological consequences of its alterations in different tumor types. I would like to finish concluding that DYRK1A is, as a matter of fact, a tumor driver, although much more remains to be investigated.

In the end, it is not always easy to distinguish good from evil.

Conclusions

1. Genes encoding for DYRK kinases are differentially expressed in cancer.

2. *DYRK1B* and *DYRK2* are overexpressed and amplified in several TCGA cohorts.

3. *DYRK1A* is downregulated in many tumor types and shows signals of positive selection in three TCGA cohorts: liver hepatocellular carcinoma, esophageal carcinoma and uterine corpus endometrial carcinoma.

4. DYRK1A cancer-associated mutations are LoF, as they cause a loss of kinase activity and/or stability.

5. DYRK1A catalytic activity and protein stability show positive correlation.

6. DYRK1A overexpression impairs the growth of *DYRK1A*-mutated endometrial cancer cell lines.

7. Reversion to wild type of the *DYRK1A*-mutated locus in the endometrial cancer cell line HEC59 negatively affects cell growth, despite unaltered cell cycle profiles.

8. HEC59 *DYRK1A*$^{-/-}$ cells show increased colony formation capability, but unaltered proliferation rates.

9. Restoring DYRK1A function in HEC59 leads to decreased cell survival, whereas *DYRK1A*$^{-/-}$ cells display the opposite phenotype.

10. Tumor xenografts derived from both the reverted *DYRK1A*$^{wt/wt}$ and *DYRK1A*$^{-/-}$ HEC59 cells show delayed growth and smaller tumor volume, compared with parental HEC59-derived tumors.

11. Whole proteome/phospho-proteome analysis shows DYRK1A dosage-dependent activation of the interferon type I pathway in HEC59 cells, as indicated by STAT1 phosphorylation and differential expression of downstream effectors of this pathway.

12. DYRK1A/STAT1/IFN signaling might represent a novel regulatory axis for DYRK1A-mediated tumor suppressive function in endometrial cancer.

Abbreviations

53BP1: p53 binding protein 1
ABC: Ammonium bicarbonate
ACC: Adrenocortical carcinoma
AD: Alzheimer disease
ALL: Acute lymphoblastic leukemia
AGC: Auto gain control
AMKL: Acute megakaryoblastic leukemia
AML: Acute myeloid leukemia
APP: Amyloid precursor protein
ASD: Autism spectrum disorders
BLCA: Bladder Urothelial Carcinoma
BRCA: Breast invasive carcinoma
cBioPortal: cBio Cancer Genomics Portal
CCLE: Cancer Cell Line Encyclopedia
CDC37: Cell division cycle 37
CDK: Cyclin-dependent kinase
CDKL: CDK-like kinase
CESC: Cervical squamous cell carcinoma and endocervical adenocarcinoma
CHOL: Cholangiocarcinoma
CLK: Cdc2-like kinase
CMV: Cytomegalovirus
CNA: Copy number alteration
CNS: Central nervous system
COAD: Colon adenocarcinoma
COSMIC: Catalogue of Somatic Mutations in Cancer
CRG: Centre for Genomic Regulation
CRISPR: clustered regularly interspaced short palindromic repeats
CUX1: Cut homeobox protein 1
DAPI: 4',6-diamino-2-phenylindole
DBS: Double-strand break
DCAF7: DDB1 and CUL4 associated factor 7
DE: Differential expression
DH: DYRK homology
DHS: DYRK1A haploinsufficiency syndrome
DID: DYRK1A-increasing-dosage
DLBC: Lymphoid Neoplasm Diffuse Large B-cell Lymphoma
DMEM: Dulbecco's Modified Eagle's Medium
DREAM: Dimerization partner (DP), RB like, E2F and multi-vulval class B (MuvB)
DS: Down syndrome
DSCR: Down Syndrome critical region

DYRK: Dual-specificity tyrosine-regulated kinase
DTT: Dithiothreitol
EDTA: Ethylendiamine tetracetic acid
EF-1: Elongation factor 1-alpha
EGCG: Epigallocatechin gallate
EGFR: Epidermal growth factor receptor
EMT: Epithelial-to-mesenchymal transition
ESCA: Esophageal carcinoma
ExAC: Exome Aggregation Consortium
FADD: Fas associated via Death Domain
FC: Fold change
FDR: False discovery rate
FBS: Fetal bovine serum
GBM: Glioblastoma multiforme
gDNA: genomic DNA
GFP: Green Fluorescent Protein
GIST: gastrointestinal stromal tumor
GLI1: Glioma-Associated Oncogene Homologous 1
GO: Gene Ontology
GTEx: Genotype-tissue expression
HEPES: 4-[2-hydroxyethyl]-1-piperazineethanesulfonic acid
HGF: Hepatocyte growth factor
HGP: Human Genome Project
HH: Hedge-hog
HIPK: Homodomain-interacting kinase
HNSC: Head and Neck squamous cell carcinoma
HPV: Human papilloma virus
HRP: Horse Radish Peroxydase
HSP90: Heat shock protein 90
ICGC: International Cancer Genome Consortium
ID2: Inhibitor of DNA binding 2
ID: Intellectual disability
IDIBAPS: Institut d'Investigacions Biomèdiques August Pi i Sunyer
IFN-I: Interferon type 1
IFNAR: IFN-I receptor
IHC: Immunohistochemistry
Indel: Insertion/Deletion
IP: Immunoprecipitation
IQR: Interquartile range
IRB: Institute for Research in Biomedicine
IRES: internal ribosomal entry site
IRF1: Interferon regulatory factor 1

ISG: IFN-stimulated genes
IVK: In vitro kinase assay
JCRB: Japanese Collection of Research Biorecourses
KICH: Kidney Chromophobe
KIRC: Kidney renal clear cell carcinoma
KIRP: Kidney renal papillary cell carcinoma
KO: knock-out
LAML: Acute Myeloid Leukemia
LATS2: Large tumor suppressor kinase 2
LC: Liquid chromatography
LGG: Brain Lower Grade Glioma
LIHC: Liver hepatocellular carcinoma
LOH: Loss of heterozygosity
LTP: Long term potentiation
LUAD: Lung adenocarcinoma
LUSC: Lung squamous cell carcinoma
MAP: microtubule associated protein
MAPK: Mitogen-activated protein kinase
MESO: Mesothelioma
Mirk: minibrain-related kinase
miRNA: microRNA
MRD7: Mental retardation autosomal dominant 7
MS: Mass spectrometry
NAPA: N-terminal autophosphorylation accessory region
NCBI: National Centre for Biotechnology Information
NCI: National Cancer Institute
NFAT: Nuclear factor of activated T-cells
NLS: nuclear localization signal
NP-40: Nonidet P-40
OMIM: Online Mendelian Inheritance in Man
OV: Ovarian serous cystadenocarcinoma
PAAD: Pancreatic adenocarcinoma
PAGE: Polyacrylamide gel electrophoresis
PARP: Poly(ADP-ribose) polymerase
PBS: Phosphate Saline Buffer
PCA: Principal component analysis
PCPG Pheochromocytoma and Paraganglioma
PCR: Polymerase Chain Reaction
PDAC: Pancreatic ductal adenocarcinoma
PDB: Protein Data Bank
PDGFR: Platelet-derived growth factor receptor
PRAD: Prostate adenocarcinoma

PRBB: Parc de Recerca Biomedica de Barcelona
PRP4K: Pre-messenger RNA processing protein 4 kinase
PSM: Peptide spectrum match
RCAN1: Regulator of calcineurin 1
READ: Rectum adenocarcinoma
REST: RE1 silencing transcription factor
RNF169: ring finger 169
RTK: Receptor tyrosine kinase
SARC: Sarcoma
SD: Standard deviation
SDS: Sodium Dodecyl Sulfate
sgRNA: single guide RNA
SKCM: Skin Cutaneous Melanoma
SNV: Single-Nucleotide Variation
SPRED: Sprouty-related protein with an EVH1 domain
SRPK: Serine-arginine-rich protein kinase
ssODN: single-stranded DNA oligonucleotides
STAD: Stomach adenocarcinoma
STAT: signal transducer and activator of transcription
TBX5: T-box transcription factor 5
TCGA: The Cancer Genome Atlas
TGCT: Testicular germ cell tumor
THCA: Thyroid carcinoma
THYM: Thymoma
TMD: Transient myeloproliferative disorder
TUSON: Tumor Suppressor and Oncogene
UCEC: Uterine Corpus Endometrial Carcinoma
UCS: Uterine Carcinosarcoma
UPF: Universidad Pompeu Fabra
UTR: Untranslated region
UVM: Uveal Melanoma
VHL: Von-Hippel Lindau
VEGFR: Vascular endothelial growht factor receptor
WB: Western Blot
wt: wild type

References

Adayev T, Chen-Hwang MC, Murakami N, Lee E, Bolton DC and Hwang YW. 2007. Dual-specificity tyrosine phosphorylation-regulated kinase 1A does not require tyrosine phosphorylation for activity in vitro. Biochemistry *46*, 7614-7624.

Ahn KJ, Jeong HK, Choi HS, Ryoo SR*, et al.* 2006. DYRK1A BAC transgenic mice show altered synaptic plasticity with learning and memory defects. Neurobiol Dis *22*, 463-472.

Al-Kasim F, Doyle JJ, Massey GV, Weinstein HJ, Zipursky A and Pediatric Oncology G. 2002. Incidence and treatment of potentially lethal diseases in transient leukemia of Down syndrome: Pediatric Oncology Group Study. J Pediatr Hematol Oncol *24*, 9-13.

Alappat EC, Volkland J and Peter ME. 2003. Cell cycle effects by C-FADD depend on its C-terminal phosphorylation site. J Biol Chem *278*, 41585-41588.

Alappat EC, Feig C, Boyerinas B, Volkland J*, et al.* 2005. Phosphorylation of FADD at serine 194 by CKIalpha regulates its nonapoptotic activities. Mol Cell *19*, 321-332.

Altafaj X, Dierssen M, Baamonde C, Marti E*, et al.* 2001. Neurodevelopmental delay, motor abnormalities and cognitive deficits in transgenic mice overexpressing Dyrk1A (minibrain), a murine model of Down's syndrome. Hum Mol Genet *10*, 1915-1923.

Alvarez M, Estivill X and de la Luna S. 2003. DYRK1A accumulates in splicing speckles through a novel targeting signal and induces speckle disassembly. J Cell Sci *116*, 3099-3107.

Alvarez M. 2004. Localización subcelular de la proteína quinasa DYRK1A: compartimentos, señales y regulación. Universitat de Barcelona, Barcelona, Spain.

Alvarez M, Altafaj X, Aranda S and de la Luna S. 2007. DYRK1A autophosphorylation on serine residue 520 modulates its kinase activity via 14-3-3 binding. Mol Biol Cell *18*, 1167-1178.

Amer MH. 2014. Gene therapy for cancer: present status and future perspective. Mol Cell Ther *2*, 27.

Anderson L, Henderson C and Adachi Y. 2001. Phosphorylation and rapid relocalization of 53BP1 to nuclear foci upon DNA damage. Mol Cell Biol *21*, 1719-1729.

Antal CE, Hudson AM, Kang E, Zanca C*, et al.* 2015. Cancer-associated protein kinase C mutations reveal kinase's role as tumor suppressor. Cell *160*, 489-502.

Aranda S, Alvarez M, Turro S, Laguna A and de la Luna S. 2008. Sprouty2-mediated inhibition of fibroblast growth factor signaling is modulated by the protein kinase DYRK1A. Mol Cell Biol *28*, 5899-5911.

Aranda S, Laguna A and de la Luna S. 2011. DYRK family of protein kinases: evolutionary relationships, biochemical properties, and functional roles. FASEB J *25*, 449-462.

Arató K. 2010. Regulation of the stability of the protein kinase DYRK1A: establishing connections with the Wnt signaling pathway. Universitat Pompeu Fabra, Barcelona, Spain.

Arbones ML, Thomazeau A, Nakano-Kobayashi A, Hagiwara M and Delabar JM. 2019. DYRK1A and cognition: A lifelong relationship. Pharmacol Ther *194*, 199-221.

Arranz J, Balducci E, Arato K, Sanchez-Elexpuru G*, et al.* 2019. Impaired development of neocortical circuits contributes to the neurological alterations in DYRK1A haploinsufficiency syndrome. Neurobiol Dis

Arron JR, Winslow MM, Polleri A, Chang CP*, et al.* 2006. NFAT dysregulation by increased dosage of DSCR1 and DYRK1A on chromosome 21. Nature *441*, 595-600.

Aster JC, Pear WS and Blacklow SC. 2017. The Varied Roles of Notch in Cancer. Annu Rev Pathol *12*, 245-275.

Atteya R, Ashour ME, Ibrahim EE, Farag MA and El-Khamisy SF. 2017. Chemical screening identifies the beta-Carboline alkaloid harmine to be synergistically lethal with doxorubicin. Mech Ageing Dev *161*, 141-148.

Avalle L, Pensa S, Regis G, Novelli F and Poli V. 2012. STAT1 and STAT3 in tumorigenesis: A matter of balance. JAKSTAT *1*, 65-72.

Baek KH, Zaslavsky A, Lynch RC, Britt C*, et al.* 2009. Down's syndrome suppression of tumour growth and the role of the calcineurin inhibitor DSCR1. Nature *459*, 1126-1130.

Bailey MH, Tokheim C, Porta-Pardo E, Sengupta S*, et al.* 2018. Comprehensive Characterization of Cancer Driver Genes and Mutations. Cell *174*, 1034-1035.

Bain J, Plater L, Elliott M, Shpiro N*, et al.* 2007. The selectivity of protein kinase inhibitors: a further update. Biochem J *408*, 297-315.

Baldwin A, Li W, Grace M, Pearlberg J*, et al.* 2008. Kinase requirements in human cells: II. Genetic interaction screens identify kinase requirements following HPV16 E7 expression in cancer cells. Proc Natl Acad Sci U S A *105*, 16478-16483.

Baldwin A, Grueneberg DA, Hellner K, Sawyer J*, et al.* 2010. Kinase requirements in human cells: V. Synthetic lethal interactions between p53 and the protein kinases SGK2 and PAK3. Proc Natl Acad Sci U S A *107*, 12463-12468.

Bamford S, Dawson E, Forbes S, Clements J*, et al.* 2004. The COSMIC (Catalogue of Somatic Mutations in Cancer) database and website. Br J Cancer *91*, 355-358.

Banerjee S, Ji C, Mayfield JE, Goel A*, et al.* 2018. Ancient drug curcumin impedes 26S proteasome activity by direct inhibition of dual-specificity tyrosine-regulated kinase 2. Proc Natl Acad Sci U S A *115*, 8155-8160.

Barallobre MJ, Perier C, Bove J, Laguna A*, et al.* 2014. DYRK1A promotes dopaminergic neuron survival in the developing brain and in a mouse model of Parkinson's disease. Cell Death Dis *5*, e1289.

Barba L. 2017. Chromatin-bound DYRK1A: promoter occupancy and implications in the regulation of ribosomal protein gene expression. Universitat Pompeu Fabra, Barcelona, Spain.

Barretina J, Caponigro G, Stransky N, Venkatesan K*, et al.* 2012. The Cancer Cell Line Encyclopedia enables predictive modelling of anticancer drug sensitivity. Nature *483*, 603-607.

Becker W, Weber Y, Wetzel K, Eirmbter K, Tejedor FJ and Joost HG. 1998. Sequence characteristics, subcellular localization, and substrate specificity of DYRK-related kinases, a novel family of dual specificity protein kinases. J Biol Chem *273*, 25893-25902.

Becker W and Sippl W. 2011. Activation, regulation, and inhibition of DYRK1A. FEBS J *278*, 246-256.

Becker W. 2012. Emerging role of DYRK family protein kinases as regulators of protein stability in cell cycle control. Cell Cycle *11*, 3389-3394.

Belgardt BF and Lammert E. 2016. DYRK1A: A Promising Drug Target for Islet Transplant-Based Diabetes Therapies. Diabetes *65*, 1496-1498.

Bhullar KS, Lagaron NO, McGowan EM, Parmar I*, et al.* 2018. Kinase-targeted cancer therapies: progress, challenges and future directions. Mol Cancer *17*, 48.

Bialk P, Rivera-Torres N, Strouse B and Kmiec EB. 2015. Regulation of Gene Editing Activity Directed by Single-Stranded Oligonucleotides and CRISPR/Cas9 Systems. PLoS One *10*, e0129308.

Birchmeier C, Birchmeier W, Gherardi E and Vande Woude GF. 2003. Met, metastasis, motility and more. Nat Rev Mol Cell Biol *4*, 915-925.

Blazek JD, Abeysekera I, Li J and Roper RJ. 2015. Rescue of the abnormal skeletal phenotype in Ts65Dn Down syndrome mice using genetic and therapeutic modulation of trisomic Dyrk1a. Hum Mol Genet *24*, 5687-5696.

Boichuk S, Parry JA, Makielski KR, Litovchick L*, et al.* 2013. The DREAM complex mediates GIST cell quiescence and is a novel therapeutic target to enhance imatinib-induced apoptosis. Cancer Res *73*, 5120-5129.

Boker LK, Blumstein T, Sadetzki S, Luxenburg O*, et al.* 2001. Incidence of leukemia and other cancers in Down syndrome subjects in Israel. Int J Cancer *93*, 741-744.

Bokhman JV. 1983. Two pathogenetic types of endometrial carcinoma. Gynecol Oncol *15*, 10-17.

Bommi-Reddy A, Almeciga I, Sawyer J, Geisen C*, et al.* 2008. Kinase requirements in human cells: III. Altered kinase requirements in VHL-/- cancer cells detected in a pilot synthetic lethal screen. Proc Natl Acad Sci U S A *105*, 16484-16489.

Bonomi P. 2003. Erlotinib: a new therapeutic approach for non-small cell lung cancer. Expert Opin Investig Drugs *12*, 1395-1401.

Borden EC. 2019. Interferons alpha and beta in cancer: therapeutic opportunities from new insights. Nat Rev Drug Discov *18*, 219-234.

Brabletz T, Kalluri R, Nieto MA and Weinberg RA. 2018. EMT in cancer. Nat Rev Cancer *18*, 128-134.

Branca C, Shaw DM, Belfiore R, Gokhale V*, et al.* 2017. Dyrk1 inhibition improves Alzheimer's disease-like pathology. Aging Cell *16*, 1146-1154.

Bronicki LM, Redin C, Drunat S, Piton A*, et al.* 2015. Ten new cases further delineate the syndromic intellectual disability phenotype caused by mutations in DYRK1A. Eur J Hum Genet *23*, 1482-1487.

Buchdunger E, Matter A and Druker BJ. 2001. Bcr-Abl inhibition as a modality of CML therapeutics. Biochim Biophys Acta *1551*, M11-18.

Campbell J, Ryan CJ, Brough R, Bajrami I*, et al.* 2016. Large-Scale Profiling of Kinase Dependencies in Cancer Cell Lines. Cell Rep *14*, 2490-2501.

Cancer Genome Atlas Research N, Weinstein JN, Collisson EA, Mills GB*, et al.* 2013. The Cancer Genome Atlas Pan-Cancer analysis project. Nat Genet *45*, 1113-1120.

Canzonetta C, Mulligan C, Deutsch S, Ruf S*, et al.* 2008. DYRK1A-dosage imbalance perturbs NRSF/REST levels, deregulating pluripotency and embryonic stem cell fate in Down syndrome. Am J Hum Genet *83*, 388-400.

Cao MR, Li Q, Liu ZL, Liu HH*, et al.* 2011. Harmine induces apoptosis in HepG2 cells via mitochondrial signaling pathway. Hepatobiliary Pancreat Dis Int *10*, 599-604.

Ceccaldi R, Rondinelli B and D'Andrea AD. 2016. Repair Pathway Choices and Consequences at the Double-Strand Break. Trends Cell Biol *26*, 52-64.

Cen L, Xiao Y, Wei L, Mo M*, et al.* 2016. Association of DYRK1A polymorphisms with sporadic Parkinson's disease in Chinese Han population. Neurosci Lett *632*, 39-43.

Cerami E, Gao J, Dogrusoz U, Gross BE*, et al.* 2012. The cBio cancer genomics portal: an open platform for exploring multidimensional cancer genomics data. Cancer Discov *2*, 401-404.

Chang HS, Lin CH, Yang CH, Yen MS*, et al.* 2007. Increased expression of Dyrk1a in HPV16 immortalized keratinocytes enable evasion of apoptosis. Int J Cancer *120*, 2377-2385.

Chen H, Shen J, Choy E, Hornicek FJ, Shan A and Duan Z. 2018. Targeting DYRK1B suppresses the proliferation and migration of liposarcoma cells. Oncotarget *9*, 13154-13166.

Chen JY, Lin JR, Tsai FC and Meyer T. 2013. Dosage of Dyrk1a shifts cells within a p21-cyclin D1 signaling map to control the decision to enter the cell cycle. Mol Cell *52*, 87-100.

Chen Y, Wang S, He Z, Sun F*, et al.* 2017. Dyrk1B overexpression is associated with breast cancer growth and a poor prognosis. Hum Pathol *66*, 48-58.

Cheng H, Liu P, Zhang F, Xu E*, et al.* 2014. A genetic mouse model of invasive endometrial cancer driven by concurrent loss of Pten and Lkb1 Is highly responsive to mTOR inhibition. Cancer Res *74*, 15-23.

Cheon H, Borden EC and Stark GR. 2014. Interferons and their stimulated genes in the tumor microenvironment. Semin Oncol *41*, 156-173.

Chin YE, Kitagawa M, Su WC, You ZH, Iwamoto Y and Fu XY. 1996. Cell growth arrest and induction of cyclin-dependent kinase inhibitor p21 WAF1/CIP1 mediated by STAT1. Science *272*, 719-722.

Chiva C, Olivella R, Borras E, Espadas G*, et al.* 2018. QCloud: A cloud-based quality control system for mass spectrometry-based proteomics laboratories. PLoS One *13*, e0189209.

Collett MS and Erikson RL. 1978. Protein kinase activity associated with the avian sarcoma virus src gene product. Proc Natl Acad Sci U S A *75*, 2021-2024.

Courcet JB, Faivre L, Malzac P, Masurel-Paulet A*, et al.* 2012. The DYRK1A gene is a cause of syndromic intellectual disability with severe microcephaly and epilepsy. J Med Genet *49*, 731-736.

Cox J, Neuhauser N, Michalski A, Scheltema RA, Olsen JV and Mann M. 2011. Andromeda: a peptide search engine integrated into the MaxQuant environment. J Proteome Res *10*, 1794-1805.

Cox J, Hein MY, Luber CA, Paron I, Nagaraj N and Mann M. 2014. Accurate proteome-wide label-free quantification by delayed normalization and maximal peptide ratio extraction, termed MaxLFQ. Mol Cell Proteomics *13*, 2513-2526.

da Costa Martins PA, Salic K, Gladka MM, Armand AS*, et al.* 2010. MicroRNA-199b targets the nuclear kinase Dyrk1a in an auto-amplification loop promoting calcineurin/NFAT signalling. Nat Cell Biol *12*, 1220-1227.

Davoli T, Xu AW, Mengwasser KE, Sack LM*, et al.* 2013. Cumulative haploinsufficiency and triplosensitivity drive aneuploidy patterns and shape the cancer genome. Cell *155*, 948-962.

de Herreros AG, Peiro S, Nassour M and Savagner P. 2010. Snail family regulation and epithelial mesenchymal transitions in breast cancer progression. J Mammary Gland Biol Neoplasia *15*, 135-147.

De la Torre R, De Sola S, Pons M, Duchon A*, et al.* 2014. Epigallocatechin-3-gallate, a DYRK1A inhibitor, rescues cognitive deficits in Down syndrome mouse models and in humans. Mol Nutr Food Res *58*, 278-288.

de la Torre R, de Sola S, Hernandez G, Farre M*, et al.* 2016. Safety and efficacy of cognitive training plus epigallocatechin-3-gallate in young adults with Down's syndrome (TESDAD): a double-blind, randomised, placebo-controlled, phase 2 trial. Lancet Neurol *15*, 801-810.

De Vita S, Canzonetta C, Mulligan C, Delom F*, et al.* 2010. Trisomic dose of several chromosome 21 genes perturbs haematopoietic stem and progenitor cell differentiation in Down's syndrome. Oncogene *29*, 6102-6114.

Delitto D, Vertes-George E, Hughes SJ, Behrns KE and Trevino JG. 2014. c-Met signaling in the development of tumorigenesis and chemoresistance: potential applications in pancreatic cancer. World J Gastroenterol *20*, 8458-8470.

Demange L, Abdellah FN, Lozach O, Ferandin Y*, et al.* 2013. Potent inhibitors of CDK5 derived from roscovitine: synthesis, biological evaluation and molecular modelling. Bioorg Med Chem Lett *23*, 125-131.

Deng X, Mercer SE, Shah S, Ewton DZ and Friedman E. 2004. The cyclin-dependent kinase inhibitor p27Kip1 is stabilized in G(0) by Mirk/dyrk1B kinase. J Biol Chem *279*, 22498-22504.

Deng X, Ewton DZ, Li S, Naqvi A*, et al.* 2006. The kinase Mirk/Dyrk1B mediates cell survival in pancreatic ductal adenocarcinoma. Cancer Res *66*, 4149-4158.

Deng X, Ewton DZ and Friedman E. 2009. Mirk/Dyrk1B maintains the viability of quiescent pancreatic cancer cells by reducing levels of reactive oxygen species. Cancer Res *69*, 3317-3324.

Deng X and Friedman E. 2014. Mirk kinase inhibition blocks the in vivo growth of pancreatic cancer cells. Genes Cancer *5*, 337-347.

Dephoure N, Zhou C, Villen J, Beausoleil SA*, et al.* 2008. A quantitative atlas of mitotic phosphorylation. Proc Natl Acad Sci U S A *105*, 10762-10767.

Di Vona C, Bezdan D, Islam AB, Salichs E*, et al.* 2015. Chromatin-wide profiling of DYRK1A reveals a role as a gene-specific RNA polymerase II CTD kinase. Mol Cell *57*, 506-520.

Dicitore A, Castiglioni S, Saronni D, Gentilini D*, et al.* 2018. Effects of human recombinant type I IFNs (IFN-alpha2b and IFN-beta1a) on growth and migration of primary endometrial stromal cells from women with deeply infiltrating endometriosis: A preliminary study. Eur J Obstet Gynecol Reprod Biol *230*, 192-198.

Dimitrakopoulos CM and Beerenwinkel N. 2017. Computational approaches for the identification of cancer genes and pathways. Wiley Interdiscip Rev Syst Biol Med *9*,

Dobin A, Davis CA, Schlesinger F, Drenkow J*, et al.* 2013. STAR: ultrafast universal RNA-seq aligner. Bioinformatics *29*, 15-21.

Dowjat WK, Adayev T, Kuchna I, Nowicki K*, et al.* 2007. Trisomy-driven overexpression of DYRK1A kinase in the brain of subjects with Down syndrome. Neurosci Lett *413*, 77-81.

Druker BJ, Tamura S, Buchdunger E, Ohno S*, et al.* 1996. Effects of a selective inhibitor of the Abl tyrosine kinase on the growth of Bcr-Abl positive cells. Nat Med *2*, 561-566.

Du Z and Lovly CM. 2018. Mechanisms of receptor tyrosine kinase activation in cancer. Mol Cancer *17*, 58.

Dunn GP, Koebel CM and Schreiber RD. 2006. Interferons, immunity and cancer immunoediting. Nat Rev Immunol *6*, 836-848.

Earl RK, Turner TN, Mefford HC, Hudac CM*, et al.* 2017. Clinical phenotype of ASD-associated DYRK1A haploinsufficiency. Mol Autism *8*, 54.

Ehe BK, Lamson DR, Tarpley M, Onyenwoke RU, Graves LM and Williams KP. 2017. Identification of a DYRK1A-mediated phosphorylation site within the nuclear localization sequence of the hedgehog transcription factor GLI1. Biochem Biophys Res Commun *491*, 767-772.

Escudier B, Eisen T, Stadler WM, Szczylik C*, et al.* 2007. Sorafenib in advanced clear-cell renal-cell carcinoma. N Engl J Med *356*, 125-134.

Eskilsson E, Rosland GV, Solecki G, Wang Q*, et al.* 2018. EGFR heterogeneity and implications for therapeutic intervention in glioblastoma. Neuro Oncol *20*, 743-752.

Ewton DZ, Hu J, Vilenchik M, Deng X*, et al.* 2011. Inactivation of mirk/dyrk1b kinase targets quiescent pancreatic cancer cells. Mol Cancer Ther *10*, 2104-2114.

Fabian MA, Biggs WH, 3rd, Treiber DK, Atteridge CE*, et al.* 2005. A small molecule-kinase interaction map for clinical kinase inhibitors. Nat Biotechnol *23*, 329-336.

Fedorov O, Marsden B, Pogacic V, Rellos P*, et al.* 2007. A systematic interaction map of validated kinase inhibitors with Ser/Thr kinases. Proc Natl Acad Sci U S A *104*, 20523-20528.

Fedorov O, Muller S and Knapp S. 2010. The (un)targeted cancer kinome. Nat Chem Biol *6*, 166-169.

Feldmann G, Beaty R, Hruban RH and Maitra A. 2007. Molecular genetics of pancreatic intraepithelial neoplasia. J Hepatobiliary Pancreat Surg *14*, 224-232.

Ferlay J, Colombet M, Soerjomataram I, Mathers C*, et al.* 2019. Estimating the global cancer incidence and mortality in 2018: GLOBOCAN sources and methods. Int J Cancer *144*, 1941-1953.

Fernandez-Martinez J, Vela EM, Tora-Ponsioen M, Ocana OH, Nieto MA and Galceran J. 2009. Attenuation of Notch signalling by the Down-syndrome-associated kinase DYRK1A. J Cell Sci *122*, 1574-1583.

Ferron SR, Pozo N, Laguna A, Aranda S*, et al.* 2010. Regulated segregation of kinase Dyrk1A during asymmetric neural stem cell division is critical for EGFR-mediated biased signaling. Cell Stem Cell *7*, 367-379.

Fish EN and Platanias LC. 2014. Interferon receptor signaling in malignancy: a network of cellular pathways defining biological outcomes. Mol Cancer Res *12*, 1691-1703.

Fleuren ED, Zhang L, Wu J and Daly RJ. 2016. The kinome 'at large' in cancer. Nat Rev Cancer *16*, 83-98.

Fotaki V, Dierssen M, Alcantara S, Martinez S*, et al.* 2002. Dyrk1A haploinsufficiency affects viability and causes developmental delay and abnormal brain morphology in mice. Mol Cell Biol *22*, 6636-6647.

Friedman E. 2013. Mirk/dyrk1B Kinase in Ovarian Cancer. Int J Mol Sci *14*, 5560-5575.

Frisch SM and Mymryk JS. 2002. Adenovirus-5 E1A: paradox and paradigm. Nat Rev Mol Cell Biol *3*, 441-452.

Futreal PA, Coin L, Marshall M, Down T*, et al.* 2004. A census of human cancer genes. Nat Rev Cancer *4*, 177-183.

Gaboriau DC, Rowling PJ, Morrison CG and Itzhaki LS. 2015. Protein stability versus function: effects of destabilizing missense mutations on BRCA1 DNA repair activity. Biochem J *466*, 613-624.

Galganski L, Urbanek MO and Krzyzosiak WJ. 2017. Nuclear speckles: molecular organization, biological function and role in disease. Nucleic Acids Res *45*, 10350-10368.

Gao J, Zheng Z, Rawal B, Schell MJ, Bepler G and Haura EB. 2009. Mirk/Dyrk1B, a novel therapeutic target, mediates cell survival in non-small cell lung cancer cells. Cancer Biol Ther *8*, 1671-1679.

Gao J, Yang X, Yin P, Hu W*, et al.* 2012. The involvement of FoxO in cell survival and chemosensitivity mediated by Mirk/Dyrk1B in ovarian cancer. Int J Oncol *40*, 1203-1209.

Gao J, Aksoy BA, Dogrusoz U, Dresdner G*, et al.* 2013. Integrative analysis of complex cancer genomics and clinical profiles using the cBioPortal. Sci Signal *6*, pl1.

Garcia-Cerro S, Martinez P, Vidal V, Corrales A*, et al.* 2014. Overexpression of Dyrk1A is implicated in several cognitive, electrophysiological and neuromorphological alterations found in a mouse model of Down syndrome. PLoS One *9*, e106572.

Gargiulo G. 2018. Next-Generation in vivo Modeling of Human Cancers. Front Oncol *8*, 429.

Garraway LA and Lander ES. 2013. Lessons from the cancer genome. Cell *153*, 17-37.

Giatromanolaki A, Koukourakis MI, Ritis K, Mimidis K and Sivridis E. 2004. Interferon regulatory factor-1 (IRF-1) suppression and derepression during endometrial tumorigenesis and cancer progression. Cytokine *26*, 164-168.

Glenewinkel F, Cohen MJ, King CR, Kaspar S*, et al.* 2016. The adaptor protein DCAF7 mediates the interaction of the adenovirus E1A oncoprotein with the protein kinases DYRK1A and HIPK2. Sci Rep *6*, 28241.

Gockler N, Jofre G, Papadopoulos C, Soppa U, Tejedor FJ and Becker W. 2009. Harmine specifically inhibits protein kinase DYRK1A and interferes with neurite formation. FEBS J *276*, 6324-6337.

Gonzalez-Navajas JM, Lee J, David M and Raz E. 2012. Immunomodulatory functions of type I interferons. Nat Rev Immunol *12*, 125-135.

Gonzalez-Perez A and Lopez-Bigas N. 2012. Functional impact bias reveals cancer drivers. Nucleic Acids Res *40*, e169.

Gonzalez-Perez A, Perez-Llamas C, Deu-Pons J, Tamborero D*, et al.* 2013. IntOGen-mutations identifies cancer drivers across tumor types. Nat Methods *10*, 1081-1082.

Gorringe KL, Boussioutas A, Bowtell DD and Melbourne Gastric Cancer Group PMMAF. 2005. Novel regions of chromosomal amplification at 6p21, 5p13, and 12q14 in gastric cancer identified by array comparative genomic hybridization. Genes Chromosomes Cancer *42*, 247-259.

Graham FL and van der Eb AJ. 1973. Transformation of rat cells by DNA of human adenovirus 5. Virology *54*, 536-539.

Greenman C, Stephens P, Smith R, Dalgliesh GL*, et al.* 2007. Patterns of somatic mutation in human cancer genomes. Nature *446*, 153-158.

Gross S, Rahal R, Stransky N, Lengauer C and Hoeflich KP. 2015. Targeting cancer with kinase inhibitors. J Clin Invest *125*, 1780-1789.

Grueneberg DA, Degot S, Pearlberg J, Li W*, et al.* 2008. Kinase requirements in human cells: I. Comparing kinase requirements across various cell types. Proc Natl Acad Sci U S A *105*, 16472-16477.

Grueneberg DA, Li W, Davies JE, Sawyer J, Pearlberg J and Harlow E. 2008. Kinase requirements in human cells: IV. Differential kinase requirements in cervical and renal human tumor cell lines. Proc Natl Acad Sci U S A *105*, 16490-16495.

Gu Z, Eils R and Schlesner M. 2016. Complex heatmaps reveal patterns and correlations in multidimensional genomic data. Bioinformatics *32*, 2847-2849.

Guedj F, Sebrie C, Rivals I, Ledru A*, et al.* 2009. Green tea polyphenols rescue of brain defects induced by overexpression of DYRK1A. PLoS One *4*, e4606.

Guerois R, Nielsen JE and Serrano L. 2002. Predicting changes in the stability of proteins and protein complexes: a study of more than 1000 mutations. J Mol Biol *320*, 369-387.

Guimera J, Casas C, Pucharcos C, Solans A*, et al.* 1996. A human homologue of Drosophila minibrain (MNB) is expressed in the neuronal regions affected in Down syndrome and maps to the critical region. Hum Mol Genet *5*, 1305-1310.

Guimera J, Casas C, Estivill X and Pritchard M. 1999. Human minibrain homologue (MNBH/DYRK1): characterization, alternative splicing, differential tissue expression, and overexpression in Down syndrome. Genomics *57*, 407-418.

Guo X, Williams JG, Schug TT and Li X. 2010. DYRK1A and DYRK3 promote cell survival through phosphorylation and activation of SIRT1. J Biol Chem *285*, 13223-13232.

Guo X, Wang X, Wang Z, Banerjee S*, et al.* 2016. Site-specific proteasome phosphorylation controls cell proliferation and tumorigenesis. Nat Cell Biol *18*, 202-212.

Gupta S, Takebe N and Lorusso P. 2010. Targeting the Hedgehog pathway in cancer. Ther Adv Med Oncol *2*, 237-250.

Guschin DY, Waite AJ, Katibah GE, Miller JC, Holmes MC and Rebar EJ. 2010. A rapid and general assay for monitoring endogenous gene modification. Methods Mol Biol *649*, 247-256.

Gwack Y, Sharma S, Nardone J, Tanasa B*, et al.* 2006. A genome-wide Drosophila RNAi screen identifies DYRK-family kinases as regulators of NFAT. Nature *441*, 646-650.

Haigis KM, Cichowski K and Elledge SJ. 2019. Tissue-specificity in cancer: The rule, not the exception. Science *363*, 1150-1151.

Hammerle B, Carnicero A, Elizalde C, Ceron J, Martinez S and Tejedor FJ. 2003. Expression patterns and subcellular localization of the Down syndrome candidate protein MNB/DYRK1A suggest a role in late neuronal differentiation. Eur J Neurosci *17*, 2277-2286.

Harrison JR and Owen MJ. 2016. Alzheimer's disease: the amyloid hypothesis on trial. Br J Psychiatry *208*, 1-3.

Hasle H, Clemmensen IH and Mikkelsen M. 2000. Risks of leukaemia and solid tumours in individuals with Down's syndrome. Lancet *355*, 165-169.

Hasle H. 2001. Pattern of malignant disorders in individuals with Down's syndrome. Lancet Oncol *2*, 429-436.

Heijink AM, Krajewska M and van Vugt MA. 2013. The DNA damage response during mitosis. Mutat Res *750*, 45-55.

Henley SJ, Miller JW, Dowling NF, Benard VB and Richardson LC. 2018. Uterine Cancer Incidence and Mortality - United States, 1999-2016. MMWR Morb Mortal Wkly Rep *67*, 1333-1338.

Herbert SP and Stainier DY. 2011. Molecular control of endothelial cell behaviour during blood vessel morphogenesis. Nat Rev Mol Cell Biol *12*, 551-564.

Hill DA, Gridley G, Cnattingius S, Mellemkjaer L*, et al.* 2003. Mortality and cancer incidence among individuals with Down syndrome. Arch Intern Med *163*, 705-711.

Hille S, Dierck F, Kuhl C, Sosna J*, et al.* 2016. Dyrk1a regulates the cardiomyocyte cell cycle via D-cyclin-dependent Rb/E2f-signalling. Cardiovasc Res *110*, 381-394.

Himpel S, Tegge W, Frank R, Leder S, Joost HG and Becker W. 2000. Specificity determinants of substrate recognition by the protein kinase DYRK1A. J Biol Chem *275*, 2431-2438.

Himpel S, Panzer P, Eirmbter K, Czajkowska H*, et al.* 2001. Identification of the autophosphorylation sites and characterization of their effects in the protein kinase DYRK1A. Biochem J *359*, 497-505.

Hoadley KA, Yau C, Hinoue T, Wolf DM*, et al.* 2018. Cell-of-Origin Patterns Dominate the Molecular Classification of 10,000 Tumors from 33 Types of Cancer. Cell *173*, 291-304 e296.

Horvath CM. 2000. STAT proteins and transcriptional responses to extracellular signals. Trends Biochem Sci *25*, 496-502.

Hu J and Friedman E. 2010. Depleting Mirk Kinase Increases Cisplatin Toxicity in Ovarian Cancer Cells. Genes Cancer *1*, 803-811.

Hu J, Nakhla H and Friedman E. 2011. Transient arrest in a quiescent state allows ovarian cancer cells to survive suboptimal growth conditions and is mediated by both Mirk/dyrk1b and p130/RB2. Int J Cancer *129*, 307-318.

Hu J, Deng H and Friedman EA. 2013. Ovarian cancer cells, not normal cells, are damaged by Mirk/Dyrk1B kinase inhibition. Int J Cancer *132*, 2258-2269.

Ilic M and Ilic I. 2016. Epidemiology of pancreatic cancer. World J Gastroenterol *22*, 9694-9705.

International Cancer Genome C, Hudson TJ, Anderson W, Artez A*, et al.* 2010. International network of cancer genome projects. Nature *464*, 993-998.

Isaka K, Nishi H, Sagawa Y, Nakada T*, et al.* 2003. Establishment of a new human cell line (EN) with TP53 mutation derived from endometrial carcinoma. Cancer Genet Cytogenet *141*, 20-25.

Ishida J, Wang HK, Bastow KF, Hu CQ and Lee KH. 1999. Antitumor agents 201. Cytotoxicity of harmine and beta-carboline analogs. Bioorg Med Chem Lett *9*, 3319-3324.

Italiano A, Bianchini L, Keslair F, Bonnafous S*, et al.* 2008. HMGA2 is the partner of MDM2 in well-differentiated and dedifferentiated liposarcomas whereas CDK4 belongs to a distinct inconsistent amplicon. Int J Cancer *122*, 2233-2241.

Ivashkiv LB and Donlin LT. 2014. Regulation of type I interferon responses. Nat Rev Immunol *14*, 36-49.

Jarhad DB, Mashelkar KK, Kim HR, Noh M and Jeong LS. 2018. Dual-Specificity Tyrosine Phosphorylation-Regulated Kinase 1A (DYRK1A) Inhibitors as Potential Therapeutics. J Med Chem *61*, 9791-9810.

Jayathilaka K, Sheridan SD, Bold TD, Bochenska K*, et al.* 2008. A chemical compound that stimulates the human homologous recombination protein RAD51. Proc Natl Acad Sci U S A *105*, 15848-15853.

Ji J, Lee H, Argiropoulos B, Dorrani N*, et al.* 2015. DYRK1A haploinsufficiency causes a new recognizable syndrome with microcephaly, intellectual disability, speech impairment, and distinct facies. Eur J Hum Genet *23*, 1473-1481.

Jin K, Ewton DZ, Park S, Hu J and Friedman E. 2009. Mirk regulates the exit of colon cancer cells from quiescence. J Biol Chem *284*, 22916-22925.

Jowsey P, Morrice NA, Hastie CJ, McLauchlan H, Toth R and Rouse J. 2007. Characterisation of the sites of DNA damage-induced 53BP1 phosphorylation catalysed by ATM and ATR. DNA Repair (Amst) *6*, 1536-1544.

Kaczmarski W, Barua M, Mazur-Kolecka B, Frackowiak J*, et al.* 2014. Intracellular distribution of differentially phosphorylated dual-specificity tyrosine phosphorylation-regulated kinase 1A (DYRK1A). J Neurosci Res *92*, 162-173.

Kan Z, Jaiswal BS, Stinson J, Janakiraman V*, et al.* 2010. Diverse somatic mutation patterns and pathway alterations in human cancers. Nature *466*, 869-873.

Kang JE, Choi SA, Park JB and Chung KC. 2005. Regulation of the proapoptotic activity of huntingtin interacting protein 1 by Dyrk1 and caspase-3 in hippocampal neuroprogenitor cells. J Neurosci Res *81*, 62-72.

Karaman MW, Herrgard S, Treiber DK, Gallant P*, et al.* 2008. A quantitative analysis of kinase inhibitor selectivity. Nat Biotechnol *26*, 127-132.

Kastan MB and Bartek J. 2004. Cell-cycle checkpoints and cancer. Nature *432*, 316-323.

Kastenhuber ER and Lowe SW. 2017. Putting p53 in Context. Cell *170*, 1062-1078.

Kentrup H, Becker W, Heukelbach J, Wilmes A*, et al.* 1996. Dyrk, a dual specificity protein kinase with unique structural features whose activity is dependent on tyrosine residues between subdomains VII and VIII. J Biol Chem *271*, 3488-3495.

Kiani A, Kuithan H, Kuithan F, Kyttala S*, et al.* 2007. Expression analysis of nuclear factor of activated T cells (NFAT) during myeloid differentiation of CD34+ cells: regulation of Fas ligand gene expression in megakaryocytes. Exp Hematol *35*, 757-770.

Kida E, Walus M, Jarzabek K, Palminiello S*, et al.* 2011. Form of dual-specificity tyrosine-(Y)-phosphorylation-regulated kinase 1A nonphosphorylated at tyrosine 145 and 147 is enriched in the nuclei of astroglial cells, adult hippocampal progenitors, and some cholinergic axon terminals. Neuroscience *195*, 112-127.

Kii I, Sumida Y, Goto T, Sonamoto R*, et al.* 2016. Selective inhibition of the kinase DYRK1A by targeting its folding process. Nat Commun *7*, 11391.

Kim D, Won J, Shin DW, Kang J*, et al.* 2004. Regulation of Dyrk1A kinase activity by 14-3-3. Biochem Biophys Res Commun *323*, 499-504.

Kim H, Sablin SO and Ramsay RR. 1997. Inhibition of monoamine oxidase A by beta-carboline derivatives. Arch Biochem Biophys *337*, 137-142.

Kim H, Lee KS, Kim AK, Choi M*, et al.* 2016. A chemical with proven clinical safety rescues Down-syndrome-related phenotypes in through DYRK1A inhibition. Dis Model Mech *9*, 839-848.

Kim J, Siverly AN, Chen D, Wang M*, et al.* 2016. Ablation of miR-10b Suppresses Oncogene-Induced Mammary Tumorigenesis and Metastasis and Reactivates Tumor-Suppressive Pathways. Cancer Res *76*, 6424-6435.

Kim TH, Yoo JY and Jeong JW. 2017. Mig-6 Mouse Model of Endometrial Cancer. Adv Exp Med Biol *943*, 243-259.

Kimura R, Kamino K, Yamamoto M, Nuripa A*, et al.* 2007. The DYRK1A gene, encoded in chromosome 21 Down syndrome critical region, bridges between beta-amyloid production and tau phosphorylation in Alzheimer disease. Hum Mol Genet *16*, 15-23.

Kinstrie R, Luebbering N, Miranda-Saavedra D, Sibbet G*, et al.* 2010. Characterization of a domain that transiently converts class 2 DYRKs into intramolecular tyrosine kinases. Sci Signal *3*, ra16.

Komorek J, Kuppuswamy M, Subramanian T, Vijayalingam S*, et al.* 2010. Adenovirus type 5 E1A and E6 proteins of low-risk cutaneous beta-human papillomaviruses suppress cell transformation through interaction with FOXK1/K2 transcription factors. J Virol *84*, 2719-2731.

Koon N, Schneider-Stock R, Sarlomo-Rikala M, Lasota J*, et al.* 2004. Molecular targets for tumour progression in gastrointestinal stromal tumours. Gut *53*, 235-240.

Koretzky GA. 2007. The legacy of the Philadelphia chromosome. J Clin Invest *117*, 2030-2032.

Krijgsman O, Carvalho B, Meijer GA, Steenbergen RD and Ylstra B. 2014. Focal chromosomal copy number aberrations in cancer-Needles in a genome haystack. Biochim Biophys Acta *1843*, 2698-2704.

Kugel S, Feldman JL, Klein MA, Silberman DM*, et al.* 2015. Identification of and Molecular Basis for SIRT6 Loss-of-Function Point Mutations in Cancer. Cell Rep *13*, 479-488.

Kuhn C, Frank D, Will R, Jaschinski C*, et al.* 2009. DYRK1A is a novel negative regulator of cardiomyocyte hypertrophy. J Biol Chem *284*, 17320-17327.

Kuleshov MV, Jones MR, Rouillard AD, Fernandez NF*, et al.* 2016. Enrichr: a comprehensive gene set enrichment analysis web server 2016 update. Nucleic Acids Res *44*, W90-97.

Kumar K, Wang P, Sanchez R, Swartz EA, Stewart AF and DeVita RJ. 2018. Development of Kinase-Selective, Harmine-Based DYRK1A Inhibitors that Induce Pancreatic Human beta-Cell Proliferation. J Med Chem *61*, 7687-7699.

Kurabayashi N, Nguyen MD and Sanada K. 2015. DYRK1A overexpression enhances STAT activity and astrogliogenesis in a Down syndrome mouse model. EMBO Rep *16*, 1548-1562.

Kuroboshi H, Okubo T, Kitaya K, Nakayama T*, et al.* 2003. Interferon regulatory factor-1 expression in human uterine endometrial carcinoma. Gynecol Oncol *91*, 354-358.

Kuuselo R, Savinainen K, Azorsa DO, Basu GD*, et al.* 2007. Intersex-like (IXL) is a cell survival regulator in pancreatic cancer with 19q13 amplification. Cancer Res *67*, 1943-1949.

Laguna A, Aranda S, Barallobre MJ, Barhoum R*, et al.* 2008. The protein kinase DYRK1A regulates caspase-9-mediated apoptosis during retina development. Dev Cell *15*, 841-853.

Laguna A, Barallobre MJ, Marchena MA, Mateus C*, et al.* 2013. Triplication of DYRK1A causes retinal structural and functional alterations in Down syndrome. Hum Mol Genet *22*, 2775-2784.

Lahiry P, Torkamani A, Schork NJ and Hegele RA. 2010. Kinase mutations in human disease: interpreting genotype-phenotype relationships. Nat Rev Genet *11*, 60-74.

Lasorella A, Benezra R and Iavarone A. 2014. The ID proteins: master regulators of cancer stem cells and tumour aggressiveness. Nat Rev Cancer *14*, 77-91.

Lawrence MS, Stojanov P, Polak P, Kryukov GV*, et al.* 2013. Mutational heterogeneity in cancer and the search for new cancer-associated genes. Nature *499*, 214-218.

Lax SF and Kurman RJ. 1997. A dualistic model for endometrial carcinogenesis based on immunohistochemical and molecular genetic analyses. Verh Dtsch Ges Pathol *81*, 228-232.

Leder S, Weber Y, Altafaj X, Estivill X, Joost HG and Becker W. 1999. Cloning and characterization of DYRK1B, a novel member of the DYRK family of protein kinases. Biochem Biophys Res Commun *254*, 474-479.

Lee P, Bhansali R, Izraeli S, Hijiya N and Crispino JD. 2016. The biology, pathogenesis and clinical aspects of acute lymphoblastic leukemia in children with Down syndrome. Leukemia *30*, 1816-1823.

Lee SB, Frattini V, Bansal M, Castano AM*, et al.* 2016. An ID2-dependent mechanism for VHL inactivation in cancer. Nature *529*, 172-177.

Lee Y, Ha J, Kim HJ, Kim YS*, et al.* 2009. Negative feedback Inhibition of NFATc1 by DYRK1A regulates bone homeostasis. J Biol Chem *284*, 33343-33351.

Leiserson MD, Vandin F, Wu HT, Dobson JR*, et al.* 2015. Pan-cancer network analysis identifies combinations of rare somatic mutations across pathways and protein complexes. Nat Genet *47*, 106-114.

Lek M, Karczewski KJ, Minikel EV, Samocha KE*, et al.* 2016. Analysis of protein-coding genetic variation in 60,706 humans. Nature *536*, 285-291.

Lemmon MA and Schlessinger J. 2010. Cell signaling by receptor tyrosine kinases. Cell *141*, 1117-1134.

Lemmon MA, Schlessinger J and Ferguson KM. 2014. The EGFR family: not so prototypical receptor tyrosine kinases. Cold Spring Harb Perspect Biol *6*, a020768.

Lepagnol-Bestel AM, Zvara A, Maussion G, Quignon F*, et al.* 2009. DYRK1A interacts with the REST/NRSF-SWI/SNF chromatin remodelling complex to deregulate gene clusters involved in the neuronal phenotypic traits of Down syndrome. Hum Mol Genet *18*, 1405-1414.

Levy DE and Darnell JE, Jr. 2002. Stats: transcriptional control and biological impact. Nat Rev Mol Cell Biol *3*, 651-662.

Li D, Jackson RA, Yusoff P and Guy GR. 2010. Direct association of Sprouty-related protein with an EVH1 domain (SPRED) 1 or SPRED2 with DYRK1A modifies substrate/kinase interactions. J Biol Chem *285*, 35374-35385.

Li M, Kales SC, Ma K, Shoemaker BA*, et al.* 2016. Balancing Protein Stability and Activity in Cancer: A New Approach for Identifying Driver Mutations Affecting CBL Ubiquitin Ligase Activation. Cancer Res *76*, 561-571.

Li Q, Zhang M, Kumar S, Zhu LJ*, et al.* 2001. Identification and implantation stage-specific expression of an interferon-alpha-regulated gene in human and rat endometrium. Endocrinology *142*, 2390-2400.

Liang YJ, Chang HS, Wang CY and Yu WC. 2008. DYRK1A stabilizes HPV16E7 oncoprotein through phosphorylation of the threonine 5 and threonine 7 residues. Int J Biochem Cell Biol *40*, 2431-2441.

Litovchick L, Florens LA, Swanson SK, Washburn MP and DeCaprio JA. 2011. DYRK1A protein kinase promotes quiescence and senescence through DREAM complex assembly. Genes Dev *25*, 801-813.

Liu Q, Liu N, Zang S, Liu H*, et al.* 2014. Tumor suppressor DYRK1A effects on proliferation and chemoresistance of AML cells by downregulating c-Myc. PLoS One *9*, e98853.

Liu Y, Hu X, Han C, Wang L*, et al.* 2015. Targeting tumor suppressor genes for cancer therapy. Bioessays *37*, 1277-1286.

Lobry C, Oh P, Mansour MR, Look AT and Aifantis I. 2014. Notch signaling: switching an oncogene to a tumor suppressor. Blood *123*, 2451-2459.

Lochhead PA, Sibbet G, Morrice N and Cleghon V. 2005. Activation-loop autophosphorylation is mediated by a novel transitional intermediate form of DYRKs. Cell *121*, 925-936.

Love MI, Huber W and Anders S. 2014. Moderated estimation of fold change and dispersion for RNA-seq data with DESeq2. Genome Biol *15*, 550.

Lu M, Zheng L, Han B, Wang L*, et al.* 2011. REST regulates DYRK1A transcription in a negative feedback loop. J Biol Chem *286*, 10755-10763.

Luco SM, Pohl D, Sell E, Wagner JD, Dyment DA and Daoud H. 2016. Case report of novel DYRK1A mutations in 2 individuals with syndromic intellectual disability and a review of the literature. BMC Med Genet *17*, 15.

Luna J, Boni J, Cuatrecasas M, Bofill-De Ros X*, et al.* 2018. DYRK1A modulates c-MET in pancreatic ductal adenocarcinoma to drive tumour growth. Gut

MacDonald J, Ramos-Valdes Y, Perampalam P, Litovchick L, DiMattia GE and Dick FA. 2017. A Systematic Analysis of Negative Growth Control Implicates the DREAM Complex in Cancer Cell Dormancy. Mol Cancer Res *15*, 371-381.

Macian F. 2005. NFAT proteins: key regulators of T-cell development and function. Nat Rev Immunol *5*, 472-484.

Maenz B, Hekerman P, Vela EM, Galceran J and Becker W. 2008. Characterization of the human DYRK1A promoter and its regulation by the transcription factor E2F1. BMC Mol Biol *9*, 30.

Maher EA, Brennan C, Wen PY, Durso L*, et al.* 2006. Marked genomic differences characterize primary and secondary glioblastoma subtypes and identify two distinct molecular and clinical secondary glioblastoma entities. Cancer Res *66*, 11502-11513.

Majoros A, Platanitis E, Kernbauer-Holzl E, Rosebrock F, Muller M and Decker T. 2017. Canonical and Non-Canonical Aspects of JAK-STAT Signaling: Lessons from Interferons for Cytokine Responses. Front Immunol *8*, 29.

Malinge S, Bliss-Moreau M, Kirsammer G, Diebold L*, et al.* 2012. Increased dosage of the chromosome 21 ortholog Dyrk1a promotes megakaryoblastic leukemia in a murine model of Down syndrome. J Clin Invest *122*, 948-962.

Mancini M and Toker A. 2009. NFAT proteins: emerging roles in cancer progression. Nat Rev Cancer *9*, 810-820.

Mandal M, Bandyopadhyay D, Goepfert TM and Kumar R. 1998. Interferon-induces expression of cyclin-dependent kinase-inhibitors p21WAF1 and p27Kip1 that prevent activation of cyclin-dependent kinase by CDK-activating kinase (CAK). Oncogene *16*, 217-225.

Manning G, Whyte DB, Martinez R, Hunter T and Sudarsanam S. 2002. The protein kinase complement of the human genome. Science *298*, 1912-1934.

Mao J, Maye P, Kogerman P, Tejedor FJ*, et al.* 2002. Regulation of Gli1 transcriptional activity in the nucleus by Dyrk1. J Biol Chem *277*, 35156-35161.

Marti E, Altafaj X, Dierssen M, de la Luna S*, et al.* 2003. Dyrk1A expression pattern supports specific roles of this kinase in the adult central nervous system. Brain Res *964*, 250-263.

Martincorena I and Campbell PJ. 2015. Somatic mutation in cancer and normal cells. Science *349*, 1483-1489.

Matsuo R, Ochiai W, Nakashima K and Taga T. 2001. A new expression cloning strategy for isolation of substrate-specific kinases by using phosphorylation site-specific antibody. J Immunol Methods *247*, 141-151.

McElyea SD, Starbuck JM, Tumbleson-Brink DM, Harrington E*, et al.* 2016. Influence of prenatal EGCG treatment and Dyrk1a dosage reduction on craniofacial features associated with Down syndrome. Hum Mol Genet *25*, 4856-4869.

McGuigan A, Kelly P, Turkington RC, Jones C, Coleman HG and McCain RS. 2018. Pancreatic cancer: A review of clinical diagnosis, epidemiology, treatment and outcomes. World J Gastroenterol *24*, 4846-4861.

Meissl K, Macho-Maschler S, Muller M and Strobl B. 2017. The good and the bad faces of STAT1 in solid tumours. Cytokine *89*, 12-20.

Mercer SE, Ewton DZ, Shah S, Naqvi A and Friedman E. 2006. Mirk/Dyrk1b mediates cell survival in rhabdomyosarcomas. Cancer Res *66*, 5143-5150.

Mermel CH, Schumacher SE, Hill B, Meyerson ML, Beroukhim R and Getz G. 2011. GISTIC2.0 facilitates sensitive and confident localization of the targets of focal somatic copy-number alteration in human cancers. Genome Biol *12*, R41.

Meyerson M, Gabriel S and Getz G. 2010. Advances in understanding cancer genomes through second-generation sequencing. Nat Rev Genet *11*, 685-696.

Miki Y, Swensen J, Shattuck-Eidens D, Futreal PA*, et al.* 1994. A strong candidate for the breast and ovarian cancer susceptibility gene BRCA1. Science *266*, 66-71.

Miller CT, Aggarwal S, Lin TK, Dagenais SL*, et al.* 2003. Amplification and overexpression of the dual-specificity tyrosine-(Y)-phosphorylation regulated kinase 2 (DYRK2) gene in esophageal and lung adenocarcinomas. Cancer Res *63*, 4136-4143.

Mimoto R, Taira N, Takahashi H, Yamaguchi T*, et al.* 2013. DYRK2 controls the epithelial-mesenchymal transition in breast cancer by degrading Snail. Cancer Lett *339*, 214-225.

Mirantes C, Eritja N, Dosil MA, Santacana M*, et al.* 2013. An inducible knockout mouse to model the cell-autonomous role of PTEN in initiating endometrial, prostate and thyroid neoplasias. Dis Model Mech *6*, 710-720.

Miwa W, Yasuda J, Murakami Y, Yashima K*, et al.* 1996. Isolation of DNA sequences amplified at chromosome 19q13.1-q13.2 including the AKT2 locus in human pancreatic cancer. Biochem Biophys Res Commun *225*, 968-974.

Modica C, Tortarolo D, Comoglio PM, Basilico C and Vigna E. 2018. MET/HGF Co-Targeting in Pancreatic Cancer: A Tool to Provide Insight into the Tumor/Stroma Crosstalk. Int J Mol Sci *19*,

Mohan R and John A. 2015. Microtubule-associated proteins as direct crosslinkers of actin filaments and microtubules. IUBMB Life *67*, 395-403.

Moller RS, Kubart S, Hoeltzenbein M, Heye B*, et al.* 2008. Truncation of the Down syndrome candidate gene DYRK1A in two unrelated patients with microcephaly. Am J Hum Genet *82*, 1165-1170.

Morris LG and Chan TA. 2015. Therapeutic targeting of tumor suppressor genes. Cancer *121*, 1357-1368.

Morton S, Davis RJ, McLaren A and Cohen P. 2003. A reinvestigation of the multisite phosphorylation of the transcription factor c-Jun. EMBO J *22*, 3876-3886.

Murakami N, Bolton D and Hwang YW. 2009. Dyrk1A binds to multiple endocytic proteins required for formation of clathrin-coated vesicles. Biochemistry *48*, 9297-9305.

Musella M, Manic G, De Maria R, Vitale I and Sistigu A. 2017. Type-I-interferons in infection and cancer: Unanticipated dynamics with therapeutic implications. Oncoimmunology *6*, e1314424.

Najas S, Arranz J, Lochhead PA, Ashford AL*, et al.* 2015. DYRK1A-mediated Cyclin D1 Degradation in Neural Stem Cells Contributes to the Neurogenic Cortical Defects in Down Syndrome. EBioMedicine *2*, 120-134.

Ng CT, Mendoza JL, Garcia KC and Oldstone MB. 2016. Alpha and Beta Type 1 Interferon Signaling: Passage for Diverse Biologic Outcomes. Cell *164*, 349-352.

Nihira NT and Yoshida K. 2015. Engagement of DYRK2 in proper control for cell division. Cell Cycle *14*, 802-807.

Nijman SM. 2011. Synthetic lethality: general principles, utility and detection using genetic screens in human cells. FEBS Lett *585*, 1-6.

Nissen RM, Amsterdam A and Hopkins N. 2006. A zebrafish screen for craniofacial mutants identifies wdr68 as a highly conserved gene required for endothelin-1 expression. BMC Dev Biol *6*, 28.

Nizetic D and Groet J. 2012. Tumorigenesis in Down's syndrome: big lessons from a small chromosome. Nat Rev Cancer *12*, 721-732.

Nolen B, Taylor S and Ghosh G. 2004. Regulation of protein kinases; controlling activity through activation segment conformation. Mol Cell *15*, 661-675.

O'Neil NJ, Bailey ML and Hieter P. 2017. Synthetic lethality and cancer. Nat Rev Genet *18*, 613-623.

Ogawa Y, Nonaka Y, Goto T, Ohnishi E*, et al.* 2010. Development of a novel selective inhibitor of the Down syndrome-related kinase Dyrk1A. Nat Commun *1*, 86.

Ohshima K, Hatakeyama K, Nagashima T, Watanabe Y*, et al.* 2017. Integrated analysis of gene expression and copy number identified potential cancer driver genes with amplification-dependent overexpression in 1,454 solid tumors. Sci Rep *7*, 641.

Oi A, Katayama S, Hatano N, Sugiyama Y, Kameshita I and Sueyoshi N. 2017. Subcellular distribution of cyclin-dependent kinase-like 5 (CDKL5) is regulated through phosphorylation by dual specificity tyrosine-phosphorylation-regulated kinase 1A (DYRK1A). Biochem Biophys Res Commun *482*, 239-245.

Oldrini B, Curiel-Garcia A, Marques C, Matia V*, et al.* 2018. Somatic genome editing with the RCAS-TVA-CRISPR-Cas9 system for precision tumor modeling. Nat Commun *9*, 1466.

Orthwein A, Fradet-Turcotte A, Noordermeer SM, Canny MD*, et al.* 2014. Mitosis inhibits DNA double-strand break repair to guard against telomere fusions. Science *344*, 189-193.

Ozaki T, Takahashi K, Kanasaki H, Iida K and Miyazaki K. 2005. Expression of the type I interferon receptor and the interferon-induced Mx protein in human endometrium during the menstrual cycle. Fertil Steril *83*, 163-170.

Papadopoulos C, Arato K, Lilienthal E, Zerweck J*, et al.* 2011. Splice variants of the dual specificity tyrosine phosphorylation-regulated kinase 4 (DYRK4) differ in their subcellular localization and catalytic activity. J Biol Chem *286*, 5494-5505.

Paquet D, Kwart D, Chen A, Sproul A*, et al.* 2016. Efficient introduction of specific homozygous and heterozygous mutations using CRISPR/Cas9. Nature *533*, 125-129.

Park J, Oh Y, Yoo L, Jung MS*, et al.* 2010. Dyrk1A phosphorylates p53 and inhibits proliferation of embryonic neuronal cells. J Biol Chem *285*, 31895-31906.

Patja K, Pukkala E, Sund R, Iivanainen M and Kaski M. 2006. Cancer incidence of persons with Down syndrome in Finland: a population-based study. Int J Cancer *118*, 1769-1772.

Payne SR and Kemp CJ. 2005. Tumor suppressor genetics. Carcinogenesis *26*, 2031-2045.

Pozo N, Zahonero C, Fernandez P, Linares JM*, et al.* 2013. Inhibition of DYRK1A destabilizes EGFR and reduces EGFR-dependent glioblastoma growth. J Clin Invest *123*, 2475-2487.

Raaf L, Noll C, Cherifi M, Benazzoug Y, Delabar JM and Janel N. 2010. Hyperhomocysteinemia-induced Dyrk1a downregulation results in cardiomyocyte hypertrophy in rats. Int J Cardiol *145*, 306-307.

Radhakrishnan A, Nanjappa V, Raja R, Sathe G*, et al.* 2016. A dual specificity kinase, DYRK1A, as a potential therapeutic target for head and neck squamous cell carcinoma. Sci Rep *6*, 36132.

Rahib L, Smith BD, Aizenberg R, Rosenzweig AB, Fleshman JM and Matrisian LM. 2014. Projecting cancer incidence and deaths to 2030: the unexpected burden of thyroid, liver, and pancreas cancers in the United States. Cancer Res *74*, 2913-2921.

Ran FA, Hsu PD, Wright J, Agarwala V, Scott DA and Zhang F. 2013. Genome engineering using the CRISPR-Cas9 system. Nat Protoc *8*, 2281-2308.

Raveau M, Shimohata A, Amano K, Miyamoto H and Yamakawa K. 2018. DYRK1A-haploinsufficiency in mice causes autistic-like features and febrile seizures. Neurobiol Dis *110*, 180-191.

Renaud JB, Boix C, Charpentier M, De Cian A*, et al.* 2016. Improved Genome Editing Efficiency and Flexibility Using Modified Oligonucleotides with TALEN and CRISPR-Cas9 Nucleases. Cell Rep *14*, 2263-2272.

Rizwani W, Allen AE and Trevino JG. 2015. Hepatocyte Growth Factor from a Clinical Perspective: A Pancreatic Cancer Challenge. Cancers (Basel) *7*, 1785-1805.

Robinson MD and Oshlack A. 2010. A scaling normalization method for differential expression analysis of RNA-seq data. Genome Biol *11*, R25.

Roewenstrunk J. 2016. RNF169 and RNF168 novel substrates of DYRK1A: connecting DYRK1A to DNA-damage repair. Universitat Pompeu Fabra, Barcelona, Spain.

Rogers S, Wells R and Rechsteiner M. 1986. Amino acid sequences common to rapidly degraded proteins: the PEST hypothesis. Science *234*, 364-368.

Rozen EJ, Roewenstrunk J, Barallobre MJ, Di Vona C*, et al.* 2018. DYRK1A Kinase Positively Regulates Angiogenic Responses in Endothelial Cells. Cell Rep *23*, 1867-1878.

Rubio-Perez C, Tamborero D, Schroeder MP, Antolin AA*, et al.* 2015. In silico prescription of anticancer drugs to cohorts of 28 tumor types reveals targeting opportunities. Cancer Cell *27*, 382-396.

Ryoo SR, Cho HJ, Lee HW, Jeong HK*, et al.* 2008. Dual-specificity tyrosine(Y)-phosphorylation regulated kinase 1A-mediated phosphorylation of amyloid precursor protein: evidence for a functional link between Down syndrome and Alzheimer's disease. J Neurochem *104*, 1333-1344.

Sabapathy K and Lane DP. 2018. Therapeutic targeting of p53: all mutants are equal, but some mutants are more equal than others. Nat Rev Clin Oncol *15*, 13-30.

Sacher F, Moller C, Bone W, Gottwald U and Fritsch M. 2007. The expression of the testis-specific Dyrk4 kinase is highly restricted to step 8 spermatids but is not required for male fertility in mice. Mol Cell Endocrinol *267*, 80-88.

Sadasivam S and DeCaprio JA. 2013. The DREAM complex: master coordinator of cell cycle-dependent gene expression. Nat Rev Cancer *13*, 585-595.

Salichs E, Ledda A, Mularoni L, Alba MM and de la Luna S. 2009. Genome-wide analysis of histidine repeats reveals their role in the localization of human proteins to the nuclear speckles compartment. PLoS Genet *5*, e1000397.

Sansregret L, Gallo D, Santaguida M, Leduy L, Harada R and Nepveu A. 2010. Hyperphosphorylation by cyclin B/CDK1 in mitosis resets CUX1 DNA binding clock at each cell cycle. J Biol Chem *285*, 32834-32843.

Santarius T, Shipley J, Brewer D, Stratton MR and Cooper CS. 2010. A census of amplified and overexpressed human cancer genes. Nat Rev Cancer *10*, 59-64.

Schindelin J, Arganda-Carreras I, Frise E, Kaynig V*, et al.* 2012. Fiji: an open-source platform for biological-image analysis. Nat Methods *9*, 676-682.

Schneider G, Schmidt-Supprian M, Rad R and Saur D. 2017. Tissue-specific tumorigenesis: context matters. Nat Rev Cancer *17*, 239-253.

Schneider P, Bayo-Fina JM, Singh R, Kumar Dhanyamraju P*, et al.* 2015. Identification of a novel actin-dependent signal transducing module allows for the targeted degradation of GLI1. Nat Commun *6*, 8023.

Schymkowitz J, Borg J, Stricher F, Nys R, Rousseau F and Serrano L. 2005. The FoldX web server: an online force field. Nucleic Acids Res *33*, W382-388.

Sebe-Pedros A, Pena MI, Capella-Gutierrez S, Anto M*, et al.* 2016. High-Throughput Proteomics Reveals the Unicellular Roots of Animal Phosphosignaling and Cell Differentiation. Dev Cell *39*, 186-197.

Seifert A, Allan LA and Clarke PR. 2008. DYRK1A phosphorylates caspase 9 at an inhibitory site and is potently inhibited in human cells by harmine. FEBS J *275*, 6268-6280.

Shah AN, Summy JM, Zhang J, Park SI, Parikh NU and Gallick GE. 2007. Development and characterization of gemcitabine-resistant pancreatic tumor cells. Ann Surg Oncol *14*, 3629-3637.

Sharma SV, Bell DW, Settleman J and Haber DA. 2007. Epidermal growth factor receptor mutations in lung cancer. Nat Rev Cancer *7*, 169-181.

Shats I, Deng M, Davidovich A, Zhang C*, et al.* 2017. Expression level is a key determinant of E2F1-mediated cell fate. Cell Death Differ *24*, 626-637.

Shen Y, Zhang L, Wang D, Bao Y*, et al.* 2017. Regulation of Glioma Cells Migration by DYRK2. Neurochem Res *42*, 3093-3102.

Shibuya M, Suzuki Y, Sugita K, Saito I*, et al.* 1992. Effect of AT877 on cerebral vasospasm after aneurysmal subarachnoid hemorrhage. Results of a prospective placebo-controlled double-blind trial. J Neurosurg *76*, 571-577.

Shield K, Ackland ML, Ahmed N and Rice GE. 2009. Multicellular spheroids in ovarian cancer metastases: Biology and pathology. Gynecol Oncol *113*, 143-148.

Shirozu T, Iwano H, Ogiso T, Suzuki T*, et al.* 2017. Estrous cycle stage-dependent manner of type I interferon-stimulated genes induction in the bovine endometrium. J Reprod Dev *63*, 211-220.

Siddiqui-Jain A, Drygin D, Streiner N, Chua P*, et al.* 2010. CX-4945, an orally bioavailable selective inhibitor of protein kinase CK2, inhibits prosurvival and angiogenic signaling and exhibits antitumor efficacy. Cancer Res *70*, 10288-10298.

Siegel RL, Miller KD and Jemal A. 2018. Cancer statistics, 2018. CA Cancer J Clin *68*, 7-30.

Sitz JH, Tigges M, Baumgartel K, Khaspekov LG and Lutz B. 2004. Dyrk1A potentiates steroid hormone-induced transcription via the chromatin remodeling factor Arip4. Mol Cell Biol *24*, 5821-5834.

Skurat AV and Dietrich AD. 2004. Phosphorylation of Ser640 in muscle glycogen synthase by DYRK family protein kinases. J Biol Chem *279*, 2490-2498.

Snell LM, McGaha TL and Brooks DG. 2017. Type I Interferon in Chronic Virus Infection and Cancer. Trends Immunol *38*, 542-557.

Sommeijer DW, Sjoquist KM and Friedlander M. 2013. Hormonal treatment in recurrent and metastatic gynaecological cancers: a review of the current literature. Curr Oncol Rep *15*, 541-548.

Sonamoto R, Kii I, Koike Y, Sumida Y*, et al.* 2015. Identification of a DYRK1A Inhibitor that Induces Degradation of the Target Kinase using Co-chaperone CDC37 fused with Luciferase nanoKAZ. Sci Rep *5*, 12728.

Song J, Yang D, Xu J, Zhu T, Chen YE and Zhang J. 2016. RS-1 enhances CRISPR/Cas9- and TALEN-mediated knock-in efficiency. Nat Commun *7*, 10548.

Song WJ, Song EA, Jung MS, Choi SH*, et al.* 2015. Phosphorylation and inactivation of glycogen synthase kinase 3beta (GSK3beta) by dual-specificity tyrosine phosphorylation-regulated kinase 1A (Dyrk1A). J Biol Chem *290*, 2321-2333.

Sonnenblick A, de Azambuja E, Azim HA, Jr. and Piccart M. 2015. An update on PARP inhibitors--moving to the adjuvant setting. Nat Rev Clin Oncol *12*, 27-41.

Soppa U, Schumacher J, Florencio Ortiz V, Pasqualon T, Tejedor FJ and Becker W. 2014. The Down syndrome-related protein kinase DYRK1A phosphorylates p27(Kip1) and Cyclin D1 and induces cell cycle exit and neuronal differentiation. Cell Cycle *13*, 2084-2100.

Soundararajan M, Roos AK, Savitsky P, Filippakopoulos P*, et al.* 2013. Structures of Down syndrome kinases, DYRKs, reveal mechanisms of kinase activation and substrate recognition. Structure *21*, 986-996.

Spina A, De Pasquale V, Cerulo G, Cocchiaro P*, et al.* 2015. HGF/c-MET Axis in Tumor Microenvironment and Metastasis Formation. Biomedicines *3*, 71-88.

Stehelin D, Varmus HE, Bishop JM and Vogt PK. 1976. DNA related to the transforming gene(s) of avian sarcoma viruses is present in normal avian DNA. Nature *260*, 170-173.

Stewart SA, Dykxhoorn DM, Palliser D, Mizuno H*, et al.* 2003. Lentivirus-delivered stable gene silencing by RNAi in primary cells. RNA *9*, 493-501.

Storey JD and Tibshirani R. 2003. Statistical significance for genomewide studies. Proc Natl Acad Sci U S A *100*, 9440-9445.

Stratton MR, Campbell PJ and Futreal PA. 2009. The cancer genome. Nature *458*, 719-724.

Swaney DL, Beltrao P, Starita L, Guo A*, et al.* 2013. Global analysis of phosphorylation and ubiquitylation cross-talk in protein degradation. Nat Methods *10*, 676-682.

Tabin CJ, Bradley SM, Bargmann CI, Weinberg RA*, et al.* 1982. Mechanism of activation of a human oncogene. Nature *300*, 143-149.

Taira N, Nihira K, Yamaguchi T, Miki Y and Yoshida K. 2007. DYRK2 is targeted to the nucleus and controls p53 via Ser46 phosphorylation in the apoptotic response to DNA damage. Mol Cell *25*, 725-738.

Taira N, Yamamoto H, Yamaguchi T, Miki Y and Yoshida K. 2010. ATM augments nuclear stabilization of DYRK2 by inhibiting MDM2 in the apoptotic response to DNA damage. J Biol Chem *285*, 4909-4919.

Taira N, Mimoto R, Kurata M, Yamaguchi T*, et al.* 2012. DYRK2 priming phosphorylation of c-Jun and c-Myc modulates cell cycle progression in human cancer cells. J Clin Invest *122*, 859-872.

Tamborero D, Gonzalez-Perez A and Lopez-Bigas N. 2013. OncodriveCLUST: exploiting the positional clustering of somatic mutations to identify cancer genes. Bioinformatics *29*, 2238-2244.

Tamborero D, Gonzalez-Perez A, Perez-Llamas C, Deu-Pons J*, et al.* 2013. Comprehensive identification of mutational cancer driver genes across 12 tumor types. Sci Rep *3*, 2650.

Tate JG, Bamford S, Jubb HC, Sondka Z*, et al.* 2019. COSMIC: the Catalogue Of Somatic Mutations In Cancer. Nucleic Acids Res *47*, D941-D947.

Tejedor F, Zhu XR, Kaltenbach E, Ackermann A*, et al.* 1995. minibrain: a new protein kinase family involved in postembryonic neurogenesis in Drosophila. Neuron *14*, 287-301.

Thompson BJ, Bhansali R, Diebold L, Cook DE*, et al.* 2015. DYRK1A controls the transition from proliferation to quiescence during lymphoid development by destabilizing Cyclin D3. J Exp Med *212*, 953-970.

Thompson FH, Nelson MA, Trent JM, Guan XY*, et al.* 1996. Amplification of 19q13.1-q13.2 sequences in ovarian cancer. G-band, FISH, and molecular studies. Cancer Genet Cytogenet *87*, 55-62.

Tokheim CJ, Papadopoulos N, Kinzler KW, Vogelstein B and Karchin R. 2016. Evaluating the evaluation of cancer driver genes. Proc Natl Acad Sci U S A *113*, 14330-14335.

Tourneur L and Chiocchia G. 2010. FADD: a regulator of life and death. Trends Immunol *31*, 260-269.

Tschop K, Conery AR, Litovchick L, Decaprio JA*, et al.* 2011. A kinase shRNA screen links LATS2 and the pRB tumor suppressor. Genes Dev *25*, 814-830.

Uhl KL, Schultz CR, Geerts D and Bachmann AS. 2018. Harmine, a dual-specificity tyrosine phosphorylation-regulated kinase (DYRK) inhibitor induces caspase-mediated apoptosis in neuroblastoma. Cancer Cell Int *18*, 82.

van Bon BW, Hoischen A, Hehir-Kwa J, de Brouwer AP*, et al.* 2011. Intragenic deletion in DYRK1A leads to mental retardation and primary microcephaly. Clin Genet *79*, 296-299.

van Bon BW, Coe BP, Bernier R, Green C*, et al.* 2016. Disruptive de novo mutations of DYRK1A lead to a syndromic form of autism and ID. Mol Psychiatry *21*, 126-132.

Varjosalo M, Keskitalo S, Van Drogen A, Nurkkala H*, et al.* 2013. The protein interaction landscape of the human CMGC kinase group. Cell Rep *3*, 1306-1320.

Vitale I, Galluzzi L, Castedo M and Kroemer G. 2011. Mitotic catastrophe: a mechanism for avoiding genomic instability. Nat Rev Mol Cell Biol *12*, 385-392.

Vogelstein B, Papadopoulos N, Velculescu VE, Zhou S, Diaz LA, Jr. and Kinzler KW. 2013. Cancer genome landscapes. Science *339*, 1546-1558.

Walte A, Ruben K, Birner-Gruenberger R, Preisinger C*, et al.* 2013. Mechanism of dual specificity kinase activity of DYRK1A. FEBS J *280*, 4495-4511.

Wang P, Alvarez-Perez JC, Felsenfeld DP, Liu H*, et al.* 2015. A high-throughput chemical screen reveals that harmine-mediated inhibition of DYRK1A increases human pancreatic beta cell replication. Nat Med *21*, 383-388.

Wang P, Karakose E, Liu H, Swartz E*, et al.* 2019. Combined Inhibition of DYRK1A, SMAD, and Trithorax Pathways Synergizes to Induce Robust Replication in Adult Human Beta Cells. Cell Metab *29*, 638-652 e635.

Waters PJ. 2001. Degradation of mutant proteins, underlying "loss of function" phenotypes, plays a major role in genetic disease. Curr Issues Mol Biol *3*, 57-65.

Wechsler J, Greene M, McDevitt MA, Anastasi J*, et al.* 2002. Acquired mutations in GATA1 in the megakaryoblastic leukemia of Down syndrome. Nat Genet *32*, 148-152.

Wegiel J, Kuchna I, Nowicki K, Frackowiak J*, et al.* 2004. Cell type- and brain structure-specific patterns of distribution of minibrain kinase in human brain. Brain Res *1010*, 69-80.

Wen Z, Zhong Z and Darnell JE, Jr. 1995. Maximal activation of transcription by Stat1 and Stat3 requires both tyrosine and serine phosphorylation. Cell *82*, 241-250.

Westbrook TF, Martin ES, Schlabach MR, Leng Y*, et al.* 2005. A genetic screen for candidate tumor suppressors identifies REST. Cell *121*, 837-848.

Widowati EW, Ernst S, Hausmann R, Muller-Newen G and Becker W. 2018. Functional characterization of DYRK1A missense variants associated with a syndromic form of intellectual deficiency and autism. Biol Open *7*,

Wiechmann S, Czajkowska H, de Graaf K, Grotzinger J, Joost HG and Becker W. 2003. Unusual function of the activation loop in the protein kinase DYRK1A. Biochem Biophys Res Commun *302*, 403-408.

Wood LD, Parsons DW, Jones S, Lin J*, et al.* 2007. The genomic landscapes of human breast and colorectal cancers. Science *318*, 1108-1113.

Woods YL, Cohen P, Becker W, Jakes R*, et al.* 2001. The kinase DYRK phosphorylates protein-synthesis initiation factor eIF2Bepsilon at Ser539 and the microtubule-associated protein tau at Thr212: potential role for DYRK as a glycogen synthase kinase 3-priming kinase. Biochem J *355*, 609-615.

Woods YL, Rena G, Morrice N, Barthel A*, et al.* 2001. The kinase DYRK1A phosphorylates the transcription factor FKHR at Ser329 in vitro, a novel in vivo phosphorylation site. Biochem J *355*, 597-607.

Wooster R, Bignell G, Lancaster J, Swift S*, et al.* 1995. Identification of the breast cancer susceptibility gene BRCA2. Nature *378*, 789-792.

Xu H, Becker CM, Lui WT, Chu CY*, et al.* 2011. Green tea epigallocatechin-3-gallate inhibits angiogenesis and suppresses vascular endothelial growth factor C/vascular endothelial growth factor receptor 2 expression and signaling in experimental endometriosis in vivo. Fertil Steril *96*, 1021-1028.

Yabut O, Domogauer J and D'Arcangelo G. 2010. Dyrk1A overexpression inhibits proliferation and induces premature neuronal differentiation of neural progenitor cells. J Neurosci *30*, 4004-4014.

Yang C, Ji D, Weinstein EJ, Choy E*, et al.* 2010. The kinase Mirk is a potential therapeutic target in osteosarcoma. Carcinogenesis *31*, 552-558.

Yang CS, Wang X, Lu G and Picinich SC. 2009. Cancer prevention by tea: animal studies, molecular mechanisms and human relevance. Nat Rev Cancer *9*, 429-439.

Yang EJ, Ahn YS and Chung KC. 2001. Protein kinase Dyrk1 activates cAMP response element-binding protein during neuronal differentiation in hippocampal progenitor cells. J Biol Chem *276*, 39819-39824.

Yang L, Paul S, Trieu KG, Dent LG*, et al.* 2016. Minibrain and Wings apart control organ growth and tissue patterning through down-regulation of Capicua. Proc Natl Acad Sci U S A *113*, 10583-10588.

Yang Q, Rasmussen SA and Friedman JM. 2002. Mortality associated with Down's syndrome in the USA from 1983 to 1997: a population-based study. Lancet *359*, 1019-1025.

Yi K and Ju YS. 2018. Patterns and mechanisms of structural variations in human cancer. Exp Mol Med *50*, 98.

Yousefelahiyeh M, Xu J, Alvarado E, Yu Y, Salven D and Nissen RM. 2018. DCAF7/WDR68 is required for normal levels of DYRK1A and DYRK1B. PLoS One *13*, e0207779.

Zemke NR and Berk AJ. 2017. The Adenovirus E1A C Terminus Suppresses a Delayed Antiviral Response and Modulates RAS Signaling. Cell Host Microbe *22*, 789-800 e785.

Zhang D, Li K, Erickson-Miller CL, Weiss M and Wojchowski DM. 2005. DYRK gene structure and erythroid-restricted features of DYRK3 gene expression. Genomics *85*, 117-130.

Zhang J, Spath SS, Marjani SL, Zhang W and Pan X. 2018. Characterization of cancer genomic heterogeneity by next-generation sequencing advances precision medicine in cancer treatment. Precis Clin Med *1*, 29-48.

Zhang P, Huang CR, Wang W, Zhang XK*, et al.* 2016. Harmine Hydrochloride Triggers G2 Phase Arrest and Apoptosis in MGC-803 Cells and SMMC-7721 Cells by Upregulating p21, Activating Caspase-8/Bid, and Downregulating ERK/Bad Pathway. Phytother Res *30*, 31-40.

Zhang Y, Liao JM, Zeng SX and Lu H. 2011. p53 downregulates Down syndrome-associated DYRK1A through miR-1246. EMBO Rep *12*, 811-817.

Zhang Z, Smith MM and Mymryk JS. 2001. Interaction of the E1A oncoprotein with Yak1p, a novel regulator of yeast pseudohyphal differentiation, and related mammalian kinases. Mol Biol Cell *12*, 699-710.

Zhu JL, Hasle H, Correa A, Schendel D*, et al.* 2013. Survival among people with Down syndrome: a nationwide population-based study in Denmark. Genet Med *15*, 64-69.

Zou Y, Ewton DZ, Deng X, Mercer SE and Friedman E. 2004. Mirk/dyrk1B kinase destabilizes cyclin D1 by phosphorylation at threonine 288. J Biol Chem *279*, 27790-27798.

Zufferey R, Nagy D, Mandel RJ, Naldini L and Trono D. 1997. Multiply attenuated lentiviral vector achieves efficient gene delivery in vivo. Nat Biotechnol *15*, 871-875.

Annexes

Luna J, Boni J, Cuatrecasas M, Bofill-De Ros X, Núñez-Manchón E, Gironella M, et al. DYRK1A modulates c-MET in pancreatic ductal adenocarcinoma to drive tumour growth. Gut. 2019 Aug 1;68(8):1465–76. DOI: 10.1136/gutjnl-2018-316128

Jacopo Boni was supported by a FPI predoctoral fellowship of the Spanish Ministry of Science, Innovation and University (BES-2014-069983). This work was supported by grants from the Spanish Ministry of Economy and Competitiveness (BFU2013-44513 and BFU2016-76141-P), and the Secretariat of Universities and Research-Generalitat de Catalunya (2014SGR674). The group belongs to the Rare Diseases Networking Biomedical Research Center (CIBERER). The CRG is a ‘Centro de Excelencia Severo Ochoa 2013-2017’.